FORMATION AND CHARACTERIZATION OF BULK METALLIC GLASSES

Thesis by

Atakan Peker

In Partial Fulfillment of the Requirements

for the Degree of

Doctor of Philosophy

California Institute of Technology

Pasadena, California

1994

(March 14, 1994)

To my family

Acknowledgements

I have found myself several times extremely fortunate being at the right time, at the right place with the right person. This includes working on bulk metallic glasses with Bill Johnson at Caltech. Having the most admirable history of research on metallic glasses, Caltech provided me an excellent environment, scientific and non-scientific, for a graduate study I have never thought of before.

This thesis has been possible not only because Bill acquired me to his group, but also because he has an exemplary vision of research and teaching in this field -- metallic glasses-- nobody can match. He has exceptional scientific intuition, enthusiasm and enjoyment of science, and he has mastered in passing these to his students. I have also found him as a great friend and am looking forward to long years of collaboration and friendship.

Carol, our gifted microscopist, performed the exquisite TEM work on our samples and provided invaluable TEM pictures, which were impossible to obtain without her incredible patience and talent.

I would like to appreciate Yoshi Abe, my former office-mate, for his kind friendship and his patience in helping me in several stages of my learning how to do research. He was the most helpful friend of mine during his stay at Caltech.

In the first three years of my graduate study, I have seen invaluable assistance, help and friendship from the senior members of Johnson group and it is a

pleasure to thank them. My special thanks go to Dave Lee, Chuck Krill, Zezhong Fu and Joe Holzer who provided my lab training which proved extremely useful for my thesis. Also, I would like to thank Jurgen Eckart, Mo Li, Rainer Birringer, Jorge Kittel and Phil Askenazy.

My acknowledgments cannot be complete without fellows with whom I had friendship and cooperation in lab: Mohit Jain, Hugh Bruck, Marissa La Madrid, my current office-mate Eric Bakke, Xiang Lin, Jian Li, Z. Gao, L. Anthony, T. Stephens and many others with whom I shared the lab.

I have met with several world-class researches and extensively benefited from them during my visit to Japan for RQ 8 conference. I would like to thank J. Perepezko, B. Cantor, R. Bormann, R. Schwarz, U. Koster, H. Fecht, A. Inoue and others which I may have forgotten to list. I would like to express my gratitude to them for the valuable discussions and their friendship. Again, I like to thank my advisor, Bill Johnson, for his encouragement to attend the conference and for his friendship during this memorial visit. I would also like to thank my former officemate, Yoshi Abe, for his kind hospitality in Japan.

Amorphous International Technologies, ATI, supported the first phase of bulk metallic glass research of Bill Johnson's group. Later stages of research described in this thesis are also supported by The United States Department of Energy.

I have seen great encouragement and help from my former professors: Dr. Sabri Altintas, Dr. Can F. Delale, and Dr. Burak Erman. They prepared me for graduate study and their help proved extremely useful. I also like to thank my friend Hakan N. Ersoy who helped me in several respects to my academic life. His help in my applications to graduate school was crucial.

I can hardly express my gratitude to Dr. Talip Alp and Dr. Korkut Ozal who provided me wise advice and inspiration for hard work before and throughout my graduate study.

Finally, I would like to express my deepest gratitude to my family, who most supported (and also most suffered) from my whole academic life. I tried my best to deserve their support and right now I have the peace of mind to accomplish that. My wife Hulya, my life-long friend in this world and hereafter, has always been supportive of my graduate study. I can hardly pay off her sacrifice. My very active son has been very generous to share his energy with me by keeping me awake day and night so that I can finish my thesis as soon as possible.

Abstract

Since the discovery of metallic glass formation by ultra-rapid melt quenching at Caltech in 1959, it was thought that metallic glasses can be processed only as very thin ribbons or fine powders, due to the required high cooling rate, and that they are not stable above the glass transition temperature. This has severely limited the technological applications of metallic glasses which combine unique and desirable properties. Also, bulk glass forming metallic alloys have long been desired to improve our scientific knowledge of nucleation, crystal growth and other properties of undercooled metallic melts.

After the discovery of solid state amorphization in early eighties, there were several years of paused research on metallic glass formation by melt quenching. At the end of the last decade, a Japanese group in Sendai discovered new metallic systems, which require substantially lower cooling rates for glass formation than previous systems and which have high thermal stability above their glass transition temperature.

As a major contribution to a new era of metallic glasses, this thesis extended the formation and the thermal stability of metallic glasses to the extent that many potential uses of metallic glasses have come to the brink of reality. For the first time, the art of metallic glass making has become as easy as a single step alloy preparation using conventional metallurgical processing. The production of the

larger bulk metallic glass specimens is limited only by the scale of equipment in our laboratory and not by limitations arising from the glass forming ability of the particular alloy. These new developments presented throughout this thesis may not only extend the applications of metallic glasses but they also allow us to study the properties of highly undercooled metallic melts which are very important in phenomena such as nucleation and crystal growth.

The thesis starts with an introductory chapter describing the art and science of metallic glasses prior to this work. Then, a critical review of the current knowledge of thermodynamics and kinetics of glass formation is given in chapter 2. In chapter 3, an example of a highly processable metallic glass alloy, $Zr_{41.2}Ti_{13.8}Cu_{12.5}Ni_{10.0}Be_{22.5}$, is presented along with its preparation methods. Its general characteristics which distinguish it from conventional metallic glasses are emphasized. This particular glassy alloy, $Zr_{41.2}Ti_{13.8}Cu_{12.5}Ni_{10.0}Be_{22.5}$, belongs to an exceptionally large family of excellent glass forming metallic systems, which were developed in the course of this thesis research. In chapter 4, various forms of heterogeneous nucleation, --an important phenomena in glass formation-- are discussed with reference to several glass forming alloys. Finally, conditions for bulk glass formation are proposed in view of our current theoretical knowledge and experimental observations. Difficulties in attaining these conditions are also discussed and suggestions are made for finding other bulk glass forming alloys.

Contents

List of Figures

List of Tables

Chapter 1:

Introduction

In this chapter I will introduce and define some of the terminology used in this thesis. After introducing glass and the glass transition, I will present a brief history of metallic glasses and their characteristics. The early work on bulk metallic glasses will then be reviewed. Finally, I will summarize the recent work on bulk metallic glasses carried out at Tohoku University, which inspired this thesis.

1.1 What is *glass?*

For the purpose of this thesis, I will use the original and the more specific definition of *glass*. A *glass* is an amorphous solid, lacking any long range order, formed by continuous hardening of a cooled liquid. The hardening is determined quantitatively by viscosity and it is common to take a viscosity of 10^{13} poise[1] to distinguish fluid from solid behavior. The amorphous structure can be determined by X-ray diffraction and transmission electron microscopy (TEM). However, the difference between an amorphous and nanocrystalline structure becomes vague when long range translational order is limited to a few nanometers. A solid will be called amorphous, when no long range order can be

[1] 1 poise = 10^{-1} Ns m^{-2}

detected down to ~2 nm. Further, we can supplement X-ray and TEM by calorimetry, which utilizes the thermal manifestations of the glass transition and the crystallization of a glassy phase.

1.2 The *glass transition*

The *glass transition* can be defined as a transition during which undercooled liquid configurationally freezes into a solid in a rather well defined temperature range during continuous cooling. Alternatively, an undercooled liquid transforms into a *glass* during the *glass transition*. This transition is roughly reversible (ignoring irreversible relaxation effects in the glass), unless crystallization intervenes, and transforms the glass into a highly undercooled liquid state during continuous heating. During glass transition the atomic mobility, which is correlated to the viscosity, changes by several orders of magnitude. In figure 1.1 (a) the temperature dependence of the viscosity of an undercooled liquid is shown schematically. Usually the glass transition occurs in a relatively small temperature interval though it is somewhat dependent on the rate of heating and cooling. The *glass transition temperature* T_g has been arbitrarily defined as the temperature at which viscosity has a value of 10^{13} poise. The *reduced glass transition temperature* T_{rg}, a crucial factor for glass formation, is defined as $T_{rg} \equiv T_g / T_m$, where T_m is the thermodynamic freezing temperature of liquid (where the liquid freezes to the equilibrium crystalline phase(s)).

It has been empirically observed that the heat capacity of undercooled liquid increases with decreasing temperature below T_m and frequently exceeds the heat capacity of the corresponding crystalline phase. Thus $\Delta C_p = C_p^l - C_p^x$, defined as the difference of heat capacity between liquid and crystal, increases with falling

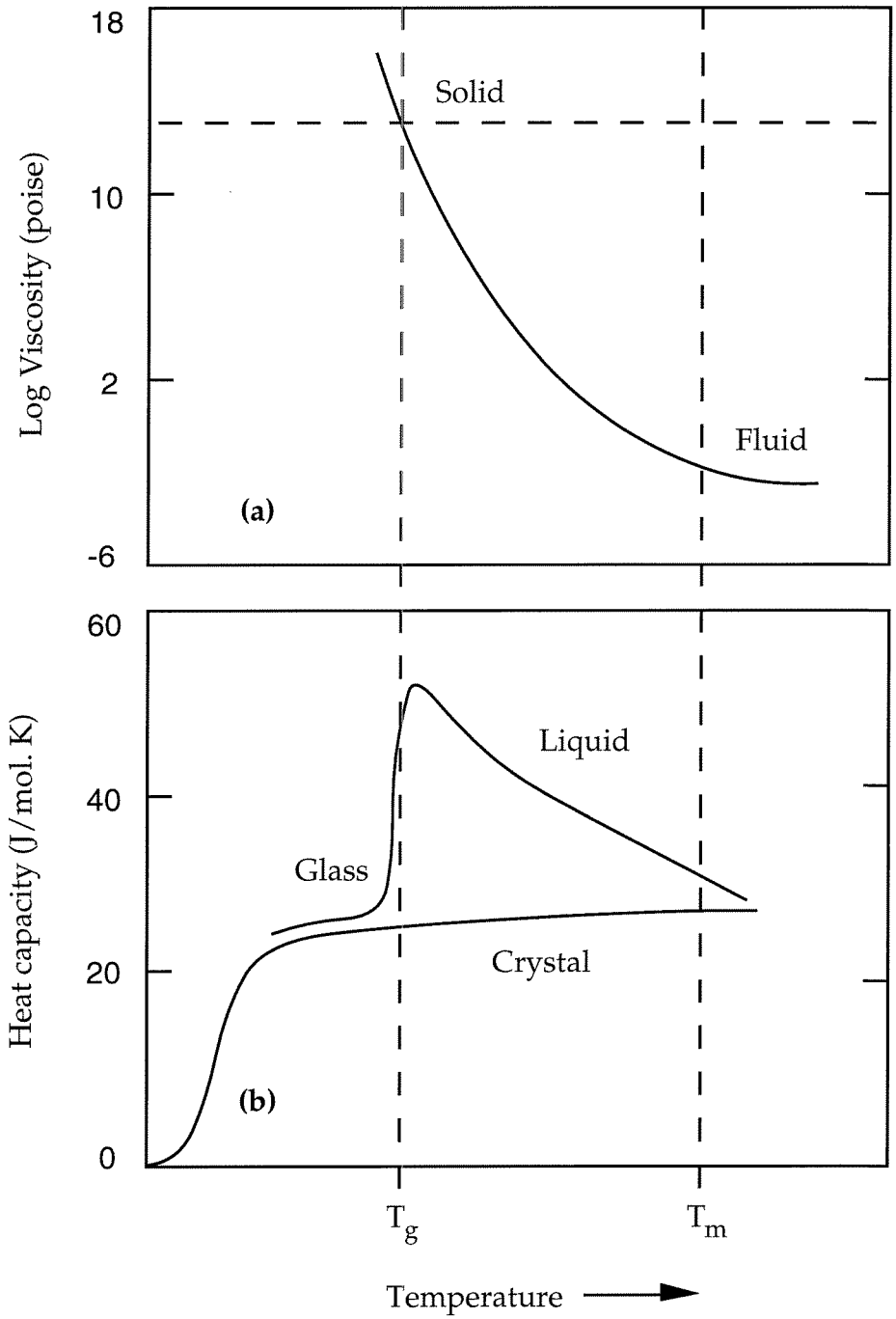

Figure 1.1: (a) Temperature dependence of the viscosity of an undercooled melt. (b) Heat capacity of an undercooled melt as a function of temperature. Also shown is the typical heat capacity of the corresponding crystalline solid at the same composition.

temperature as shown in figure 1.1 (b). Alternatively, liquid loses entropy faster relative to the corresponding crystal with decreasing temperature. According to the "*Kauzmann Paradox*," this cannot continue indefinitely as entropy of melting would fall to zero with decreasing temperature and become negative at some temperature below the thermodynamic melting point [1]. This trend must therefore be terminated at some low temperature by a solidification process. The solidification can be either crystallization or the formation of an amorphous solid, glass. When the crystallization is suppressed by the kinetic constraints, the formation of an amorphous solid is realized through the glass transition. Figure 2 shows the heat capacity of undercooled liquid decreasing abruptly during the glass transition thus avoiding the "*Kauzmann Paradox*." This abrupt change in heat capacity has been traditionally exploited to determine the glass transition temperature of undercooled liquids by the calorimetric techniques.

1.3 A brief history of metallic glasses

The history of metallic glasses formed by melt quenching starts in 1959, here at Caltech, with an unexpected result of an experimental search for extended solid solubility in the immiscible Au-Si binary system by very rapid quenching from the molten state [2]. The very rapid quenching of liquid was achieved by a gun quenching technique which can give exceptionally high cooling rates of 10^7 K/s for samples having a thickness of a few microns or less [2, 3]. Previously it had been shown that extended solid solutions and new crystalline metastable phases can form in binary systems having solid immiscibility upon rapid quenching from the molten state using the same technique. For example, extended solid solutions were found in Ag-Cu and Ag-Ge systems, and a new metastable hexagonal phase was found in Ag-Ge system [2, 3]. As the Au-Si system

resembles the Ag-Ge system in several respects, extended solid solutions and new metastable crystalline phases were expected in the Au-Si system upon very rapid quenching of the liquid alloy. However, at the composition of $Au_{75}Si_{25}$, a new metastable glassy phase was found which was called *"non-crystalline phase"* at that time [4]. The main difference between Au-Si and Ag-Ge is that Au-Si has a much deeper eutectic, at 18 atom percent Si, where metallic glass formation was observed. This was quickly pointed out by Cohen and Turnbull [5] and they proposed subsequently that glass formation is favored near deep eutectics. Later, Turnbull used the classical theory of nucleation and growth of crystalline phases in undercooled liquids to account for the glass forming ability of materials [6]. He concluded that glass formation is favored at high reduced glass transition temperatures, T_{rg}, defined as $T_{rg} \equiv T_g / T_m$. As glass transition temperature slowly varies with composition, deep eutectic compositions have higher reduced glass transition temperature, hence better glass forming ability. Since then, this has become a very popular guide to finding new metallic glass forming systems.

However, metallic glasses didn't attract the attention of the scientific community for a decade and were even referred to as "Pol Duwez' s stupid alloys" by one visiting professor [7]. After the discovery of strong ferromagnetism in Fe- base metallic glasses [8], the level of research in this new field accelerated due, not only to scientific interest in ferromagnetism, but also to possible exploitation in industrial applications. Since then, numerous new metallic glass forming systems have been studied and glass transition has been found in a large number of binary systems. Initially, it was thought that glass formation was unique to late transition metal-metalloid type eutectic systems such as Au-Si, Pd-Si, Fe-B, etc. Here, the composition of metalloid element is typically found to be near 20

atom percent. The first counter example was reported by Giessen and co-workers in 1967 [9]. Nb-Ni and Ta-Ni binary alloys with 60 atom percent Ni were quenched into the glassy phase by splat-quenching. Later they reported glass formation in Zr-TM (TM=Ni, Co, Cu, Pd) with late transition metal concentration ranging from 25 atom percent to 60 atom percent [10]. By the mid eighties, several different types of glass forming metallic systems had been discovered by rapid quenching techniques. These included metallic systems containing up to 50 atom percent metalloid atoms, e.g., $Ru_{42}Zr_8B_{50}$ [11], metallic systems with no transition metal or metalloid, e.g., $Mg_{70}Zn_{30}$ [12], and transition metal-simple metal systems, e.g., $Ti_{50}Be_{40}Zr_{10}$ [13].

In the late sixties Chen and Turnbull successfully carried out the first experimental studies of the glass transition in metallic glasses. This was a very difficult task for metallic systems, as crystallization kinetics in metallic systems are much faster than in oxide glasses such as fused silica. Crystallization generally intercedes and precludes the glass transition in the time scale of laboratory measurements. In the first system they studied, $Au_{81.4}Si_{18.6}$, they were not able to observe the glass transition calorimetrically (i.e., abrupt change in heat capacity of glass) as crystallization intervened [14]. However, they found that at the melting point, the liquid has a higher heat capacity than the crystal, and ΔC_p increases further with increasing liquid undercooling, whereas the heat capacity difference between the glass and the crystalline phases from room temperature up to the crystallization temperature is less than the heat capacity difference of liquid and crystalline phases below the melting point. They concluded that there should be a glass transition temperature, between the crystallization temperature and melting point of the crystalline alloy, where the trend of increasing ΔC_p with falling temperature terminates. This was an indirect

proof for the existence of a glass transition in metallic glasses. Later, they obtained direct thermal evidence that a glassy $Au_{77}Ge_{13.6}Si_{9.4}$ alloy --a better glass former-- exhibits a transition from the glass to a metastable supercooled liquid state highlighted by the abrupt change in heat capacity as predicted [15]. They further confirmed their thermal results by viscosity measurements around the glass transition [16]. In summary, they observed that upon continuous heating, metallic glasses go through a glass transition, becoming a highly undercooled liquid in a short temperature interval. When the transition is complete, the typical force needed to sustain deformation of the undercooled liquid is many orders of magnitude less than for the glass. This may have practical applications such as easy fabrication of glassy alloys at temperatures far below the melting temperature of crystalline alloy. However, the utilization of the glass transition in fabrication of metallic glasses has never been realized, since metallic glasses have not been stable enough against crystallization above the glass transition. Since these early experiments, relatively very little experimental work has been done on glass transition and related phenomena such as viscosity change at the glass transition in metallic glass systems.

Until the early seventies, the reported studies of metallic glasses have concentrated on measurement of physical properties which do not depend on sample geometry such as electrical, magnetic, thermodynamic and structural properties. At that time, the available rapid quenching techniques could not produce metallic glass samples with suitable geometry for large scale mechanical testing. Masumoto and Maddin were the first to report on the comprehensive mechanical properties of metallic glasses [17]. They adapted the rotating crucible technique, which was originally developed for the production of the crystalline metal filaments from the melt [18], to produce uniform and long enough Pd-Si

glassy ribbons to carry out mechanical tests. They found that metallic glasses have exceptional high strength and show limited ductility in tension. However, this apparent "brittleness" was completely different from that of oxide glasses as there was evidence of plastic flow at failure surfaces. Deformation markings -- shear bands-- were observed on the yield surfaces of metallic glass ribbons which were pulled above the yield point. The first experiment to show the intrinsic ductility of metallic glasses was actually carried out by Pol Duwez et al., though not reported [19]. They were able to cold roll 40 micron thick glassy foil down to 13 micron without any cracking. Another good example of ductility in metallic glasses was given by Chen and Polk [20]. They bent a Ni- base metallic glassy ribbon around a radius of the order of magnitude of its thickness without any breaking and crack formation. However, the ductility of metallic glasses depends on the preparation method as well as on the composition. For example, no sign of ductility was observed in bending $Cu_{60}Zr_{40}$ glassy alloy [21].

As the properties of metallic glasses have been measured and sorted out, it has been found that these new glassy alloys have unique features and combine several desirable properties which do not exist in their crystalline counterparts. For example, metallic glassy alloys have very high elastic limit, high hardness, very high strength --close to the theoretical limit--, good bend ductility, better soft magnetic properties, increased corrosion resistance, low coefficient of friction and other useful properties [22]. Although metallic glasses have very useful properties for many technological applications, they were largely ignored by industrial researchers for some time. Clearly, the single most important reason was the difficulty in production of metallic glasses which requires very high cooling rates. Since heat had to be extracted in at least one direction at 10^5-10^7 K/s, metallic glasses should have a thickness of less than 100 micron at least in

one direction. The early rapid quenching techniques were not convenient for the large scale production of metallic glasses. By the mid seventies, the development of new rapid quenching techniques for industrial production, such as single roller chill-block casting [23], opened the way for the applications of metallic glasses [24]. The first applications utilized the unusual soft magnetic properties of Fe-base metallic glasses to produce transformer cores which could be wound from thin sheets. This also permitted the researchers to obtain better samples in the form of uniform foils for more comprehensive testing and characterization of metallic glasses. The absence of bulk specimens nevertheless continued to hinder use in structural applications.

In the first three decades of metallic glass research, the common wisdom has been that metallic glass formation is generally limited to high cooling rates of 10^5 K/s or more. In turn, this cannot give glassy samples having a minimum dimension greater than a few hundreds microns. There were a few exceptions. For example, certain noble metal based alloy systems were found to exhibit glass formation at somewhat lower cooling rates. To obtain bulk samples in more practical alloys, several methods have been tried to consolidate metallic glasses; however, most of them either failed or achieved moderate success at enormous effort and cost [25]. One method used by Shingu deserves particular attention [26]. This method exploits the homogenous deformation of metallic glasses above the glass transition and requires relatively much smaller consolidation pressures due to very low viscosity. However, known metallic glasses at the time of this work were generally prone to crystallization above the glass transition. In fact, most of them were observed to crystallize below the glass transition temperature making the Shingu process very tricky and difficult to implement and control. Another method which worked well in consolidation of

metallic glasses is shock wave consolidation [27,28]. However, this method is very expensive and its practical applications are very limited. Ironically, until the 1990's research efforts to find metallic glasses which do not require high cooling rates (thus making bulk glass formation easier), or efforts to find metallic glasses with better thermal stability above the glass transition, were relatively rare compared to efforts on consolidation of metallic glasses.

The interest in metallic glass formation from the melt diminished quickly with the discovery of solid state amorphization by R. B. Schwarz and W. L. Johnson (a Ph.D. student of Pol Duwez) in 1983 [29]. There has been little work reported on melt quenched metallic glasses due to increased research interest in solid state amorphization since then.

Starting in 1989, the group of Masumoto and Inoue, at Tohoku University, discovered several novel metallic glass forming systems, which were all reported in the journal of "JIM Materials Transactions." These systems are especially distinguished from earlier ones by much lower critical cooling rates required to produce glass. This enables glass formation in thicker samples and better thermal stability above the glass transition. Moreover, these systems do not contain expensive noble metals unlike earlier "thick" glass formers. It is also obvious that these alloys are better suited for scientific work, such as viscosity and heat capacity measurements, and for possible technological applications. Interestingly, there was little response in the scientific community to this breakthrough work until 1993 [30].

1.4 Previous work on bulk metallic glasses

For the purpose of this thesis, I will define the terms of "thick glass" and "bulk glass." The term "thick glass" refers to glassy samples having a minimum dimension of one mm or more, whereas "bulk glass" will refer to glassy samples having a minimum size of one cm or more.

The first thick metallic glass formation was reported by Chen and Turnbull in 1969 [31]. They added Cu, Ag, and Au to the well known Pd-Si glass forming binary system [32]. By dropping liquid droplets onto copper substrates, they made 1.0 mm thick glassy samples. A typical composition was $Pd_{77.5}M_6Si_{16.5}$ (M=Ag, Au, Cu). They also found that these metallic glasses have better thermal stability than others. For example, they heated a glassy $Pd_{77.5}Cu_6Si_{16.5}$ alloy 40 K above the glass transition without crystallization at a heating rate of 20 K/min. Most other metallic glasses crystallize before the glass transition temperature has been reached.

Later, Chen investigated glass formation in $(Pd_{1-X}M_X)_{0.835}Si_{0.165}$, $(Pd_{1-X}T_X)_{1-Z}P_Z$, $(Pt_{1-X}Ni_X)_{1-Z}P_Z$ (T = Ni, Co, and Fe and M = Rh, Au, Ag, Cu and T) systems [33]. He found that the replacement of Pd and Pt with elements of smaller size (e.g., Ni, Co, Fe, and Cu) greatly facilitated the formation of metallic glass and lowered the critical cooling rates down to 10^3 K/s. Ni was especially effective; giving the largest replacement of Pd and Pt and thicker glass formation. 1-3 mm diameter rods of glassy samples were obtained by quenching the melt, sealed in a capillary quartz tube, into water. He attributed this enhanced glass formation to the increased reduced glass transition temperature T_{rg} due to additional alloying. These alloys have been found especially useful for

more reliable and comprehensive mechanical testing of metallic glasses. Two of the well known compositions are $Pd_{40}Ni_{40}P_{20}$ and $Pd_{77.5}Cu_6Si_{16.5}$. The Pt- base alloys were not extensively studied due to their prohibitive cost.

In 1982, Lee, Kendall and Johnson [34] reported thick glass formation in another noble metal based alloy, $Au_{55}Pb_{22.5}Sb_{22.5}$. 1.5 mm diameter spheres of this alloy formed metallic glass upon quenching molten droplets into LN_2. They noticed heterogeneous nucleation on surfaces of bigger samples. This glassy alloy has such good thermal stability that its heat capacity was measured up to 50 K above the glass transition temperature [35].

In 1982, David Turnbull and his colleagues demonstrated the first cm thick glass formation in a $Pd_{40}Ni_{40}P_{20}$ alloy though with a cumbersome method. Turnbull had predicted that when the reduced glass transition temperature T_{rg} reaches a value of 0.67, bulk glass formation should occur provided heterogeneous nucleation of crystals is prevented [6]. To demonstrate the pronounced effect of heterogeneous nucleation on glass formation, they tried to obtain unusually thick metallic glass by eliminating the heterogeneous surface nucleation. They used $Pd_{40}Ni_{40}P_{20}$, since it had the highest reported T_{rg} =0.66 [36], and is thus favorable for bulk glass formation. Initially, they tried to eliminate the surface heterogeneities by successive melting, solidification and etching cycles. This resulted in a 6 mm diameter spheroidal glassy alloy with marginal crystallization [37]. Later, they improved the elimination of heterophase nucleants by using a molten surface flux of dehydrated boron oxide [38]. This technique proved to be powerful, producing more massive, wholly glassy specimens more consistently. They obtained a glassy sample having a minimum dimension of 1.0 cm with no superficial crystallinity at cooling rates of ~1 °C/s. This was the largest metallic

glass specimen formed by melt cooling until 1993 [30]. They also demonstrated that glassy alloys with a proper flux, which deactivates heterogeneous crystal nucleation sites, have better thermal stability. They successfully heated a fluxed $Pd_{40}Ni_{40}P_{20}$ glassy alloy from room temperature to the melting temperature of the equilibrium crystal at the rates of ~1 °C/s without any crystallization [39]. However, this very interesting work did not receive broad attention and in some cases was totally ignored.

Another noteworthy alloy is $Ni_{62}Nb_{38}$ which was found to be a glass former in 1967 [10]. Until the 1990's, it was the only reported alloy with no noble metals, having a high reduced glass transition temperature, T_{rg} =0.66, and an estimated critical cooling rate of approximately 10^3 K/s [36]. We have been able to cast 1.0 mm thick glassy strip of this alloy which is consistent with the estimated critical cooling rate [40]. However, there has been very little reported information on its "thick glass formation," and no work has been reported on efforts to improve its glass forming ability.

1.5 Bulk metallic glass work at Tohoku University

The first extensive and systematic search for bulk glass forming alloys was carried out by the group of Masumoto and Inoue at Tohoku University, Japan. Recently they published several papers on metallic glasses having exceptional glass forming ability and high thermal stability. Their starting point was that better thermal stability of a metallic glass above the glass transition leads to a lower critical cooling rate for glass formation. This is generally true for the earlier thick glass forming alloys such as $Pd_{77.5}Cu_6Si_{16.5}$ and $Au_{55}Pb_{22.5}Sb_{22.5}$. First they tried to form metallic glasses by melt spinning which gives a cooling rate of 10^5-10^6 K/s. Then, they performed calorimetric measurements on readily

glass forming alloys to determine their glass transition temperature and crystallization temperatures at a typical heating rate of 40 K/min. They looked for a wide super cooled liquid region which is quantitatively given by $\Delta T=T_x-T_g$, defined as the difference between crystallization and glass transition temperatures. Assuming higher ΔT values reflect lower critical cooling rates, they tried to find thick metallic glasses from the alloys exhibiting high ΔT values. Various methods were employed to form thick metallic glasses such as water quenching and metallic mold casting. They found La-base, Mg-base, and Zr-base metallic glasses, which require cooling rates less than 10^3 K/s and exhibit good thermal stability above the glass transition.

1.5.1 La-base alloys

The first thick glass forming alloy they reported is $La_{55}Ni_{20}Al_{25}$ having ΔT=70 K [41]. Glassy samples of this alloy having cylindrical shapes with a 1.2 mm diameter were prepared by quenching the melt, sealed in a quartz capillary, into water. The enhanced glass forming ability was attributed to a high value of the reduced glass transition temperature T_{rg}, which was reported to be 0.68. From the correlation between reduced glass transition and critical cooling rate, proposed by Davies and co-workers [36], they expected a critical cooling rate of 10^2 K/s which was in agreement with the water quenching experiment. Later, they increased the maximum diameter of glassy cylindrical samples up to 2.5 mm by metallic mold casting [42]. The detailed study of La-Al-Ni ternary system revealed that ΔT correlates with reduced glass transition temperature T_{rg}, both having maximum values around the composition of $La_{55}Ni_{20}Al_{25}$ [43]. Replacement of Ni with Cu gave similar good results, i.e., high ΔT and T_{rg} with maximum values of 59 K and 0.68 respectively at the composition of

$La_{55}Al_{25}Cu_{20}$ [44]. Water quenching yielded glassy samples with cylindrical shapes up to 1.0 mm diameter.

The mixture of ternary alloys, $La_{55}Ni_{20}Al_{25}$ and $La_{55}Cu_{20}Al_{25}$, resulted in a better glass forming alloy, $La_{55}Ni_{10}Cu_{10}Al_{25}$. The quaternary alloy can be cast in up to 7 mm diameter glassy rods by high pressure die casting, whereas ternary alloys can be cast only up to 3 mm diameter glassy rods [45]. Even better is a pentiary alloy, $La_{55}Cu_{10}Ni_5Co_5Al_{25}$, which can be cast into 9 mm diameter glassy rods. Similar improvement was reported for ΔT, which is 60 K, 90 K and 100 K for ternary, quaternary, and pentiary alloys respectively. All the alloys, ternary, quaternary and pentiary, have values of T_{rg} around 0.69, although they show a significant difference in critical cooling rates. It was proposed that the increase in ΔT is the dominant factor for the drastic decrease in the critical cooling rates. This proposal has been further supported by work on Mg-base and Zr-base glass forming alloys.

1.5.2 Mg-base alloys

The first alloy system reported having a wide supercooled liquid region is the ternary Mg- base system, Mg-Ni-La, having a maximum ΔT=58 K at the optimum composition of $Mg_{50}Ni_{30}La_{20}$ [46]. However, no work has been reported on the thick glass forming ability of this alloy. In a later work, the Tohoku group studied Mg-Cu-Y and Mg-Ni-Y ternary systems [47]. Maximum values of ΔT were reported to be 41 K for Mg-Ni-Y at the composition of $Mg_{50}Ni_{30}Y_{20}$ and 61 K for Mg-Cu-Y at the composition of $Mg_{65}Cu_{25}Y_{10}$. Thick glass formation was demonstrated in the Mg-Cu-Y ternary system by the metallic mold casting method [48]. The largest glassy sample was obtained at the $Mg_{65}Cu_{25}Y_{10}$ composition as a 4 mm diameter rod. Surprisingly, the reduced

glass transition temperature T_{rg} has a relatively low value of 0.60 compared to the very low critical cooling rate. Further, T_{rg} values change slowly with respect to the composition, whereas ΔT and critical cooling rates are strongly dependent on the composition. This conflicts with the well known correlation between the T_{rg} and critical cooling rate proposed by Davies [36]. It was proposed that the compositional dependence of the required cooling rates is mainly dominated by the ΔT value.

1.5.3 Zr-base alloys

Although Zr-base binary glass forming alloys, Zr-Cu and Zr-Ni, have been among the most studied glassy alloys, very little work has been reported for glass formation in Zr-base ternary systems. The group of Masumoto and Inoue carried out extensive work on ternary and higher order Zr-base alloys. The values of ΔT were especially well characterized as a function of composition. The glass formation in the ternary Zr-TM-Al (TM=Mn, Fe, Co, Ni, Cu) system was well determined and the highest values of ΔT were found in Zr-Cu-Al and Zr-Ni -Al ternaries, e.g., 77 K for $Zr_{60}Ni_{25}Al_{15}$ [49]. The reduced glass transition was reported to be highest, 0.64, around the vicinity of $Zr_{60}Ni_{20}Al_{20}$ and gradually changing to 0.60 around the composition of $Zr_{60}Ni_{25}Al_{15}$ [50]. Usually high ΔT values were reported to be associated with high T_{rg}. Using the empirical relation between T_{rg} and critical cooling rate [36], they expected a low cooling rate for the composition of $Zr_{60}Ni_{20}Al_{20}$ which was confirmed by water quenching yielding a 1.4 mm diameter glassy rod.

The detailed study of higher order systems, $Zr_{65}Al_{7.5}Cu_{2.5}TM_{25}$ (TM=Co, Ni, Cu), revealed that the quaternary system has improved glass formation compared to the ternary systems [51]. The optimization of composition for a

high value of ΔT gave rise to a remarkably high ΔT= 127 K at the composition of $Zr_{65}Cu_{17.5}Ni_{10}Al_{7.5}$. Unexpectedly, no glassy alloy was found with a T_{rg} value above 0.60 and no close relation was found between T_{rg} and ΔT. Metallic mold casting yielded glassy rods as large as 7.0 mm diameter at the composition of $Zr_{65}Cu_{17.5}Ni_{10}Al_{7.5}$, having the largest ΔT. Although the T_{rg} is almost independent of the TM composition, the maximum diameter of glassy rod shows a strong dependence on composition, decreasing with the value of ΔT down to 1.5 mm at ΔT=40 K. Later, it was claimed that glassy rods having a diameter as large as 16 mm were obtained by water quenching at the composition of $Zr_{65}Cu_{17.5}Ni_{10}Al_{7.5}$ [52]. However, we have failed to reproduce this result. Further, we couldn't get a glassy rod of 7 mm diameter by water quenching at the composition of $Zr_{65}Cu_{17.5}Ni_{10}Al_{7.5}$ [53].

The effect of adding other metals to the Zr-Cu binary glass forming alloys has also been studied. Ternary systems have always been found to have larger ΔT values with a strong dependence on the specific element added, Al being the most effective [54,55].

References

[1] W. Kauzmann, Chem. Rev., **43**, 216 (1948).

[2] For a review of historical development of liquid quenching, see: P. Duwez, Trans. ASM, **60**, 607 (1967).

[3] P. Duwez, R. H. Willens, and W. J. Klement, J. Appl. Phys., **31**, 1136 (1960).

[4] W. J. Klement, R. H. Willens, and P. Duwez, Nature, **187**, 869 (1960).

[5] M. H. Cohen and D. Turnbull, Nature, **189**, 131 (1961).

[6] D. Turnbull, Contemp. Phys., **10**, 473 (1969).

[7] W. L. Johnson, Int. J. Rap. Sol., **1**, 331 (1985).

[8] P. Duwez and S. C. H. Lin, J. Appl. Phys., **38**, 4096 (1967).

[9] R. Ray, B. C Giessen, and N. J. Grant, Script. Met., **2**, 357 (1968).

[10] R. C. Ruhl, B. C. Giessen, M. Cohen, and N. J. Grant, Acta. Met., **15**, 1693 (1967).

[11] M., Mehra, A. Williams, and W. L. Johnson, Phys. Rev., B **28**, 624 (1983).

[12] A. Calka, M. Madhava, D. E. Polk, and B. C Giessen, Script. Met., **11**, 65 (1977).

[13] L. E. Tanner, R. Ray, Script. Met., **11**, 783 (1977).

[14] H. S. Chen and D. Turnbull, J. Appl. Phys., **38**, 3646 (1967).

[15] H. S. Chen and D. Turnbull, Appl. Phys. Letts., **10**, 284 (1967).

[16] H. S. Chen and D. Turnbull, J. Chem. Phys., **48**, 2560 (1968).

[17] T. Masumoto and R. Maddin, Acta. Met., **19**, 725 (1971).

[18] R. Pond, and R. Maddin, Trans. Metall. Soc. A. I. M. E., **245**, 2475 (1969).

[19] P. Duwez, Annl. Rev. Mat. Sci, **6**, 83 (1976).

[20] H. S. Chen and D. E. Polk, J. Non Cryst. Solids, **15**, 174 (1974).

[21] J. Vitek and N. J. Grant, Met. Trans., **6A**, 1472 (1975).

[22] For a recent review of properties and applications of metallic glasses. see: *Rapidly Solidified Alloys: Processes, Structures, Properties, Applications*, H.H. Liebermann (ed.), (Marcel Dekker Inc., New York, 1993).

[23] J. R. Bedell, U.S. Patent No. 3,862,658, assigned to Allied Chemical Corp. (Jan. 1975).

[24] For a detailed account of rapid quenching techniques, see: T. R. Anantharaman and C. Suryanarayana, in *Rapidly Solidified Metals: A Technological Overview*, (Trans Tech Pub, Switzerland, 1987).

[25] For a recent review of consolidation of metallic glasses, see: R. B. Schwarz, in *Rapidly Solidified Alloys: Processes, Structures, Properties, Applications*, H. H. Liebermann (ed.), (Marcel Dekker Inc., New York, 1993).

[26] P. Shingu, Mater. Sci. Eng., **97**, 137 (1988).

[27] J. Kasiraj, D. Kostka, T. Vreeland, T. J. Ahrens, J. Non-Cryst. Solids, **61**, 967 (1984).

[28] J. Bach, B. Krueger, B. Fultz, Mater. Mat. Lett., **11**, 383 (1991).

[29] R. B. Schwarz and W. L. Johnson, Phys. Rev. Lett., **51**, 415 (1983).

[30] A. Peker and W. L. Johnson, Appl. Phys. Lett., **63**, 2342 (1993).

[31] H. S. Chen and D. Turnbull, Acta. Met., **17**, 1021 (1969).

[32] P. Duwez, R. H. Willins, and R. C. Crewdson, J. Appl. Phys., **36**, 2267 (1965).

[33] H. S. Chen, Acta. Met., **22**, 1505 (1974).

[34] M. C. Lee, J. M. Kendall, and W. L. Johnson, Appl. Phys. Lett., **40**, 382 (1982).

[35] H. J. Fecht, J. H. Perepezko, M. C. Lee, and W. L. Johnson, J. Appl. Phys., **68**, 4494 (1990).

[36] H. A. Davies, *Rapidly Quenched Metals III*, edited by B. Cantor (Metals Soc., London, 1978), Vol. 1, p. 1.

[37] A. J. Drehman, A. L. Greer, and D. Turnbull, Appl. Phys. Lett., **41**, 716 (1982).

[38] H. W. Kui, A. L. Greer, and D. Turnbull, Appl. Phys. Lett., **45**, 615 (1984).

[39] H. W. Kui and D. Turnbull, Appl. Phys. Lett., **47**, 796 (1985).

[40] A. Peker and W. L. Johnson, unpublished research (1992).

[41] A. Inoue, K. Kita, T. Zhang, and T. Masumoto, Mater. Trans., JIM, **30**, 722 (1989).

[42] A. Inoue, T. Zhang, and T. Masumoto, Mater. Trans., JIM, **31**, 425 (1990).

[43] A. Inoue, T. Zhang, and T. Masumoto, Mater. Trans., JIM, **30**, 965 (1989).

[44] A. Inoue, H. Yamaguchi, T. Zhang, and T. Masumoto, Mater. Trans., JIM, **31**, 104 (1990).

[45] A. Inoue, T. Nakamura, T. Sugita, T. Zhang, and T. Masumoto, Mater. Trans., JIM, **34**, 351 (1993).

[46] A. Inoue, M. Kohinata, A. P. Tsai, and T. Masumoto, Mater. Trans., JIM, **30**, 378 (1989).

[47] S. G. Kim, A. Inoue, and T. Masumoto, Mater. Trans., JIM, **31**, 929 (1990).

[48] A. Inoue, A. Kato, T. Zhang, S. G. Kim, and T. Masumoto, Mater. Trans., JIM, **32**, 609 (1991).

[49] A. Inoue and T. Masumoto, U.S. Patent 5,032,190 (July 1991).

[50] A. Inoue, T. Zhang, and T. Masumoto, Mater. Trans., JIM, **31**, 177 (1990).

[51] T. Zhang, A. Inoue, and T. Masumoto, Mater. Trans., JIM, **32**, 1005 (1991).

[52] T. Masumoto, *Rapidly Quenched Metals 8*, Sendai, Japan (1993).

[53] A. Peker and W. L. Johnson, unpublished research (1993).

[54] T. Zhang, A. Inoue, and T. Masumoto, J. Mat. Sci. Lett., **12**, 700 (1993).

[55] A. P. Tsai, D. Kawase, A. Inoue, and T. Masumoto, Script. Met., **29**, 657 (1993).

Chapter 2

Thermodynamics and kinetics of glass formation

What is the stable form of solid substances? Is it crystal or glass? Unfortunately we don't have any rigorous proofs that can answer these questions as yet. However, experience tells us that crystalline phases are thermodynamically more stable with respect to the glass in most or all substances we know. Unless we meet a big surprise, we might well assume that new materials will behave similarly. As such, glass formation in known (and unknown) substances should be a kinetic phenomenon. This raises another question. Can we put an arbitrary substance into the glassy form? Theoretical and experimental accomplishments of the last three decades encourage us to believe that the answer is "yes." The single most important factor for glass formation in a given substance has been found to be the cooling rate from the liquid state. A higher cooling rate is associated with an easier glass formation in all classes of materials. Turnbull and Cohen predicted that liquids will form glasses through the glass transition if cooled sufficiently fast to bypass crystallization [1]. As new techniques have been developed to provide higher cooling rates from the liquid state, more materials have been put into the glassy form [2]. Then a more practical question is "which materials can be put into glass with available quenching techniques?" Alternatively, "what is the required cooling rate to put a given material into

glassy form?" Answering this question is not an easy task, as the ease of glass formation shows enormous variation. When we classify materials according to the their bonding nature, there are some glass formers in every category of materials. From this we can deduce that the factors that govern the glass formation may have universal features. Turnbull used the classical theory of nucleation and growth of crystalline phases in an undercooled melt to account for the kinetics of glass formation in general and successfully underlined its overall features [3]. It turned out that glass formation is not a purely kinetic process. Rather, thermodynamic properties, such as crystal-liquid interfacial energy, free energy difference between the undercooled liquid and the corresponding crystalline phase, play important roles in governing kinetics of glass formation.

In this chapter I will give a critical review of kinetic analyses of glass formation and its relation to the thermodynamics of a system. First, the derivation of the classical theory of nucleation in undercooled melts will be presented without attempting any rigorous justification. After discussing the effects of thermodynamic parameters appearing in the steady state nucleation rate, I will present the well accepted kinetic treatment of glass formation by Davies and Uhlmann. Finally, the T_0 criterion of glass formation will be introduced.

2.1 Classical theory of homogeneous nucleation in undercooled liquids

The liquid becomes thermodynamically unstable with respect to the crystal when it is cooled below its equilibrium freezing or crystallization temperature, the melting point of the crystal. As shown in figure 2.1, the liquid has higher Gibbs'

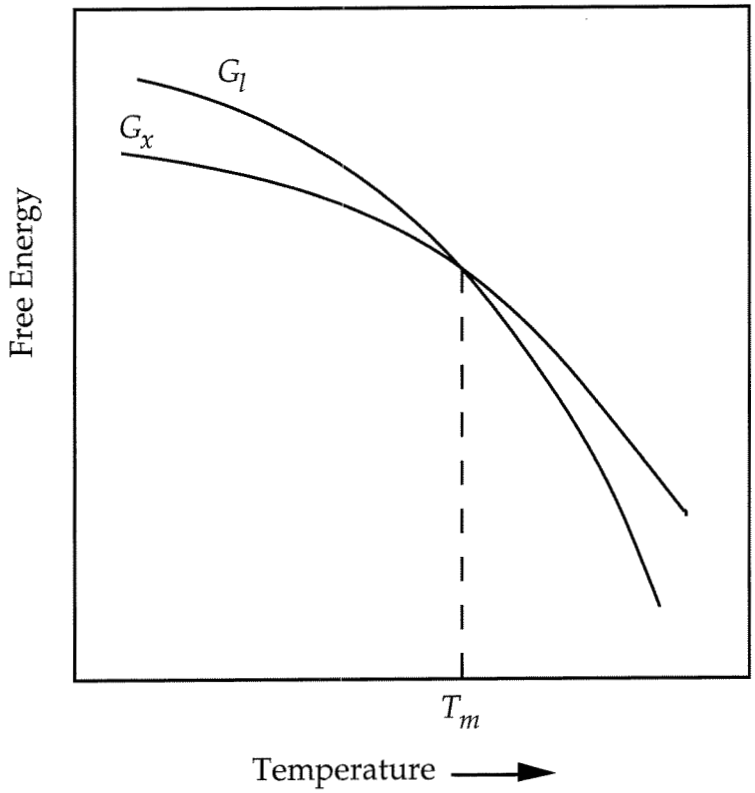

Figure 2.1: Gibbs' free energy curves for liquid and corresponding crystal with respect to the temperature.

free energy than the crystal below the thermodynamic melting of the crystal. This free energy difference gives the driving force for the nucleation of crystals from the liquid. In general, the free energy difference per unit volume, ΔG_v, is given by [3]

$$\Delta G_v = -\left\{ \Delta H_m^f(\Delta T_r) + T_m \int_1^{Tr} \left[\int_1^{T_r} \frac{\Delta C_p dT_r}{T_r} \right] dT_r \right\} \frac{1}{V_m} \qquad (2.1)$$

where ΔH_m^f is the molar heat of fusion, ΔC_p is the molar difference in heat capacity between the liquid and the crystal, V_m is the molar volume of the crystal, T_r is the reduced temperature, and ΔT_r is reduced undercooling. T_r and ΔT_r are defined as

$$T_r \equiv \frac{T}{T_m}, \qquad \Delta T_r \equiv \frac{T_m - T}{T_m}$$

where T_m and T are, respectively, the equilibrium melting temperature and actual absolute temperature.

However, the creation of a liquid/crystal interface discourages the homogenous nucleation of the crystal. This is the main cause of the resistance of the liquid to crystal nucleation. The competition between the interface energy and bulk free energy difference depends on the crystal nucleus size which in turn determines the stability of a crystalline embryo. For a spherical nucleus with radius r, the total Gibbs' free energy change upon nucleation is given by [4]:

$$\Delta G = 4\pi r^2 \sigma + \frac{4\pi}{3} r^3 \Delta G_v \qquad (2.2)$$

where σ ($\sigma > 0$) is the interfacial energy per unit area. In figure 2.2, ΔG is shown as a function of r, where ΔG_v and σ are assumed to be independent of r.

The ΔG has a maximum at r^* which is given as

$$r^* = -\frac{2\sigma}{\Delta G_v} \tag{2.3}$$

and a maximum of ΔG^* is given by

$$\Delta G^* = \left(\frac{16\pi}{3}\right)\left(\frac{\sigma^3}{\Delta G_v^2}\right). \tag{2.4}$$

The r^* and ΔG^* are the result of the balancing of two competing factors, one increasing with the area due to the interfacial tension, and one decreasing with the volume due to the free energy difference between liquid and crystal. As seen in figure 2.2, crystalline nuclei larger than r^* will grow with decreasing free energy and be stabilized. They will be nuclei for further crystal growth. Crystalline nuclei having a radius smaller than r^* will tend to remelt, as growth will increase overall free energy. Thus, ΔG^* is an activation energy for homogenous nucleation of crystals from the liquid.

Then, the classical theory of nucleation developed by Volmer, Becker, and co-workers gives the rate of homogenous nucleation as

$$I_v = K \exp\left[-\frac{(q + \Delta G^*)}{kT}\right] \tag{2.5}$$

where q is the free energy activation for atomic diffusion across the phase boundary, k is the Boltzman constant, and K is a constant to be determined [5].

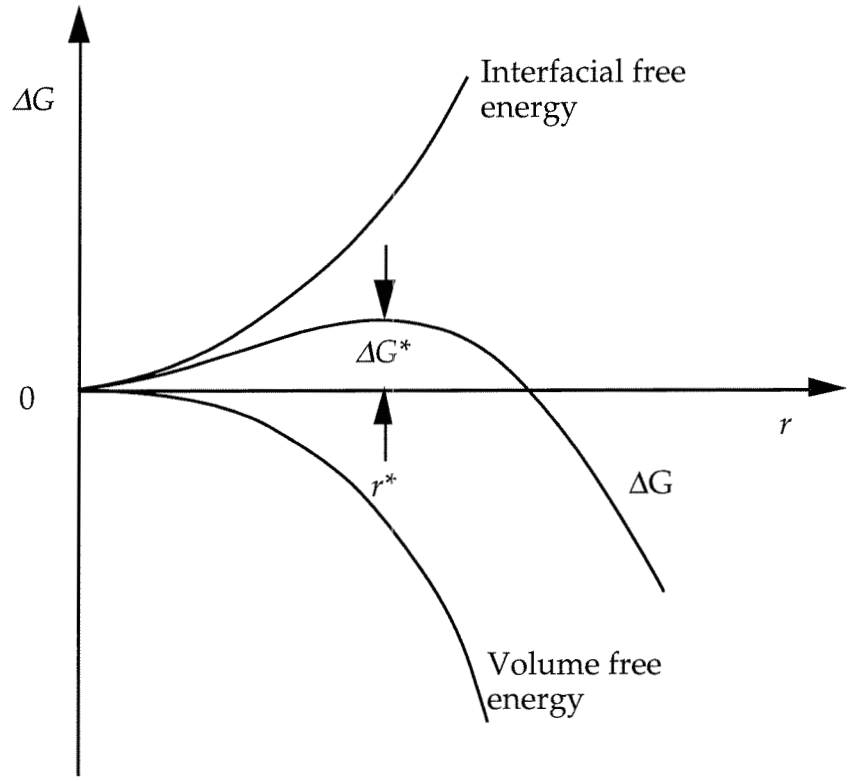

Figure 2.2: Gibbs' free energy change of nucleation of a crystalline embryo as a function of its radius.

Turnbull and Fischer derived the absolute rate of homogenous nucleation, thus determining K, based on the previous nucleation theory and the rate of absolute reaction rates [6]. According to their analysis, the rate of homogenous nucleation, to an order of magnitude, is given as

$$I_v = N_v v_0 \exp\left[-\frac{(q+\Delta G^*)}{kT}\right] \tag{2.6}$$

in units of the number of nuclei per unit volume per unit time. Here, N_V is number of atoms per unit volume and v_0 is the frequency of attempts by atoms to cross the phase boundary. It is a characteristic vibration frequency and is given as $v_0 = kT/h$ by the classical atomic theory.

Another alternative expression has been proposed for the rate of homogenous nucleation, which is

$$I_v = \frac{N_v D_i}{a_0^2}\exp\left(-\frac{\Delta G^*}{kT}\right) \tag{2.7}$$

where D_i is diffusion coefficient for atomic transport across the nucleus matrix interface, and a_0 is the interatomic distance [7]. This expression reduces to previous equation [8], when atomic transport at the interface is assumed to be an activated process:

$$D_i = a_0^2 v_0 \exp\left(-\frac{q}{kT}\right). \tag{2.8}$$

Usually, D_i is taken to be equal to the liquid diffusivity D, which is in turn related to the viscosity by the Stokes-Einstein relation [8]:

$$D_i = D = \frac{kT}{3\pi a_0 \eta}. \tag{2.9}$$

However, equation 2.9 is valid for single component simple liquids and its applicability to more complex systems such as good glass formers is questionable.

It should be noted that the above description of homogenous nucleation apply only to the limiting conditions in which a quasi-steady distrubution of embryos has been established. When the assembly is suddenly changed from a stable to a metastable condition, the nucleation rate is then a function of time until the quasi-steady state is attained. This effect will be unimportant if the transient is of short duration compared with the period of the observation [8, 9]. The transient nucleation behavior of a condensed system is approximated by

$$I_t = I_v \exp\left(-\tau/t\right) \tag{2.10}$$

where I_t is the nucleation frequency at time t and τ is the transient time [8, 9]. τ is given with order-of-magnitude accuracy by the relation:

$$\tau \approx (n^*)^2/vN_s \tag{2.11}$$

where N_s is the number of atoms on the surface of a critical nucleus, $v = D_i/a_0^2$ is the frequency of atomic transport at the nucleus-matrix interface and the n^* is the number of atoms in the critical nuclei given by equation 2.3.

The transient effects have been usually neglected in kinetic analyses of glass formation and same will be followed in this thesis. This can be justified whenever the time required to establish the steady-state conditions is small relative to the total transformation time and to the time scale of the experiment. When transient effects are important, their negligence will usually underestimate

the glass forming ability and thermal stability of glass above the glass transition [10].

2.2 The effect of thermodynamic parameters on the rate of homogenous nucleation

Turnbull analyzed the rate of homogenous nucleation with respect to the thermodynamic parameters such as reduced glass transition $T_{rg} = T_g/T_m$, interfacial tension and entropy of fusion, and presented the overall features of their effect [3]. Further, he predicted the glass forming ability for certain values of thermodynamic parameters. He assumed that formation of one nucleus precludes the glass formation. Thus the total number of appearing nuclei, n,

$$n = V\int_0^t I_v dt \tag{2.12}$$

should be less than one in the course of cooling of liquid. In this equation V is the sample volume, t is the time in which liquid is cooled. This condition of bypassing crystallization is valid for high crystal growth velocity (~1 cm/sec.) and small sizes of sample (~100 microns).

To calculate the homogenous nucleation rate, he assumed that the atomic jump time scales with the viscosity and no difference between the heat capacity of liquid and crystal, i.e., $\Delta C_p = 0$. Putting $\Delta C_p = 0$ into the equation 2.1 gives the famous "Turnbull approximation" for free energy difference between the undercooled liquid and the corresponding crystal:

$$\Delta G_v = \Delta H_m^f(\Delta T_r)\frac{1}{V_m} = \Delta S_m^f(T_m - T)\frac{1}{V_m} \tag{2.13}$$

where ΔS_m^f is the molar entropy of fusion at equilibrium melting point. ΔS_m^f corresponds to the difference between the slopes of free energies of liquid and crystal. Further, he introduced two new parameters α and β which replaces the interfacial tension and entropy of fusion respectively. They are defined as:

$$\alpha \equiv \frac{\left(NV_m^2\right)^{1/3}\sigma}{\Delta H_m^f} \tag{2.14}$$

$$\beta \equiv \frac{\Delta H_m^f}{RT_m} = \frac{\Delta S_m^f}{R} \tag{2.15}$$

where N is Avogadro's number and R is the gas constant. Physically, α is the number of monolayers of crystal which would be melted at T_m by an enthalpy equivalent in magnitude to interfacial energy, and it is the principal resistance of the liquid to the nucleation.

Then, the steady rate of homogenous nucleation becomes

$$I_v = \frac{k_n}{\eta}\exp\left(-\frac{16\pi}{3}\frac{\alpha^3\beta}{\Delta T_r^2 T_r}\right) \tag{2.16}$$

where N is the Avogadro's number, and k_n is a constant to be determined. k_n is taken from Turnbull and Fischer's kinetic analysis [5], which is set approximately to 10^{32} dyne. cm. (10^{23} N m).

To calculate the steady rate of nucleation as a function of $\alpha\beta^{1/3}$, viscosity was set to a constant value of 10^{-2} poise, a typical value for liquid metals. This will give an upper bound for the nucleation rate as viscosity increases with undercooling. Accordingly the computed values of $log\ I_v$ as a function of reduced temperature is shown in figure 2.3. The corresponding values of $\alpha\beta^{1/3}$ are also indicated.

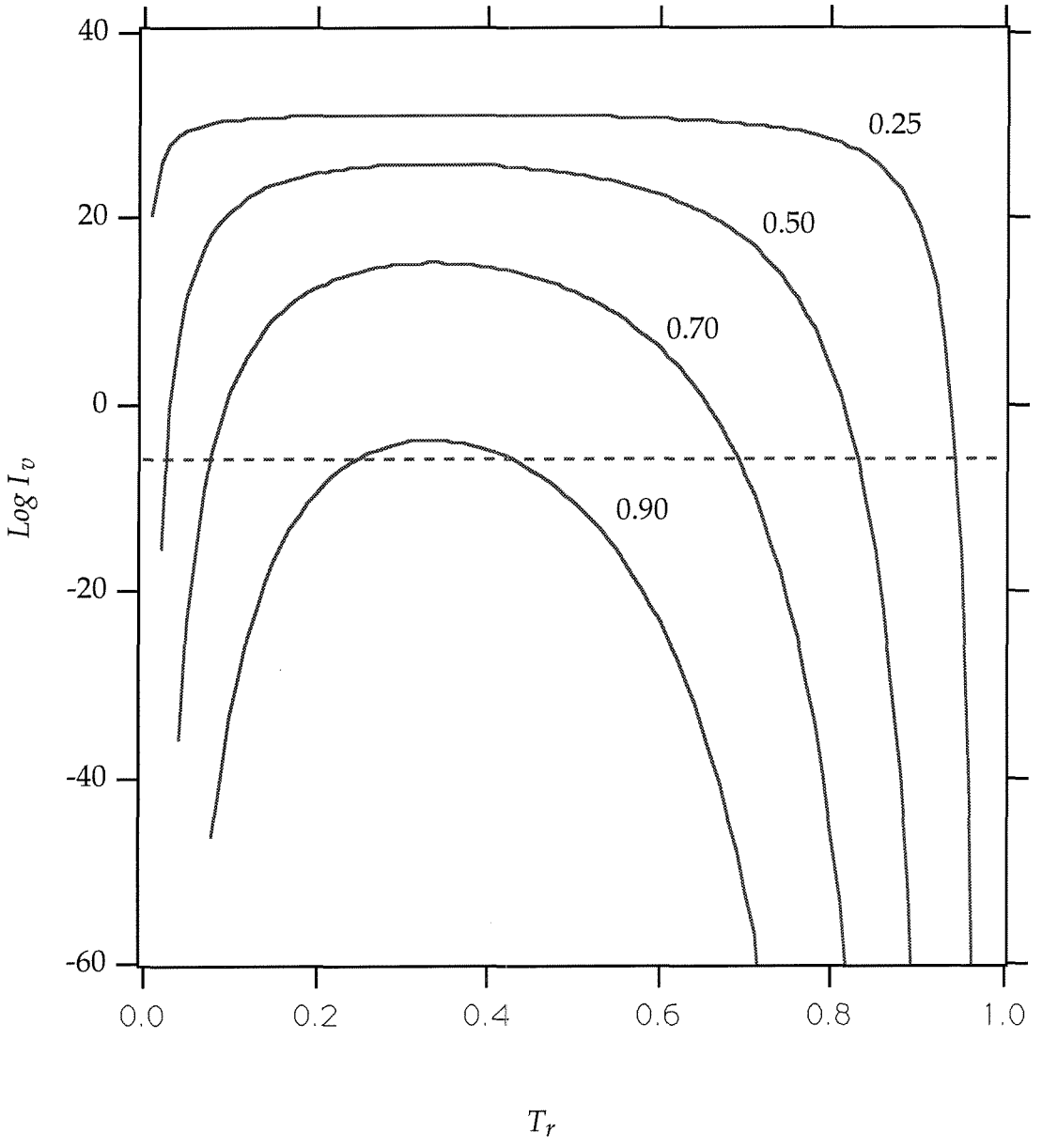

Figure 2.3: Variation of the logarithm of the frequency (in $cm^{-3}s^{-1}$) of homogenous nucleation of crystals in undercooled liquid with reduced temperature for various assignments of $\alpha\beta^{1/3}$ calculated from equation 2.16. Viscosity was set to a constant value of 10^{-2} poise. Reproduced from ref. 3.

As seen from figure 2.3, the homogenous nucleation rate has a broad peak around two thirds of reduced temperature independent of the values of $\alpha\beta^{1/3}$. The value of the maximum nucleation rate depends strongly on the value of $\alpha\beta^{1/3}$, becoming larger at small values. Typically, a nucleation event cannot be detected on the laboratory time scale when its rate is below 10^{-6} nuclei/ cm^3 s. When $\alpha\beta^{1/3} = 0.9$, the liquid, unless seeded, will freeze to glass since the rate of homogenous nucleation is extremely small. Metals have been found to have typical values of $\alpha = 0.5$ and $\beta = 1.0$ [11], so their nucleation rates will be around 10^{25} $cm^{-3}s^{-1}$ at the maximum. The rapid cooling techniques would not be sufficient to quench any metallic liquid into a glass unless T_g were much greater than 0 K.

The undercooled liquid has another means to resist nucleation far below melting point. This is due to the drastic decrease of atomic mobility which is related to viscosity. As undercooled liquid freezes configurationally during the glass transition, no nucleation is expected below the glass transition temperature. Further, the nucleation frequency should drastically decrease around the glass transition in accordance with the atomic mobility. Thus the relative position of melting point and glass transition temperature should be very important in nucleation kinetics.

To express the temperature dependence of the viscosity, Turnbull used a Fulcher type equation [12], which reasonably describes the viscosities of glass forming liquids in the range of 10^{-2} -10^{7} poise. The viscosity η was equated to:

$$\eta = 10^{-3.3} \exp\left[\frac{3.34}{\left(T_r - T_{rg}\right)}\right] \text{ poise.} \qquad (2.17)$$

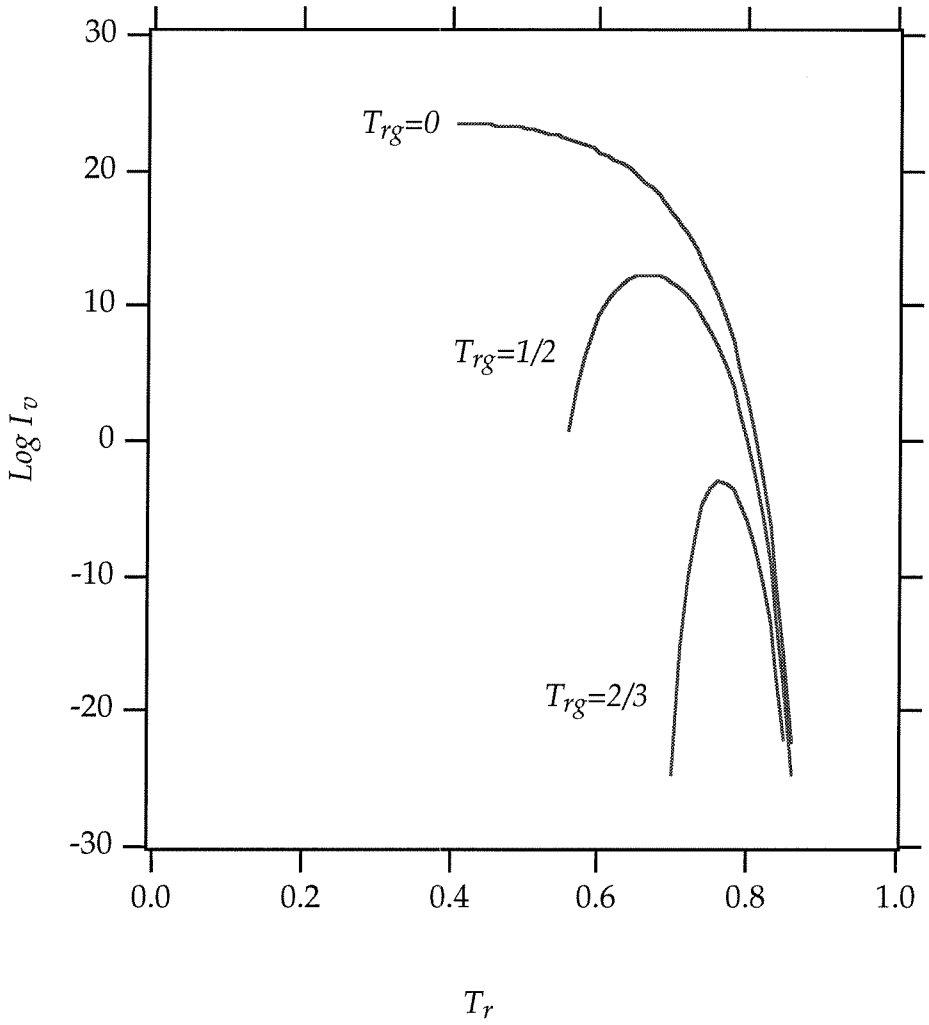

Figure 2.4: Variation of the logarithm of the frequency (in $cm^{-3}s^{-1}$) of homogenous nucleation of crystals in undercooled liquid with reduced temperature calculated from equation 2.16. $\alpha\beta^{1/3}$ was set equal to *1/2* and viscosity was calculated from equation 2.17 with indicated assignments of T_{rg}. Reproduced from ref. 3.

Notice that the Fulcher equation fails at temperatures very close to T_{rg}, the reduced glass transition temperature.

The effect of different values of T_{rg} on the rate of homogenous nucleation is calculated from equation 2.16, with $\alpha\beta^{1/3} = 0.5$ and using equation 2.17 for the viscosity. The computed I_v -T_{rg} relation with indicated values of T_{rg} is shown in figure 2.4. The peak of the nucleation frequency is lowered, sharpened and shifted to higher T_r at high values of T_{rg}. Particularly, liquids with $T_{rg} = 2/3$ can crystallize only within a narrow temperature range and very slowly provided heterogeneous nucleation is prevented. These liquids have the best potential to form bulk glasses easily. Taking an average value of $I_v = 10^{-3}$ $cm^{-3}s^{-1}$, a sample size of 1 cm, and a temperature range of 100 K to cool, equation 2.12 will predict a low critical cooling rate of 0.1 K/s for glass formation when $T_{rg} = 2/3$ in the absence of heterogeneous nucleation. Most of the early-known metallic glass formers have T_{rg} ~0.5 [13] and can only form glasses in small volume and high cooling rates. Taking an average value of $I_v = 10^{12}$ $cm^{-3}s^{-1}$, and a temperature range of 100 K to cool, the equation 2.12 will predict a critical cooling rate of 10^6 K/s for a sample size of 20 microns for metallic glass formation. This is in broad agreement with experimental observations.

2.3 Davies - Uhlmann kinetic analysis

Uhlmann was first[1] to introduce formal transformation theory into the kinetic treatment of glass formation [14]. He was concerned with the magnitude of cooling rate required to avoid a certain amount of crystallization in the course of cooling of liquid. The maximum amount of crystalline fraction for glass formation was set to the 10^{-6} with the justification that this is the limit of the routinely used analytical techniques such as X-ray diffraction and TEM. Later we shall see that this value can be set somewhat arbitrarily provided it is small, as the final results depend on this value very weakly. Using the accepted theories of homogenous nucleation and crystal growth, he constructed the TTT (Time-Temperature-Transformations) diagrams for a certain fraction of crystal formation from the liquid and estimated the critical cooling rates for classical glass forming systems. This was an improvement to Turnbull's criteria of glass formation in which formation of one nucleus precludes glass formation [3].

Then, Davies applied this formalism to the glass formation of metallic systems and successfully estimated the critical cooling rates [15-17]. Here, I will present this formalism as applied to metallic systems by Davies [18].

The Johnson-Mehl-Avrami isothermal transformation kinetics gives the volume fraction of transformed material, X, as:

$$X = 1 - \exp\left[\left(\pi/3\right) I_v \, u_c^3 \, t^4\right] \tag{2.18}$$

---

[1] D. Turnbull and M. H. Cohen noted the formal transformation theory for glass formation in "Modern Aspects of Vitreous State, J. D. Mackenzie (ed.) Butterwoths, London 1960." As they found the calculations complicated, they haven't used the actual formulation. Instead, they used limiting cases for glass formation and took an average value of 10^{-12} nuclei/sec. cm^3 for $I_v \, u_c^3$ to calculate the critical cooling rate for glass formation.

where I_v is the nucleation frequency and u_c is the crystal growth rate and t is time taken to transform X [19]. In the early stages of transformations, or for small values of X, the value of X can be approximated as:

$$X \cong \left(\frac{\pi}{3}\right) I_v u_c^3 t^4. \tag{2.19}$$

It was assumed that only the homogenous nucleation is occurring and the same expression as equation 2.7 has been used for the rate of homogenous nucleation. Using the "Hoffman approximation" [20] for ΔG_v, the volume free energy difference between the liquid and crystal,

$$\Delta G_v = T_r \Delta T_r \, \Delta H_v^f \,, \tag{2.20}$$

and following Turnbull [3, 11]

$$\alpha \equiv \frac{\left(N V_m^2\right)^{1/3} \sigma}{\Delta H_m^f}, \tag{2.21}$$

the activation energy for homogenous nucleation is given by the expression:

$$\Delta G^* = \left(\frac{16\pi}{3}\right)\left(\frac{\alpha^3 \Delta H_m^f}{N \Delta T_r^2 T_r^2}\right). \tag{2.22}$$

$\Delta G^*/kT$ has been expressed more appropriately as:

$$\frac{\Delta G^*}{kT} = \frac{A}{\Delta T_r^2 T_r^3} \tag{2.23}$$

where the constant A is given by $A = 16\Pi \alpha^3 \Delta S_m^f / 3R$. The constant A can be estimated by taking $\Delta G^*/kT \sim 50$ when $\Delta T_r = 0.20$ [7], which is equivalent to the $\Delta G^*/kT \sim 60$ when $\Delta T_r = 0.18$ [19]. Then the rate of homogeneous nucleation becomes:

$$I_v = \frac{N_v D_i}{a_o^2} \exp\left(-\frac{1.07}{\Delta T_r^2 T_r^3}\right). \tag{2.24}$$

Following the previous derivation, the crystal growth rate is given by [22]

$$u_c = \frac{f D_g}{a_o}\left[1 - \exp\left(-\frac{\Delta G_m}{RT}\right)\right] \tag{2.25}$$

where D_g is a diffusion coefficient for atomic motion required for crystal growth , ΔG_m is the molar free energy change, and f is the fraction of sites at the interface where growth occurs. For rough interfaces, as in the case for closely packed crystal structures having low entropy of fusion,

$$\Delta S_m^f = \frac{\Delta H_m^f}{T_m} < 2R, \tag{2.26}$$

all sites are considered to be equally available for growth and $f = 1$. For alloys having high entropy of fusion, $f = 0.2\ \Delta T_r$ was chosen. Using the Turnbull approximation (equation 2.13), the crystal growth rate becomes [8]:

$$u_c = \frac{f D_g}{a_o}\left[1 - \exp\left(-\frac{\Delta T_r\, \Delta H_m^f}{RT}\right)\right] \tag{2.27}$$

It is interesting to note an inconsistency. The Turnbull approximation has been used for free energy difference in the expression of crystal growth rate, whereas other approximations, such as the Hoffman approximation, have been used for the free energy difference in the expression of homogenous nucleation rate.

For simplicity, it was assumed that $D_i = D_g = D$ where D is the bulk diffusion coefficient and it was related to viscosity by Stokes-Einstein relation:

$$D_i = D_g = D = \frac{kT}{3\pi a_o \eta}. \tag{2.28}$$

After combining and arranging equations 2.28, 2.27, 2.24 and 2.19, the time t to form a small fraction of crystal, X, at temperature T is given by

$$t \cong \frac{9.3\eta}{kT}\left[\frac{a_o^9 X}{f^3 N_v}\left\{\exp\left(-\frac{1.07}{\Delta T_r^2 T_r^3}\right)\right\}\Big/\left\{1-\exp\left(-\frac{\Delta T_r\,\Delta H_m^f}{RT}\right)\right\}^3\right]^{1/4} . \quad (2.29)$$

Notice that t depends on the $1/4^{th}$ power of X which gives a relatively weak dependence of t on X. In calculation of TTT diagrams, interpolated viscosities based on the empirical Fulcher relation

$$\eta = A\exp\left[\frac{B}{(T-T_\eta)}\right] \quad (2.30)$$

have been used [13]. The constants A, B and T_η were derived by fitting the expression to respective estimated η values at the experimentally measured liquidus temperature T_l, and assuming $\eta = 10^{13}$ poise at experimentally measured T_g [13]. Where T_g has not been thermally manifested, the crystallization temperature was assumed as the lower bound for the value of T_g. The viscosity at the liquidus point is estimated from the extrapolation of the Arrhenius relation for liquid Ni above its melting point T_m [17].

CCT (Continuous - Cooling - Transformations) diagrams have been constructed from the TTT diagrams by the method of Grange-Keifer [23]. Thus the critical cooling rate $\dot{T}_c$ was calculated by the cooling curve that just avoids interception of the nose of the CCT curve, i.e., $\dot{T}_c \approx (T_l - T_n)/t_n$ where T_n and t_n are the temperature and the time at the nose respectively. Accordingly, the estimated critical cooling rates of several metallic glass forming alloys are shown against the corresponding T_{rg} in figure 2.5, which is reproduced from ref. 13. The predicted cooling rates agree with experimental observations within uncertainty

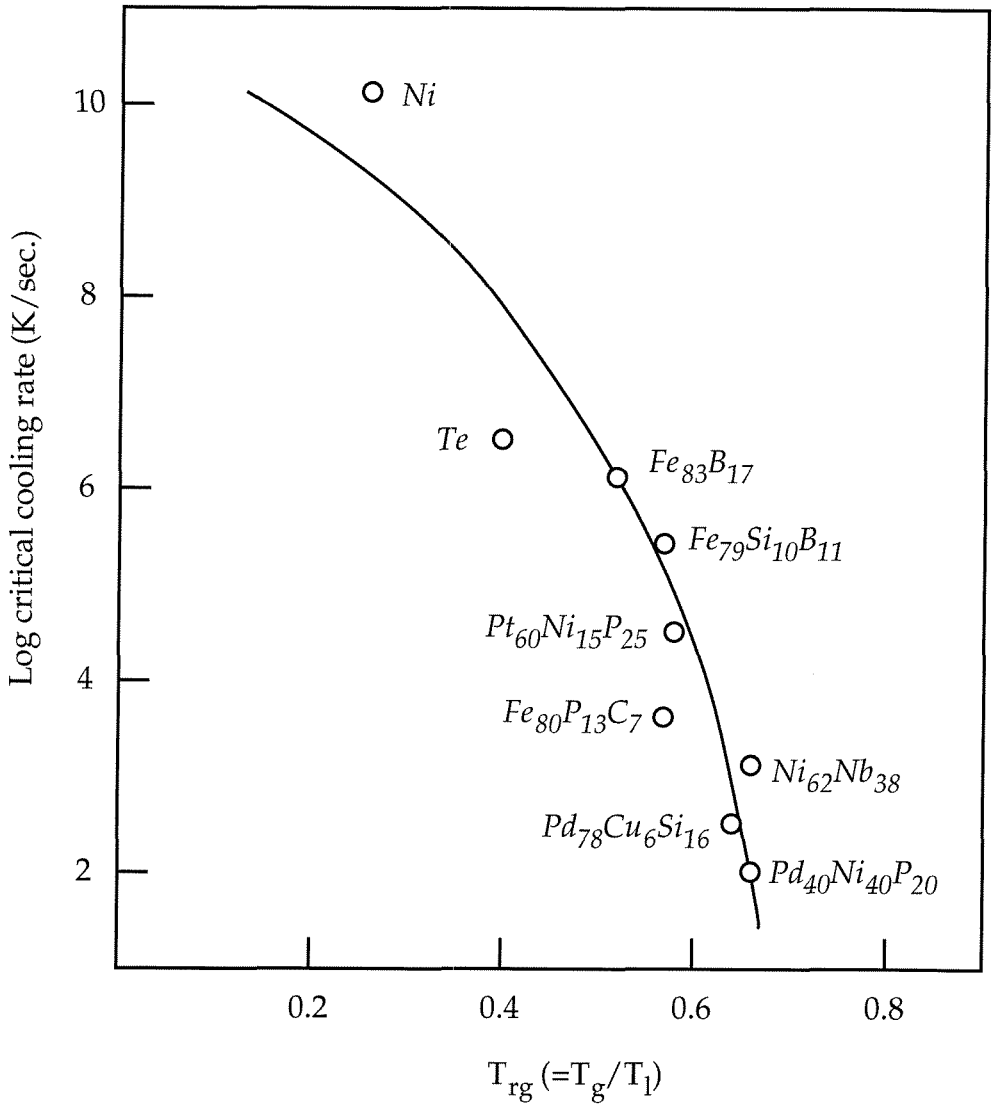

Figure 2.5: Calculated critical cooling rates for glass formation (based on CCT curves for the formation of a fraction crystal of 10^{-6}) plotted against reduced glass transition temperature T_{rg} for a representative range of elements and alloys. Reproduced from ref. 13.

of calculations and errors in estimating cooling rates in rapid solidification techniques. Obviously, T_{rg} appears as a crucial parameter in glass formation. The higher T_{rg} corresponds to the lower critical cooling rates. Notice that the critical cooling rate decreases much more rapidly as T_{rg} approaches the value of 0.67. However, the case of $Pd_{40}Ni_{40}P_{20}$ needs further attention. Initially, the observed critical cooling rate of $Pd_{40}Ni_{40}P_{20}$ was reported to be ~10^3 K/sec. [24]. Later, Turnbull and his colleagues successfully undercooled a cm thick $Pd_{40}Ni_{40}P_{20}$ alloy into glass by employing fluxing to eliminate surface heterogeneous nucleation at cooling rates of 1-2 K/sec [25]. According to the Davies-Uhlmann analyses, the critical cooling rate of $Pd_{40}Ni_{40}P_{20}$ was predicted ~ 100 K/sec., thus overestimating it by two orders of magnitude. In this case, the observed cooling rate is determined much more accurately than with other techniques such as splat quenching and melt spinning [25], and the discrepancy can be explained only in the uncertainties in the kinetic analyses. These uncertainties and possible improvements will be discussed in the next section.

Later, several refinements were added to this model by several researchers. Saunders and Miodownik used the thermodynamic parameters obtained from phase diagram calculations to derive the values of energy barrier for nucleation, free energy driving forces, and melting points, and used them in calculation of TTT diagrams [27]. This approach makes it possible to calculate the critical cooling rates for metastable crystalline phases. Other approximations for ΔG_v have been proposed as an improvement to the Hoffman approximation [28, 29]. However, none of them give satisfactory results compared to the extrapolation of experimental data for ΔG_v [10].

Ramachandrarao et al. suggested a Doolittle type expression [30] to represent the viscosity of undercooled liquid [30]:

$$\eta = A\exp\left[B\Big/\exp\left[-\frac{C}{RT}\right]\right]. \tag{2.31}$$

They argued that this expression gives better approximation to experimental values of viscosity over the full range of T_m to T_g for $Au_{77}Ge_{13.6}Si_{9.4}$ [32].

Tanner and Ray used Davies-Uhlmann analysis to account for the difference between the critical cooling rates of $Zr_{65}Be_{35}$ and $Ti_{63}Be_{37}$ [33]. Their calculations did not give satisfactory results and they proposed that the energy barrier for homogenous nucleation should be modified. They were able to account for the difference in glass forming ability by taking $\Delta G^*/kT \sim 55$ for $Zr_{65}Be_{35}$ and $\Delta G^*/kT \sim 40$ for $Ti_{63}Be_{37}$ at $\Delta T_r = 0.20$.

2.4 Limitations of Davies - Uhlmann kinetic analysis

The main limitations of Davies-Uhlmann kinetic analyses stem from the limited theoretical understanding of nucleation and crystal growth and inadequate experimental data for parameters used in these equations.

First of all, the expressions used for the homogenous nucleation rate and crystal growth velocities are valid only for single component or congruently melting multi-components systems, which is usually not the case for metallic glass forming systems, i.e., this model is true for partitionless crystallization [8,14]. In principle this deficiency can be eliminated by using models for nucleation and crystal growth of multi component systems which are not congruently melting. For example, Thompson and Spaepen developed a model for homogenous crystal nucleation in binary metallic melts [34]. In the light of apparent success of

their model, Davies argued that [18] the main competing crystalline phase with glass formation is a metastable crystalline phase having the same composition as the liquid. This is experimentally evidenced in some cases [33], but cannot be generalized. Assuming there is a competing metastable crystalline phase which crystallizes polymorphically, then the parameters should be adjusted accordingly. The most important of these is the melting point, and thus the critical T_{rg}, as the metastable phase will have a lower melting point than the equilibrium crystalline phases. Moreover, the free energy difference should be modified, as it will be smaller between the liquid and metastable crystalline phase. However, these corrections are difficult to install, because of the experimental difficulties in obtaining the thermodynamic parameters of metastable crystalline phases.

Further, the existing theories of nucleation and crystal growth rates are solely based on experiments at small undercooling ($\Delta T_r \leq 0.2$) of liquid metals. Their applicability to the high undercooling regime is also questionable. Assuming these theories are valid for the whole range of T_m to T_g, we need the properties of the highly undercooled liquid ($\Delta T_r > 0.2$), such as viscosity, diffusion constants and heat capacity. These are important parameters in determining the nucleation rate and crystal growth rate. Unfortunately, we lack a good knowledge of these parameters in the highly undercooled regime, which is the most crucial temperature region between T_m and T_g for glass formation. Moreover, we have very little data on viscosity of multi component metallic alloys at the melting point. This further lack of knowledge causes pronounced uncertainties in the calculations, since it may affect critical cooling rates significantly [18].

Recently it has been shown that heterogeneous nucleation can be an important factor for glass formation even at very high cooling rates [35]. The critical thickness of glassy $Ni_{75}B_{17}Si_8$ alloy was increased by four times when further purification of liquid alloy was employed eliminating heterogeneous nucleation. If we assume that all of the observed metallic glass formation is limited by heterogeneous nucleation rather than homogenous nucleation as suggested by many experimental observations, then the rate of homogenous nucleation should be significantly overestimated in the Davies-Uhlmann kinetic analysis. Alternatively, the resistance of a liquid to homogenous nucleation is highly underestimated. This was also proposed by Perepezko, based on the undercooling studies of fine droplets of liquid metals [36,37]. Similar observations was also reported by others [38]. Then, the interfacial energy constant α should have a larger value than the ~0.5 suggested by Turnbull [9]. This may explain the case of $Pd_{40}Ni_{40}P_{20}$, where the critical cooling rate was earlier predicted to be two orders of magnitude less. As we shall see in chapter 4, the heterogeneous nucleation rate can be expressed in the same form of equation 2.7 with an extra parameter appearing in the energy barrier for nucleation. Taking this extra parameter and interfacial energy constant α together as an effective interfacial energy constant α_e, the formalism of Davies-Uhlmann kinetic analyses can be preserved to use in cases where heterogeneous nucleation is the rate limiting factor. From the good agreement between the calculations of Davies (and others) and experimental observations of metallic glass formation , it seems that $\alpha_e \sim 0.5$ is a good choice for metallic glass formation at high cooling rates.

Finally, the assumption of $D_i = D_g = D$ requires some caution. It was already noted by Davies that [16] these diffusion constants can be quite different. For example, D_g was found to be substantially greater than the corresponding D in

the Fe-Ni alloys [39]. For the time being, the lack of experimental data and theoretical understanding of diffusion phenomena in highly undercooled liquids leaves us no choice. Recently, the group of Inoue and Masumoto reported a novel Al-base alloy, which formed nanometer sized crystallites embedded in an amorphous matrix upon rapid solidification [40]. Though no valid explanation for the formation of this unusual microstructure has been given, a possible mechanism is that the diffusion constants involved in nucleation and crystal growth may differ by several orders of magnitude.

2.5 T_0 criterion of glass formation

The T_0 temperature is the temperature at which the free energies of the liquid and crystalline phases, G_x and G_l, are equal. $T_0\,(c)$ curve is the locus of T_0 temperatures as a function of composition c [41]. The $T_0(c)$ curve can be constructed if G_x and G_l are known as a function of temperature and composition as shown in figure 2.6. Since the $T_0(c)$ curve must lie between the solidus and liquidus curves (because of the common tangent construction, see fig. 2.6), the $T_0(c)$ curve in a system can be roughly inferred from its equilibrium phase diagram. For the purposes of glass formation, the position of $T_0(c)$ curve can be roughly approximated as a curve lying halfway between the solidus and liquidus curves.

We can infer from the definition of T_0 temperature that it becomes thermodynamically possible to solidify a liquid completely into a single crystalline phase below the $T_0(c)$ curve (figure 2.7). Alternatively, the $T_0(c)$ curve represents the thermodynamic composition limit for a composition invariant crystallization (partitionless crystallization). In the early seventies, the concept of T_0 temperatures was proposed for the interpretation of extended solid solubility

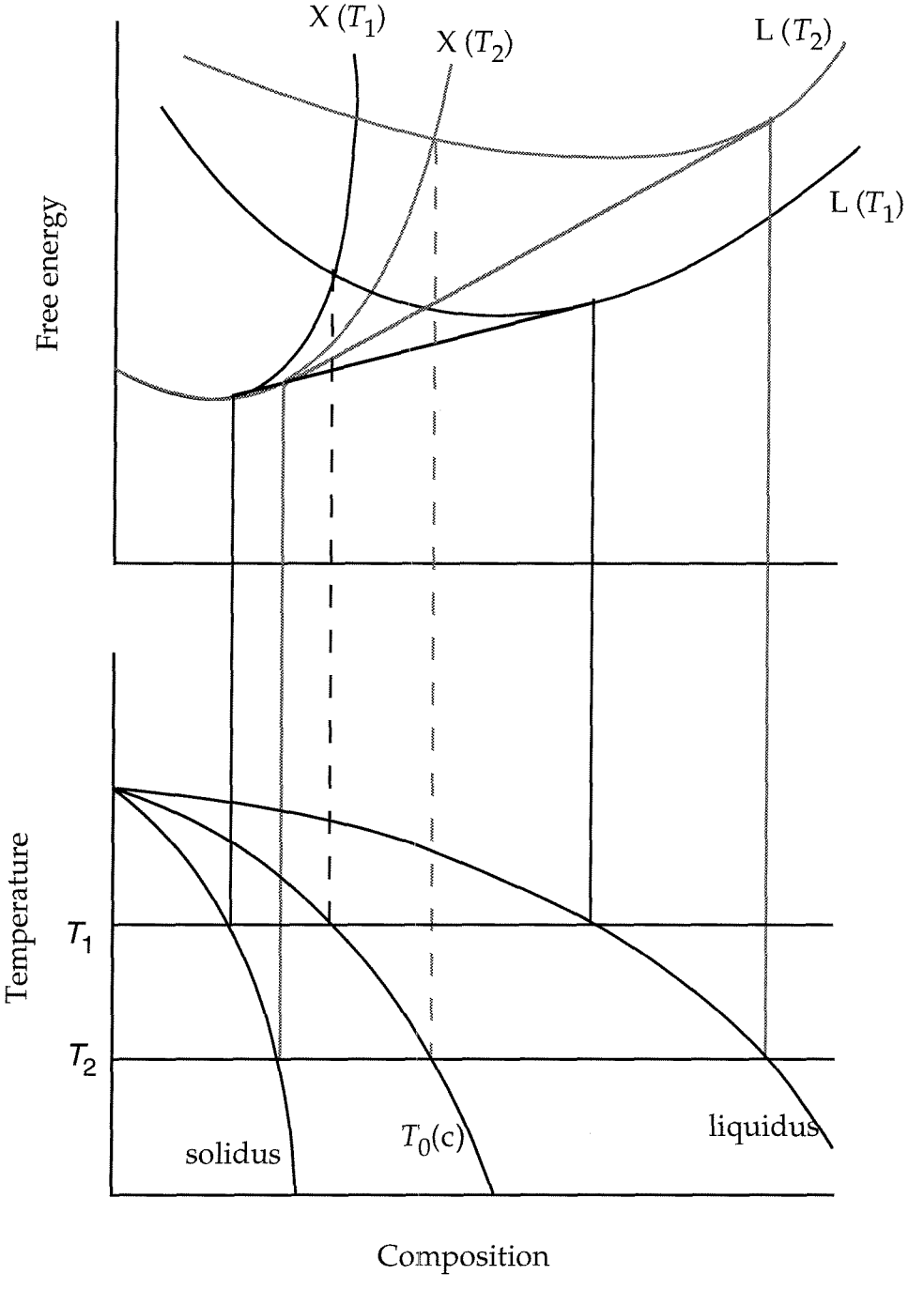

Figure 2.6: Construction of the $T_0(c)$ curve from the free energy curves of the crystalline and liquid phase.

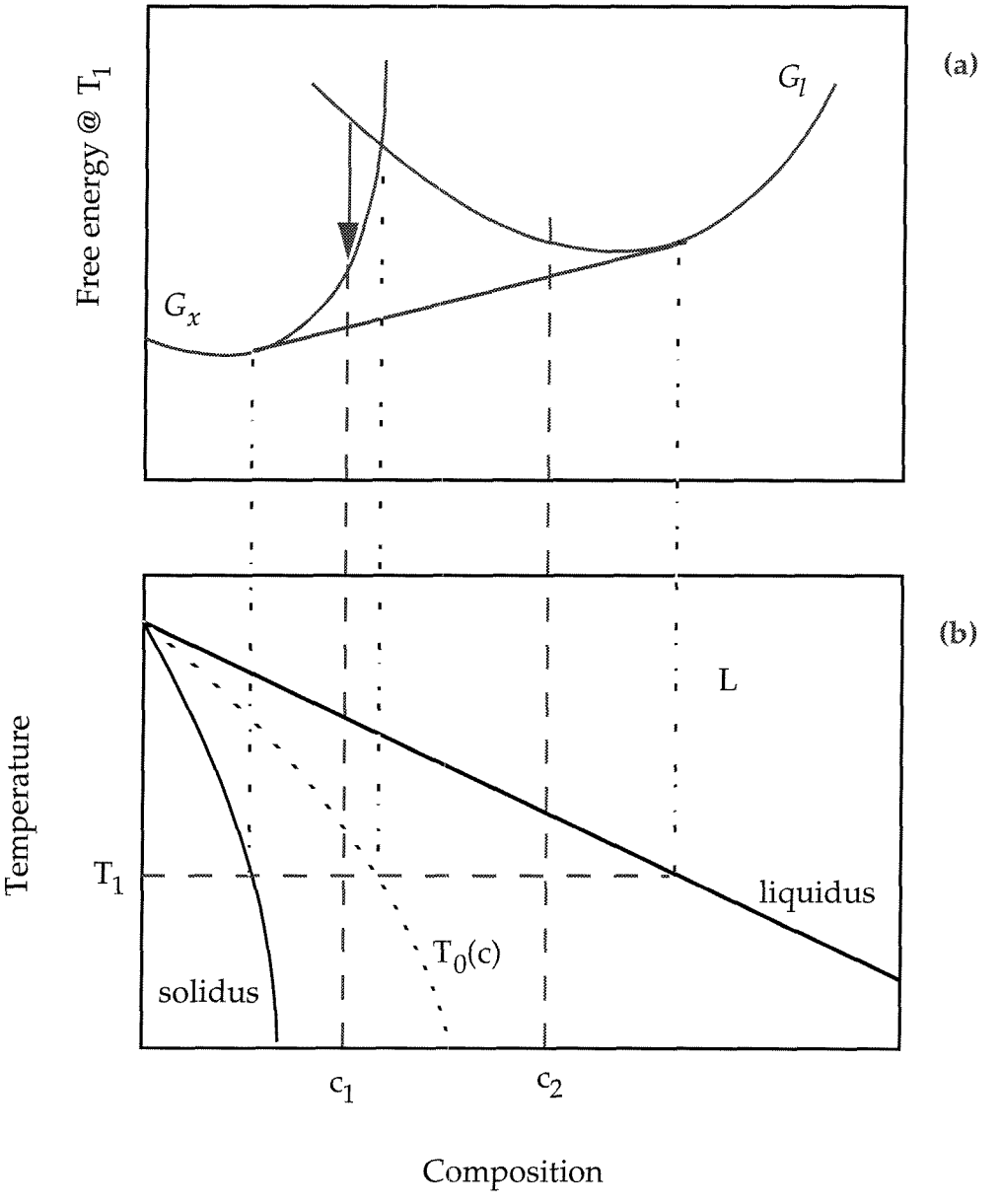

Figure 2.7: The possibility of partitionless solidification of an undercooled liquid at two different compositions. Partitionless solidification is possible at c_1 (below the $T_0(c)$ curve) and impossible at c_2 (beyond the $T_0(c)$ curve).

observed during rapid solidification of metallic melts [42]. Later, Massalski used the $T_0(c)$ curve to give a thermodynamic account of metallic glass formation near deep eutectics. He proposed that glass formation occurs at compositions beyond the intersection of the $T_0(c)$ curve with the $T_g(c)$ curve (the composition dependence of the glass transition temperature). This is known as "T_0 criterion of glass formation" and is presented in the following paragraph.

The possibility of a composition-invariant single phase crystallization, in the form of a metastable phase, constitutes the main competition to the glass formation in the eutectic region [42]. If crystallization of a single phase is not possible, a eutectic must form (growth may start with dendrite formation, but it should end up with eutectic solidification). Since eutectic growth requires solute partitioning and simultaneous growth of several phases, the growth velocity of a composition invariant single crystalline phase should be much faster than for eutectic crystallization. Thus, factors which facilitate single-phase composition invariant crystallization into an easy forming crystal structure should sharply reduce the glass forming ability. According to the T_0 criterion, the possibility of a single-phase metastable crystallization should be excluded for glass formation; i.e., no driving force should exist for partitionless solidification. This is determined by the relative position of $T_0(c)$ curve and $T_g(c)$ curve of the system in question, i.e., by the thermodynamics.

Since the glass transition is taken as the configurational freezing of liquid, no nucleation and growth of crystalline phases is allowed below the glass transition temperature. The thermodynamic possibility of partionless crystallization precludes glass formation according to the T_0 criterion. Thus, glass formation is possible only if both $T_0(c)$ curves of terminal solid solutions (or compounds)

plunge deep enough to cross the $T_g(c)$ curve and the borders of possible glass forming compositions are given by the intersection points of $T_0(c)$ and $T_g(c)$ curves as shown for the third type of binary system where its glass forming composition range is given by the shaded area in figure 2.8c.

Figure 2.8 shows three possible $T_0(c)$ curves for a simple binary eutectic phase diagram. These are:

(i) A continuous $T_0(c)$ curve above the $T_g(c)$ curve. This is true for shallow eutectics like Ag-Cu.

(ii) $T_0(c)$ curves of α and β phases crossing above the $T_g(c)$ curve.

(iii) $T_0(c)$ curves of α and β phases not crossing above the $T_g(c)$ curve. This is the case for deep eutectics with plunging $T_0(c)$ curves such as Au-Si. Only this type of phase diagram gives a good glass former. The possible glass forming range is shown by the shaded area.

Since diving $T_0(c)$ curves are invariably associated with deep eutectics, the T_0 criterion gives a good account of metallic glass formation since it has been primarily observed around deep eutectics. In principle, T_0 criterion can be extended to ternary and higher systems, where the $T_0(c)$ and $T_g(c)$ curves are replaced by the $T_0(c_1, c_2)$ and $T_g(c_1, c_2)$ surfaces.

Some apparent violations of the T_0 criterion has been observed experimentally [43, 44]. It was found that the T_0 criterion significantly underestimates the glass forming range, especially at very high cooling rates of 10^{10} K/s. These exposed two difficulties encountered in applying the T_0 criterion quantitatively. Schwarz et al. gave a good description of these difficulties [45,46]. First of all, in the

calculation of $T_0(c)$ curves, a good knowledge of the free energies of the phases as a function of composition and temperature is needed. However, our knowledge of these thermodynamic properties, especially the thermodynamic properties of the highly undercooled liquid, is very poor. Though several free energy models provide satisfactory fits to the experimentally determined solidus and liquidus curves of a binary system, these models give severely conflicting T_0 temperatures in the high undercooling regime which is experimentally not accessible.

The second difficulty arises from the complete neglect of kinetic constraints in partionless crystallization, which then underestimates the glass forming ability as compared with the experiments. As we have seen in the earlier sections of this chapter, a significant undercooling ($\Delta T_r > 0.2$) is required for the onset of copious homogenous nucleation. In fact, the Davies -Uhlmann kinetic analysis is exactly valid for partionless crystallization. When other kinetic constraints are taken into account, a better description of the glass forming range can be obtained as shown by Nash and Schwarz [46].

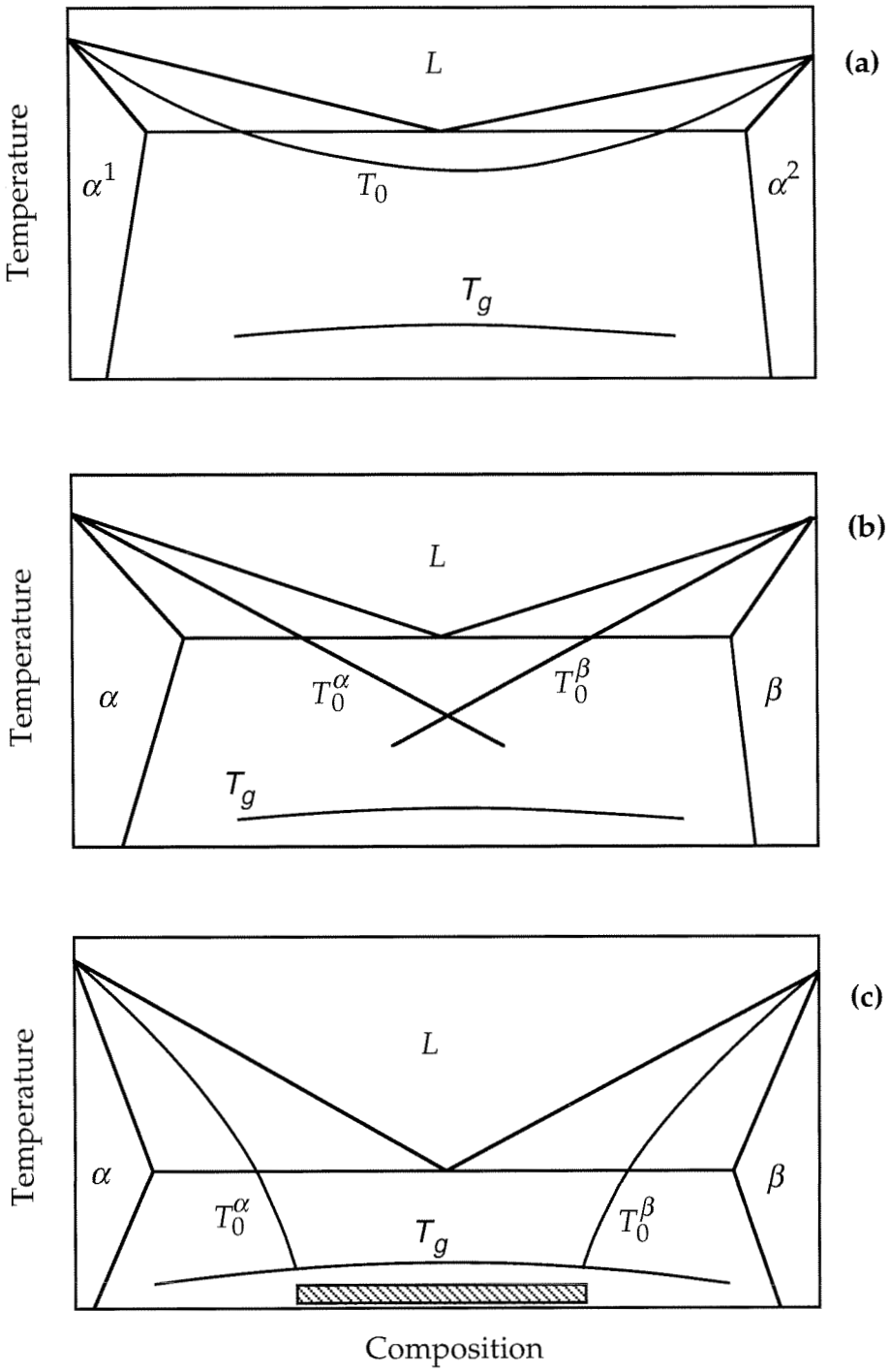

Figure 2.8: Three possible arraignments of T_0 curves for simple eutectic systems.

References

[1] M. H. Cohen and D. Turnbull, J. Chem. Phys., **31**, 1164 (1959).

[2] W. J. Klement, R. H. Willens, and P. Duwez, Nature, **187**, 869 (1960).

[3] D. Turnbull, Contemp. Phys., **10**, 473 (1969).

[4] W. Kurz and D. J. Fisher, *Fundamentals of Solidification* (Trans Tech Publications, Switzerland, 1986), Chap. 2.

[5] R. Becker, Ann. Physik, **32**, 128 (1938).

[6] D. Turnbull and J. C. Fischer, J. Chem. Phys., **17**, 71 (1949).

[7] D. R. Uhlmann, J. F. Hays, and D. Turnbull, Phys. Chem. Glasses, **7**, 159 (1966).

[8] D. R. Uhlmann, in *Materials Science Research*, Vol. 4 (Plenum, New York, 1969).

[9] J. W. Christian, *The Theory Of Phase Transformations In Metals And Alloy*, 2nd ed. (Oxford, Pergamon Press., 1975), p. 442.

[10] H. J. Fecht, J. H. Perepezko, M. C. Lee, and W. L. Johnson, J. Appl. Phys., **68**, 4494 (1990).

[11] D. Turnbull, J. Appl. Phys., **21**, 1022 (1950).

[12] G. S. Fulcher, J. Am. Ceram. Soc., **6**, 339 (1925).

[13] H. A. Davies, in *Rapidly Quenched Metals III*, B. Cantor (ed.) (Metals Soc., London, 1978), Vol. 1, p. 1.

[14] D. R. Uhlmann, J. Non-Cryst. Solids, **7**, 337 (1972).

[15] H. A. Davies, J. Aucote, and J. B. Hull, Scripta., Metall, **8**, 1179 (1974).

[16] H. A. Davies, J. Non-Cryst. Solids, **17**, 266 (1975).

[17] H. A. Davies and B. G. Lewis, Scripta. Metall., **9**, 1107 (1975).

[18] H. A. Davies, Phys. Chem. Glasses, **17**, 159 (1976).

[19] J. W. Christian, *The Theory Of Phase Transformations In Metals And Alloy* (Oxford, Pergamon Press., 1965), p. 377.

[20] J. D. Hoffman, J. Chem. Phys., **29**, 1192 (1958).

[21] E. R. Buckle, Nature, **186**, 875 (1960).

[22] D. Turnbull, J. Chem. Phys., **66**, 609 (1962).

[23] R. A. Grange and J. M. Keifer, Trans. Am. Soc. Metals, **29**, 85 (1941).

[24] H. S. Chen, Acta. Met., **22**, 1505 (1974).

[25] H. W. Kui, A. L. Greer, and D. Turnbull, Appl. Phys. Lett., **45**, 615 (1984).

[26] C. F. Lau and H. W. Kui, J. Appl. Phys., **73**, 2599 (1993).

[27] N. Saunders and A. P. Miodownik, J. Mater. Res., **1**, 38 (1986).

[28] K. S. Dubey and P. Ramachandrarao, Acta. Metall., **32**, 91 (1984).

[29] C. V. Thompson and F. Spaepen, Acta. Metall., **27**, 1855 (1979).

[30] A. K. Doolittle, J. Appl. Phys., **22**, 471 (1951).

[31] P. Ramachandrarao, B. Cantor, and R. W. Cahn, J. Non-Cryst. Solids, **24**, 109 (1977).

[32] H. S. Chen and D. Turnbull, J. Chem. Phys., **48**, 2560 (1968).

[33] L. E. Tanner and R. Ray, Acta. Metall., **27**, 1727 (1979).

[34] C. V. Thompson and F. Spaepen, Acta. Metall., **31**, 2021 (1983).

[35] L. Q. Xing, D. Q. Zhao, X. C. Chen, and X. S. Chen, Mat. Sci. Engg., **A157**, 211 (1992).

[36] J. H. Perepezko, Mat. Sci. Engg., **65**, 125 (1984).

[37] J. H. Perepezko and D. H. Rasmussen, Met. Trans, **9A**, 1490 (1978).

[38] D. W. Gomersall, S. Y. Shiraishi, and R. G. Ward, J. Aust. Inst. Met., **10**, 220 (1965).

[39] D. Turnbull, Trans. Metall. Soc. AIME, **221**, 422 (1961).

[40] Y. H. Kim, A. Inoue, and T. Masumoto, Mater. Trans., JIM, **32**, 599 (1991).

[41] T. B. Massalski, in *The Proceedings of the 4th International Conference on Rapidly Quenched Metals*, T. Masumoto and K. Suzuki (eds.) (Japan Institute of Metals, Sendai, Japan, 1981), p. 203.

[42] J. C. Baker and J. W. Cahn, in *Thermodynamics of Solidification* (ASM, Metals Park, Ohio, 1971), p. 23.

[43] C. J. Lin, F. Spaepen, and D. Turnbull, J. Non-Cryst. Solids, **61/62**, 767 (1984).

[44] C. J. Lin and F. Spaepen, Appl. Phys. Lett., **41**, 716 (1982).

[45] R. B. Schwarz, P. Nash, and D. Turnbull, J. Mater. Res., **2**, 456 (1987).

[46] P. Nash and R. B. Schwarz, Acta. Metall., **36**, 3047 (1988).

Chapter 3

$Zr_{41.2}Ti_{13.8}Cu_{12.5}Ni_{10.0}Be_{22.5}$: An example of bulk metallic glass forming alloys

We have seen in chapter 2 that the kinetics of crystallization strongly depend on the properties of the highly undercooled liquid. The knowledge of viscosity, diffusion constants and heat capacity of the highly undercooled liquid is highly desirable for understanding the kinetics of nucleation and crystal growth. However, the high undercooling regime has not been easily accessible to laboratory measurements in metallic systems. This poses severe limitations on the classical theory of nucleation as well as the kinetic treatment of glass formation. The properties of highly undercooled metallic liquids can play important roles in understanding of the microstructures developed during crystallization and in designing novel materials. Highly processable and bulk forming metallic glasses are useful not only for technological applications but for the advancement of scientific knowledge as well. Obviously, the highly undercooled regime is easier to access in good glass formers since the liquid has higher resistance to the crystallization. Until recently, there were not many good bulk glass forming alloys on which to measure the properties in the highly undercooled regime.

In this chapter, I will present an example of a highly processable metallic glass: $Zr_{41.2}Ti_{13.8}Cu_{12.5}Ni_{10.0}Be_{22.5}$ [1]. This metallic alloy is far superior to its predecessors for its bulk glass forming ability and high thermal stability above the glass transition. The alloy belongs to an exceptionally large family of excellent glass forming metallic system, which was found and developed in the course of this thesis. The bulk glass forming range of this system will be presented in Appendix I. The general characteristics of this alloy will be discussed and its properties which distinguish it from conventional metallic glass formers will be emphasized. First I will introduce the various preparation methods of the glassy alloy. Then a description of the mechanical properties will be given. The measured thermal properties will be presented and a preliminary attempt will be made to construct a TTT (Time - Temperature - Transformations) diagram for this alloy. The TTT diagram will be used to account the observed thermal properties of the glassy alloy. Finally the origins of exceptional glass forming ability will be discussed.

3.1 Preparation

Initial ingots, having the nominal composition $Zr_{41.2}Ti_{13.8}Cu_{12.5}Ni_{10.0}Be_{22.5}$, were prepared by induction melting of the constituent elements in a closed system on a water cooled copper or silver boat under a Ti-gettered argon atmosphere. Raw elements of two different purities were used according to the purpose of work. Raw elements of higher purity have been used for characterization of glassy alloys such as thermal analyses. Their purity, form and suppliers are shown in table 3.1.

Table 3.1: The purity, form and suppliers of raw elements used in characterization of glassy alloy.

Element	Form	Purity	Supplier
Zr	crystal bar turnings	99.5 %	Johnson Matthey
Ti	pellets	99.99 %	Cerac
Cu	rod	99.999 %	Johnson Matthey
Ni	pellets	99.97 %	Cerac
Be	pieces	99.9 %	ESPI

Table 3.2: The purity, form and suppliers of raw elements used in production of bulky glassy alloy.

Element	Form	Purity	Supplier
Zr	lump	99.2 %	Johnson Matthey
Ti	pellets	99.7 %	Johnson Matthey
Cu	rod	99.9 %	Johnson Matthey
Ni	rod	99.5 %	Johnson Matthey
Be	pieces	99.9 %	ESPI

Raw elements of lower grade were used in the preparation of larger pieces to demonstrate the bulk glass forming ability of $Zr_{41.2}Ti_{13.8}Cu_{12.5}Ni_{10.0}Be_{22.5}$ alloy. Their purity, form and suppliers are shown in table 3.2.

Typically, samples of 3-9 grams were used in preparation of preliminary ingots. The nominal compositions have been accepted for the rest of the work, as the total mass loss during alloying was consistently less than 0.01 percent (actually below detectable limits of our electronic balance which is 0.1 mg). The master ingots were found to freeze without any significant crystallization upon completion of alloying irrespective of the purity of the elements used. Only slight traces of crystallinity were observed on the lower surface of the glassy ingots, where casual contact with the copper boat occurs during solidification. Contact with the boat apparently can induce heterogeneous nucleation of crystals with limited growth. The remainder of the ingots were completely amorphous as confirmed by TEM, X-ray and DSC analyses. It is worth noting that the upper part of the ingot exhibits a free frozen glass surface as heat extraction is only in one direction. The glassy surface can be easily distinguished with its very smooth and highly reflective appearance. The largest glassy ingot made weighed 25 grams, where the size limitation stems from the size of the copper boat used and not from the glass forming ability of the alloy. These biggest glassy ingots have a typical thickness of 1.0 cm. Recent experiments by Schwarz have demonstrated that ingots of 200 grams readily freeze to bulk glass when constituent elements are alloyed by plasma melting on an electropolished copper hearth [2]. The ingots were further processed into more useful shapes by metallic mold casting or water quenching of molten alloy sealed in a silica glass tube.

The schematic picture of a metallic mold casting unit has been shown in figure 3.1. The unit consists of a vacuum chamber containing a cold copper block, which is used as a quenching media, a silica glass tube containing the sample, and rf heating coils surrounding the silica tube. The silica tube has a small orificeat the bottom end which is firmly seated into a channel which feeds a hole in the copper block. The top end of the silica tube is connected to a pressure reservoir. Upon melting of the alloy, the valve connecting the pressure reservoir is opened and the flow of inert gas, He or Argon, injects the molten sample into the hole of copper block through the orifice of the silica tube. Typically, a pressure of 10-20 psi has been used for injection of molten sample. The copper block has internal cavities with different shapes and sizes resulting in glassy samples in the form of rods and plates.

Water quenching has been performed after sealing the samples in a silica tube, General Electric 99.9 % fused quartz, under an inert atmosphere. The sealed sample has been melted by rf heating and plunged into water and stirred until solidification is complete. Typically, glass tubes with one mm wall thickness have been used. Large fully amorphous rods up to 14 mm in diameter have been prepared by this method. We have not as yet established an upper bound on the rod diameter which can be quenched to the glassy state.

Figure 3.2 shows several glassy samples obtained by various processes described above. Two rods, 7 mm and 12.6 mm diameter, were prepared by water quenching in silica tubes. Figure 3.2 also includes a rectangular bar and a plate prepared by casting in copper molds. The figure shows both a top view and cross-sectional views of bar, plate and rods. Also shown are top views of three glassy ingots, readily frozen into glass on a copper boat. X-ray diffraction

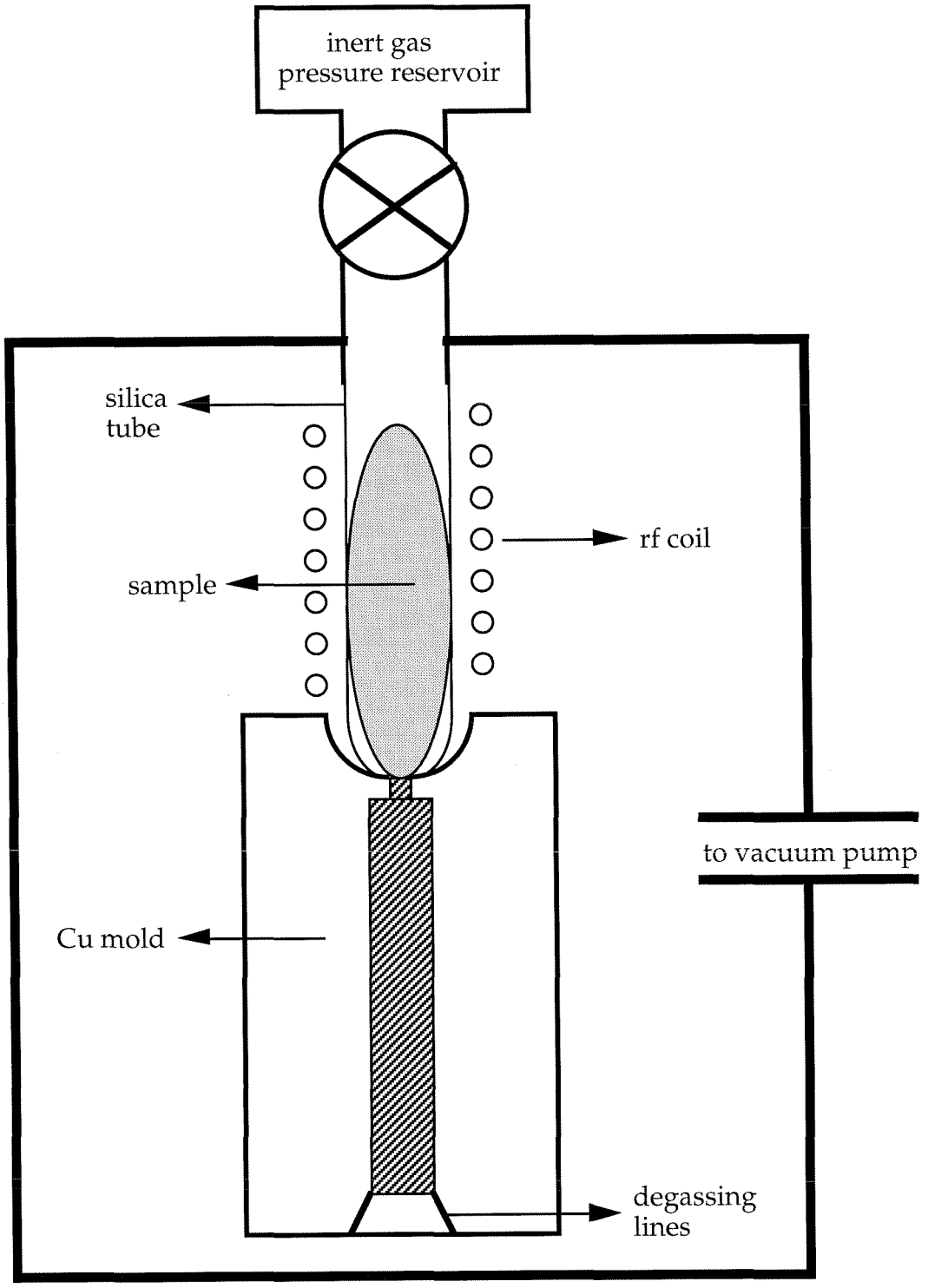

Figure 3.1: Schematic picture of metallic mold casting unit.

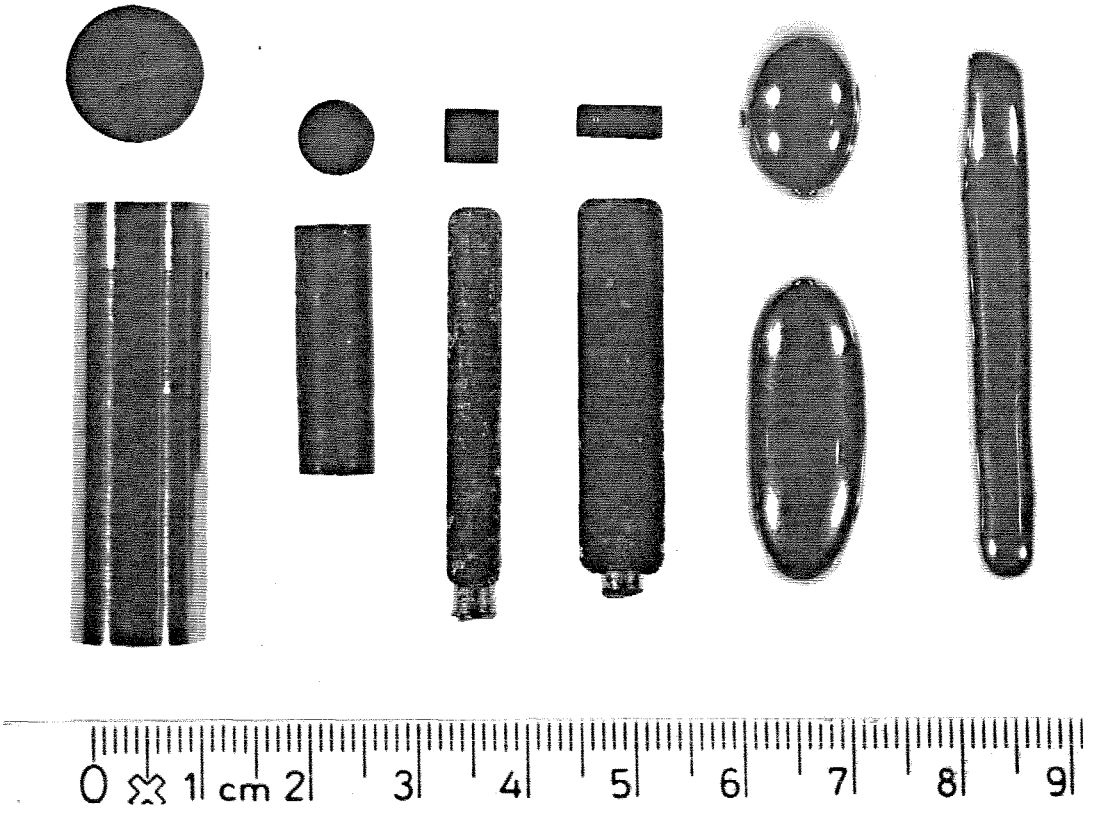

Figure 3.2: Samples of glassy alloy prepared by various processes, from left to right: 12.6 mm diameter rod and its cross-section, 7.0 mm diameter rod and its cross-section, 5X5 mm bar and its cross-section, 3X8 mm plate and its cross-section, 2 oval shape of ingots of 9 g each, bar-like ingot of 8 g.

patterns were obtained from the outer surfaces as well as on various cross-sectioned surfaces of the samples. No evidence of crystallization has been found in any of the X-ray patterns.

Figure 3.3 shows a typical x-ray pattern of glassy $Zr_{41.2}Ti_{13.8}Cu_{12.5}Ni_{10.0}Be_{22.5}$ alloy, taken from the cross-sectional surface of the 12.6 mm rod obtained by water quenching in a silica tube. This X-ray diffraction pattern was obtained with an Inel position sensitive detector using *Co* $K\alpha$ radiation (λ=0.1790 nm). The sample is completely amorphous as evidenced by the absence of any Bragg peak. This is further supported by TEM characterization. Several transmission electron microscopy samples were prepared and neither electron diffraction patterns nor dark field images gave any evidence of crystalline inclusions. Figure 3.4 shows typical bright and dark field images of $Zr_{41.2}Ti_{13.8}Cu_{12.5}Ni_{10.0}Be_{22.5}$ alloy taken from a glassy ingot of 6 grams. Figure 3.5 shows the corresponding electron diffraction. The sample is completely amorphous, as evidenced by featureless gray TEM micrographs and broad halos in the electron diffraction pattern.

Figure 3.6 shows a high resolution TEM image of a similar sample. No lattice fringes are observed beyond the range of 1.0 nm. The observed short range ordering should be interpreted as ordering of liquid due to entropy loss upon cooling rather crystallization. As we have seen in chapter 1, undercooled liquids tend to have higher heat capacity than the corresponding crystal. We shall see in section 3.3 that the same is true for our Zr alloy and it should therefore lose substantial configurational entropy thus becoming more ordered during cooling. This kind of short range ordering is generally not as pronounced in conventional metallic glasses, since the very high rate of cooling results in entropy trapping

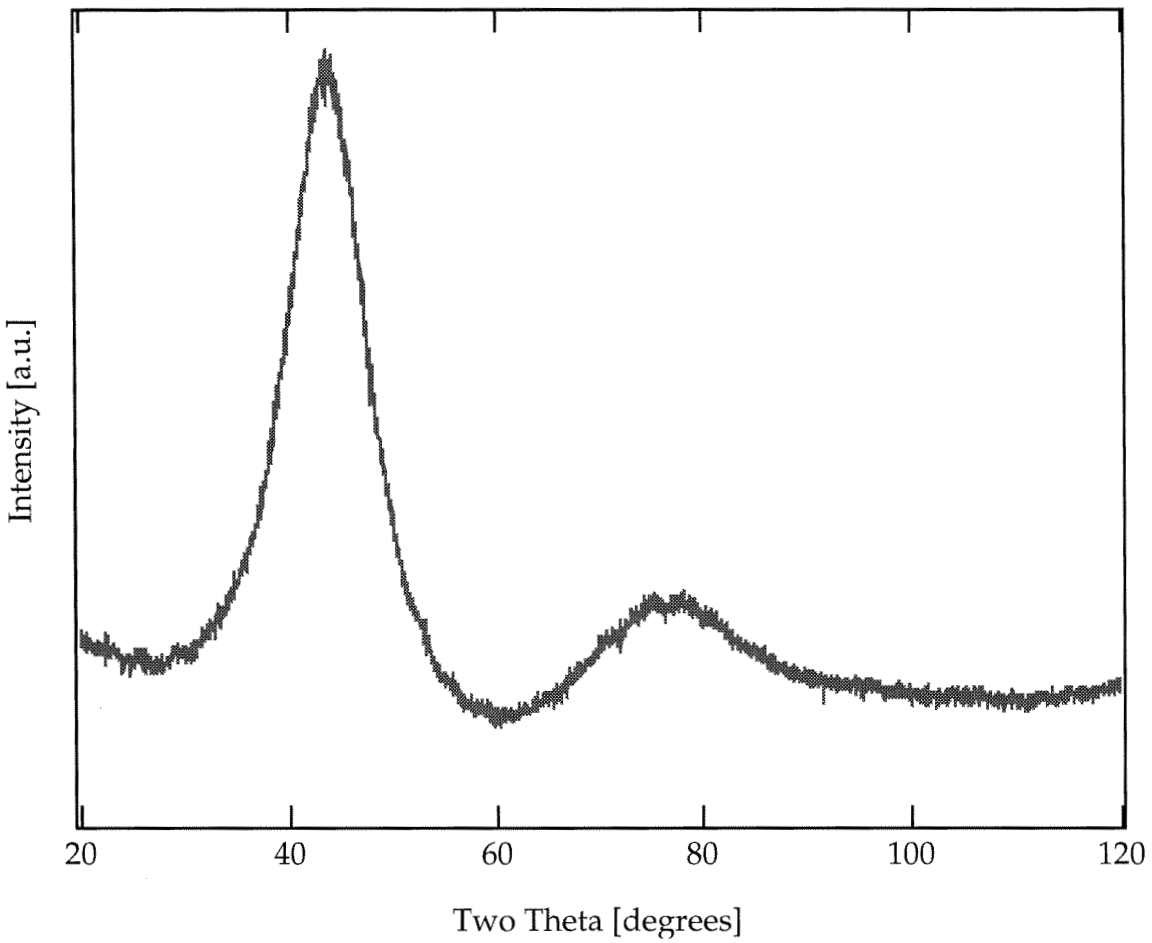

Figure 3.3: X-ray diffraction pattern (Co Kα radiation) taken from the cross-sectional surface of 12.6 mm diameter rod obtained by water quenching in a silica tube.

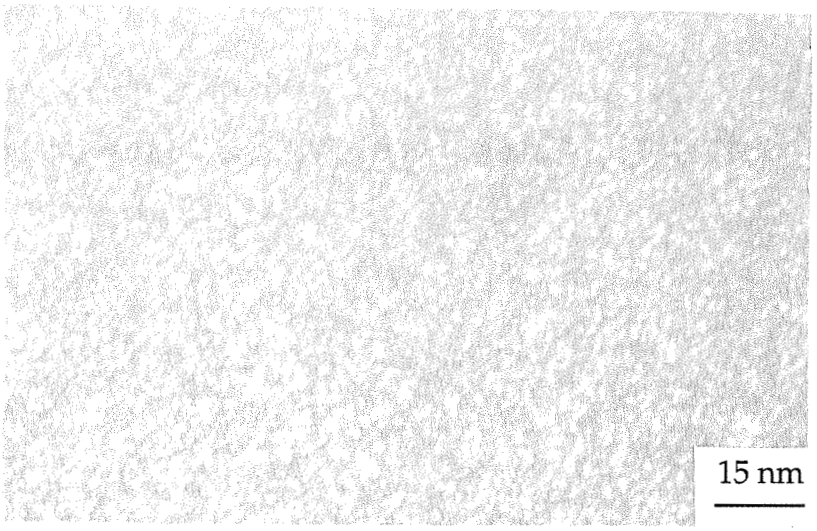

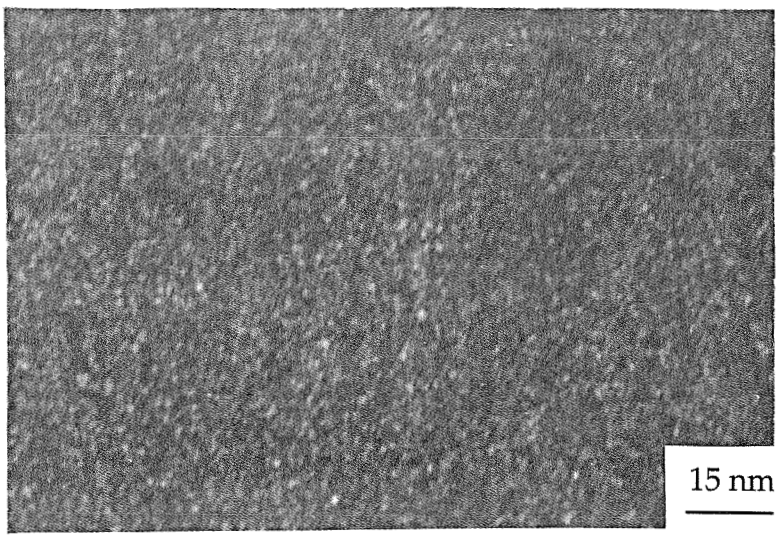

Figure 3.4: TEM micrographs of $Zr_{41.2}Ti_{13.8}Cu_{12.5}Ni_{10.0}Be_{22.5}$ alloy taken from a glassy ingot of 6 grams: (a) bright field and (b) dark field.

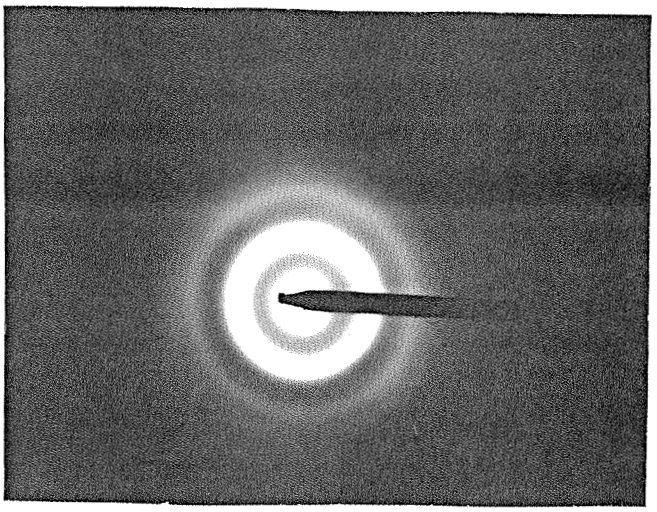

Figure 3.5: The electron diffraction pattern of $Zr_{41.2}Ti_{13.8}Cu_{12.5}Ni_{10.0}Be_{22.5}$ alloy taken from a glassy ingot of 6 grams.

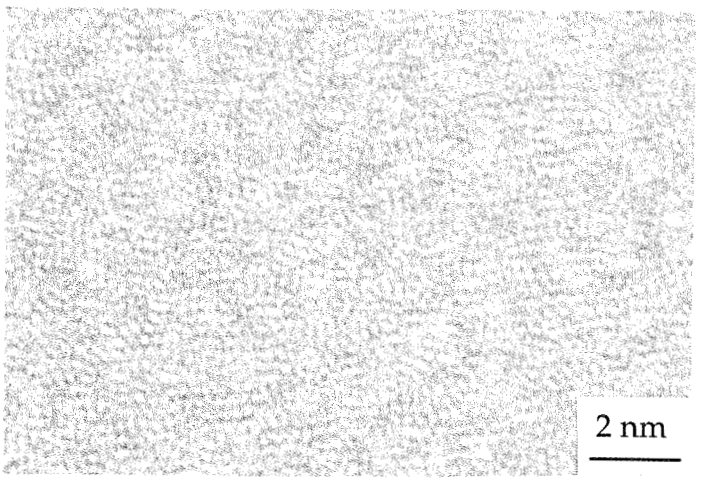

Figure 3.6: The high resolution TEM image of $Zr_{41.2}Ti_{13.8}Cu_{12.5}Ni_{10.0}Be_{22.5}$ alloy taken from a glassy ingot of 6 grams.

during the glass transition from undercooled liquid to the glass. As the atomic mobility is drastically reduced around the glass transition, the undercooled liquid may not have enough time to sample its configurational phase space completely during cooling, thus keeping some of its communal entropy which it would otherwise lose. The glassy $Zr_{41.2}Ti_{13.8}Cu_{12.5}Ni_{10.0}Be_{22.5}$ alloy has been cooled slower by several orders of magnitude, ~ 10 K/s, hence it has had more time to come to configurational equilibrium during the glass transition. As such it tends to lose more configurational entropy as reflected in a higher heat capacity and more ordered structure.

3.2 Mechanical properties

The $Zr_{41.2}Ti_{13.8}Cu_{12.5}Ni_{10.0}Be_{22.5}$ bulk glassy alloy preserves the traditional ductility and high strength of metallic glasses [1]. Vickers hardness measurements on this bulk glassy alloy shows a typical value of H_v = 585 kg/mm^2. Using the well known relation $H_v = 3\ \sigma_y$ for metallic glasses [3], the yield strength has been estimated to be σ_y = 1.95 GPa, which is in good agreement with the recently reported value of σ_y = 1.89 GPa obtained from both tensile and compression tests of the bulk samples [4]. The density of this glassy alloy has been measured as 6.11 g/cm^3 using the Archimedes principle. With the given values of density and yield strength, the glassy $Zr_{41.2}Ti_{13.8}Cu_{12.5}Ni_{10.0}Be_{22.5}$ alloy has a very high specific strength. The bulk glassy alloys are very ductile at ambient temperature when deformed under confined geometries. For example, a plate of 1.5 mm thickness was cold rolled at ambient temperature down to 15 micron thick ribbon without any crack formation. The final ribbon can still sustain a 90° bend as shown in figure 3.7. The hardness values of glassy samples before and after cold rolling do not show

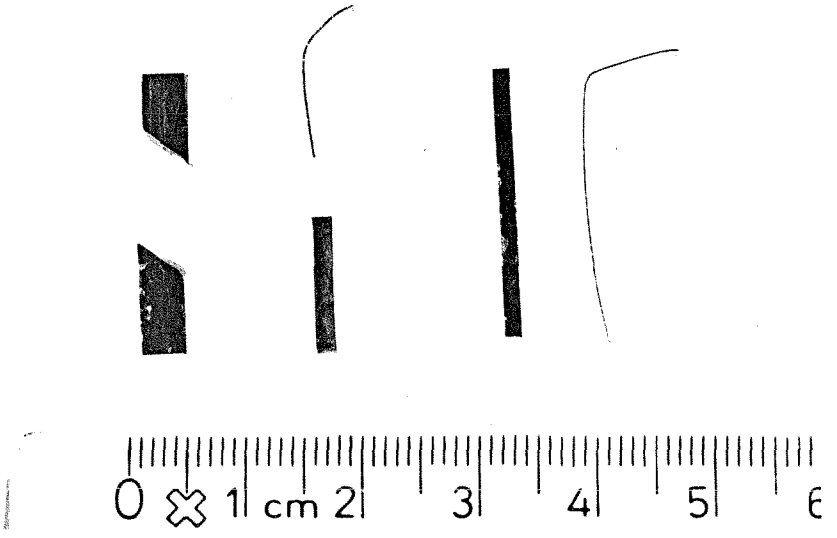

Figure 3.7: Samples of cold-rolled $Zr_{41.2}Ti_{13.8}Cu_{12.5}Ni_{10.0}Be_{22.5}$ glassy alloy. From left to right: 3mm thick glassy sample failed during cold rolled, 1.5 mm thick glassy sample cut from 3mm thick glassy alloy and its final form after rolling down to 30 micron thick ribbon, 1.5 mm thick glassy alloy, final form of 1.5 mm thick glassy alloy after rolling down to 15 micron thick ribbon.

any significant difference implying the absence of any work (strain) hardening. Localized deformation markings --shear bands-- perpendicular to the rolling direction have been observed on the rolled samples as reported by previous researchers on other metallic glasses [5].

The sample aspect ratio is a critical geometric factor, defining the confined geometry, in determining the ductility of glassy sample. It is given by l/d, where l is the length of the sample in the direction of the applied force, and d is the smallest dimension of the sample under stress in the plane perpendicular to the applied force. When the aspect ratio is greater than a critical value, the sample fails in the direction of maximum resolved shear stress (at 45° degrees to the applied force) without any apparent ductility. For example, a 3mm thick glassy plate, which has twice the aspect ratio of 1.5 mm thick glassy plate for the same rolling mill arrangement, failed during cold rolling without exhibiting any apparent ductility. The fracture surface shows the typical veiny patterns evidencing localized plastic deformation [6]. It seems that a localized shear mechanism causes the sample failure before global deformation can begin. Figure 3.7 shows the glassy sample pieces which failed during rolling. The same 3 mm thick glassy sample was longitudinally cut to reduce the thickness to 1.5 mm. This eliminated any effect due to cooling rate and exposed the pure geometrical effect on the deformation behavior of the glassy alloy. The cut sample, 1.5 mm thick, can be cold rolled indefinitely and still keep its bending ductility. The initial and final form of the cut sample after rolling has been shown in figure 8. Similar results have been obtained in compression testing of the glassy $Zr_{41.2}Ti_{13.8}Cu_{12.5}Ni_{10.0}Be_{22.5}$ alloy where a critical aspect ratio was found to be 1.0 [4, 7]. These results can be interpreted as follows. When the

applied stress on the glassy sample reaches the yield strength, a localized shear band forms in the direction of the maximum resolved shear stress (at 45° degrees to the applied force). The shear band will propagate (or expand) crossing throughout the sample in a rather narrow band shearing the sample in two pieces. The two pieces of the sample tend to move relative to each other by sliding. When the aspect ratio is less than one, the confined geometry will prevent sliding. Then two pieces of glassy sample will rotate rather than sliding on each other as shown in figure 3.8 (a). This will result in deformation of the glassy sample by a length comparable to the thickness of shear band. As new shear bands form, their combined effect will give a significant overall ductility. A good example of this is given by the rolling of glassy alloys where deformation markings have been observed in the direction perpendicular to the rolling. When the aspect ratio is greater than one, two pieces of glassy sample split by the shear band will slide freely on each other resulting in failure as illustrated in figure 3.8 (b). If there were work hardening in the glassy alloy, the propagation of a shear band and free sliding of parts of the glassy sample would be terminated in favor of new shear band formation. Thus, it is the complete absence of work hardening that results in the localization of shear deformation into narrow bands.

The Young's modulus of $Zr_{41.2}Ti_{13.8}Cu_{12.5}Ni_{10.0}Be_{22.5}$ glassy alloy has been reported to be 93 GPa, from which we find the ratio of $E/\sigma_y = 50$ in close agreement with other metallic glasses [3]. However, its constituent elements have a weighted average value of 165 GPa for Young Modulus [8] which gives the ratio of $E_{glass}/E_{crystal} \approx 0.56$. This number averages around 0.75 for other metallic glasses [3, 9]. This extra "softening" may be due to the abnormally high Young's modulus of Be , which is 356 GPa, compared to 98 GPa for Zr [8].

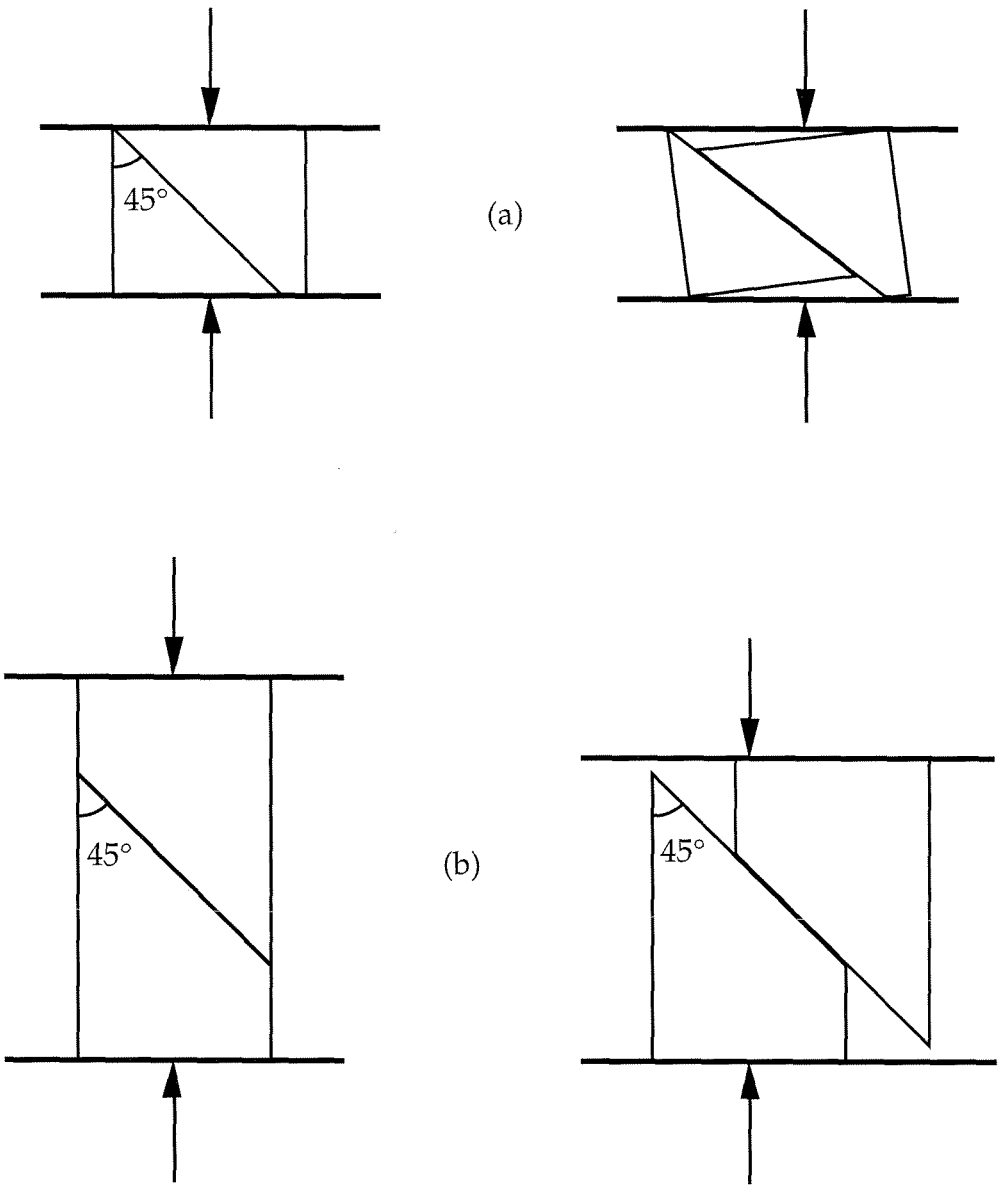

Figure 3.8: (a) Deformation of glassy alloy when aspect ratio is less than one.

(b) Failure of glassy alloy when aspect ratio is greater than one.

Relatively low concentration of Be may substantially reduce its contribution to Young's modulus of the glassy alloy. In particular, this may be related to the absence of direct Be-Be bonding in the glass.

As $Zr_{41.2}Ti_{13.8}Cu_{12.5}Ni_{10.0}Be_{22.5}$ glassy alloy can be easily produced in bulk forms, it is exceptionally well suited for highly reliable mechanical tests which were not possible with earlier metallic glass forming systems. Recently, comprehensive quasistatic mechanical tests on the $Zr_{41.2}Ti_{13.8}Cu_{12.5}Ni_{10.0}Be_{22.5}$ bulk glassy alloy were reported [4]. Further mechanical properties such as fracture toughness are under investigation [7].

3.3 Thermal analyses

Thermal analysis of the glassy alloy was carried out using a Perkin-Elmer DSC 4 scanning calorimeter interfaced to a personal computer for data processing and analysis. The samples were contained in aluminum pans and scanned in a flowing argon atmosphere. To determine the crystalline alloy melting point, a Seteram DSC 2000 K high temperature calorimeter was used in the DSC mode.

Figure 3.9 shows DSC (Differential Scanning Calorimetry) scans of the glassy $Zr_{41.2}Ti_{13.8}Cu_{12.5}Ni_{10.0}Be_{22.5}$ alloy using a heating rate of 20 K/min. and 200 K/min. In the 20 K/min. scan, a heat capacity anomaly characteristic of the glass transition can be seen beginning at 625 K with a heat capacity maximum at slightly higher temperature. At higher temperatures, two crystallization events are seen. The onset of the first occurs at 705 K while the onset of the second is at 735 K. The location of both peaks depends strongly on the rate of heating as can be seen by comparison with the DSC scan at higher heating rate. This relatively large supercooled liquid range has been successfully utilized in fabrication and

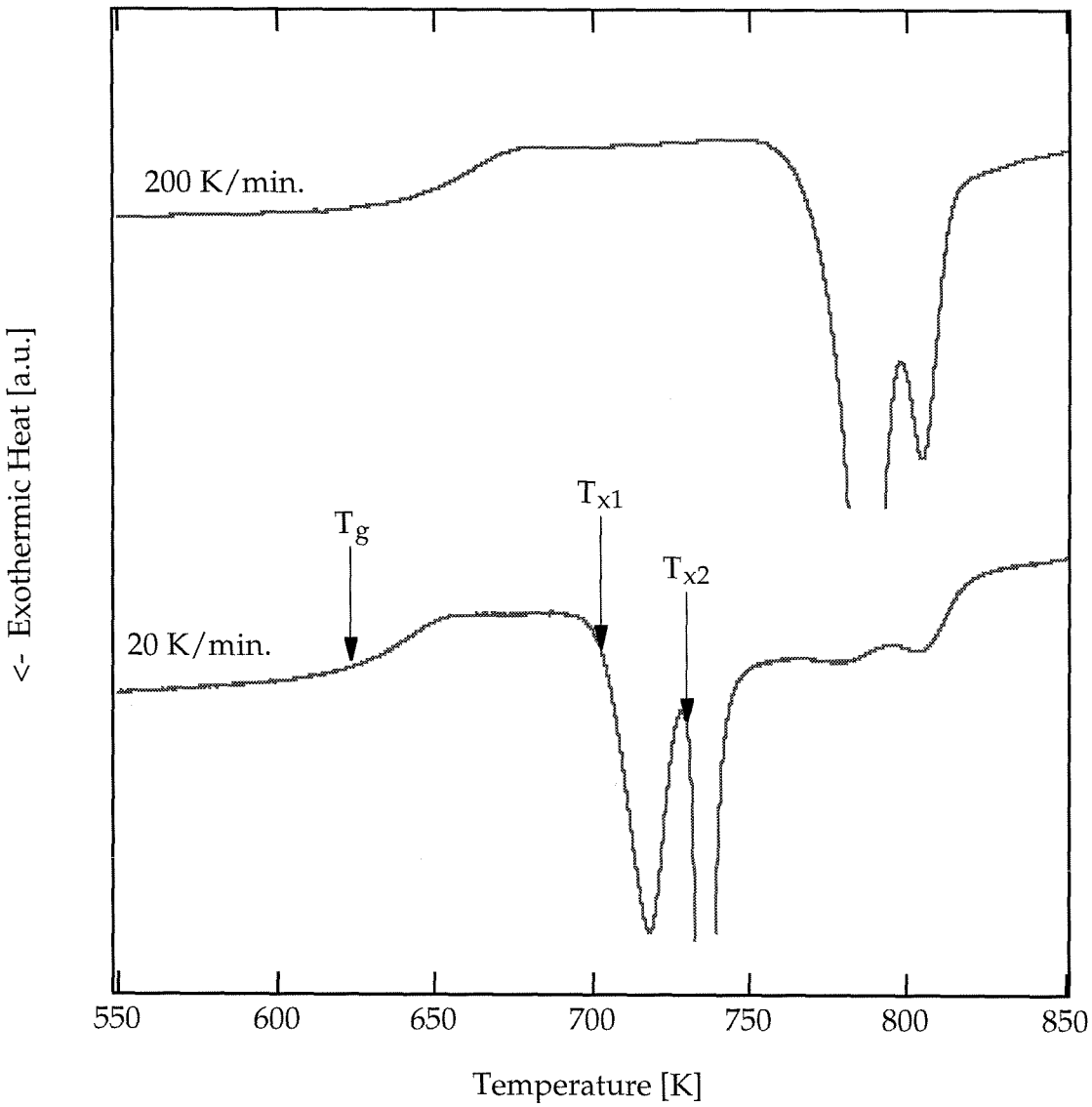

Figure 3.9: DSC scans of $Zr_{41.2}Ti_{13.8}Cu_{12.5}Ni_{10.0}Be_{22.5}$ glassy alloy at heating rates of 20 K/min. and 200 K/min. The corresponding glass transition temperature and crystallization temperatures are shown for the heating rate of 20 K/min.

shaping of the $Zr_{41.2}Ti_{13.8}Cu_{12.5}Ni_{10.0}Be_{22.5}$ bulk glassy alloys. Thickness reductions of 90 percent were easily obtained with small pressures of ~ 5 MPa at 50-70 K above the glass transition temperature during a time duration of 10-20 minutes [10]. Also, fine details of the mold pattern can be reproduced at the scale of less than one micron [10]. The samples still keep their glassy nature after the fabricating and shaping process as would be suggested by the DSC results.

Figure 3.10 shows a high temperature DSC scan of the crystalline Zr alloy at the heating rate of 20 K/min. There are two endothermic peaks, the first one being much stronger. The solidus temperature is determined to be 937±3 K taking the onset of first endothermic peak. The liquidus temperature is determined by taking the offset of second peak and found to be 993±5 K. The heat of fusion was measured as $\Delta H_m^f = 6.3 \pm 0.3$ kJ/mole. We believe that the solidus temperature should be a eutectic temperature for the five component Zr-Ti-Cu-Ni-Be system. From the comparison of relative magnitudes of endothermic signals, we can deduce that the alloy is very close to a eutectic composition. Therefore, the $Zr_{41.2}Ti_{13.8}Cu_{12.5}Ni_{10.0}Be_{22.5}$ alloy will be assumed to represent the eutectic alloy for the rest of the thesis. The boundaries of the bulk glass forming range include a rather large region of the pentiary phase diagram. The $Zr_{41.2}Ti_{13.8}Cu_{12.5}Ni_{10.0}Be_{22.5}$ alloy composition lies somewhere near the center of this region. The exact eutectic composition should have similar or possibly better glass forming ability. Further, the properties of the glassy alloys do not show any drastic change with composition, thus our assumption should be valid for purposes such as calculation of the TTT diagram.

The experimentally observed heat capacity difference between the undercooled liquid and crystalline phases was approximated with a linear equation. DSC

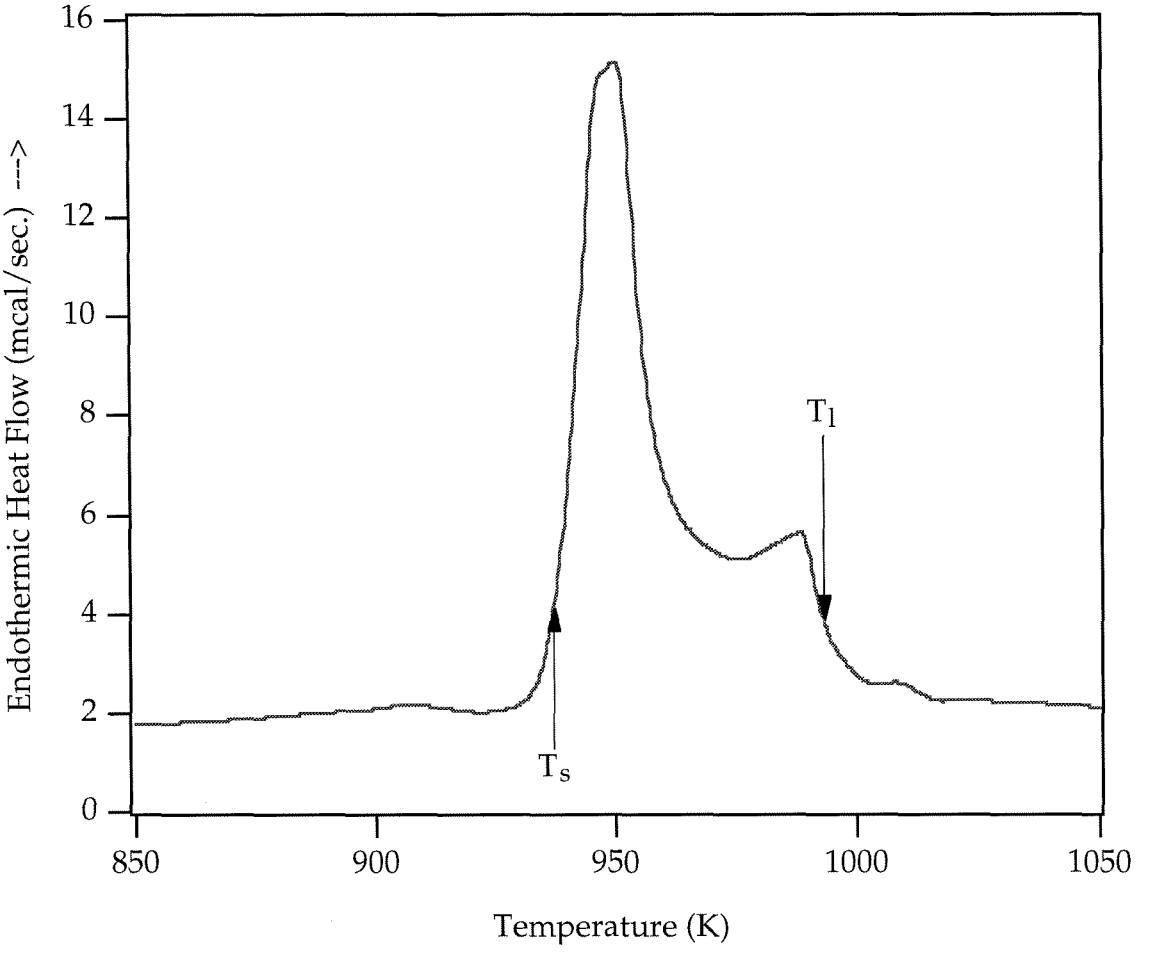

Figure 3.10: High temperature DSC scans of $Zr_{41.2}Ti_{13.8}Cu_{12.5}Ni_{10.0}Be_{22.5}$ crystalline alloy at heating rates of 20 K/min. The corresponding solidus T_s and liquidus T_l temperatures are also shown.

scans of the glassy alloy and crystalline alloy with a continuous heating rate were used to obtain the linear fit to the heat capacity difference in the supercooled liquid region. The linear equation is given by

$$\Delta C_p = -0.0233\ T + 21.91\ (\text{cal/mol}). \tag{3.1}$$

Accordingly, the calculated molar free energy difference between the liquid and corresponding crystal is plotted as a function of reduced temperature in figure 3.11. Turnbull's approximation is also shown [22]. It is clear that Turnbull's approximation diverges significantly from the experimentally extrapolated values at high undercooling, whereas it gives satisfactory values at small undercooling (ΔT_r<0.15).

3.4 The critical cooling rate

A molten sample of typical dimension R and initial temperature T_m (the melting point of the material) will require a total cooling time τ to ambient temperature (below glass transition) which is given by

$$\tau = (R^2/\kappa) \tag{3.2}$$

where κ is the thermal diffusivity of the material [11]. It is given by

$$\kappa = K/C_p \tag{3.3}$$

where K is the thermal conductivity and C_p is the heat capacity per unit volume. Then we can find an average value of cooling rate from the melting point to the ambient temperature by the equation

$$\dot{T} = \frac{\Delta T}{\tau} = \frac{\left(T_m - T_g\right)}{R^2}\frac{K}{C_p} \tag{3.4}$$

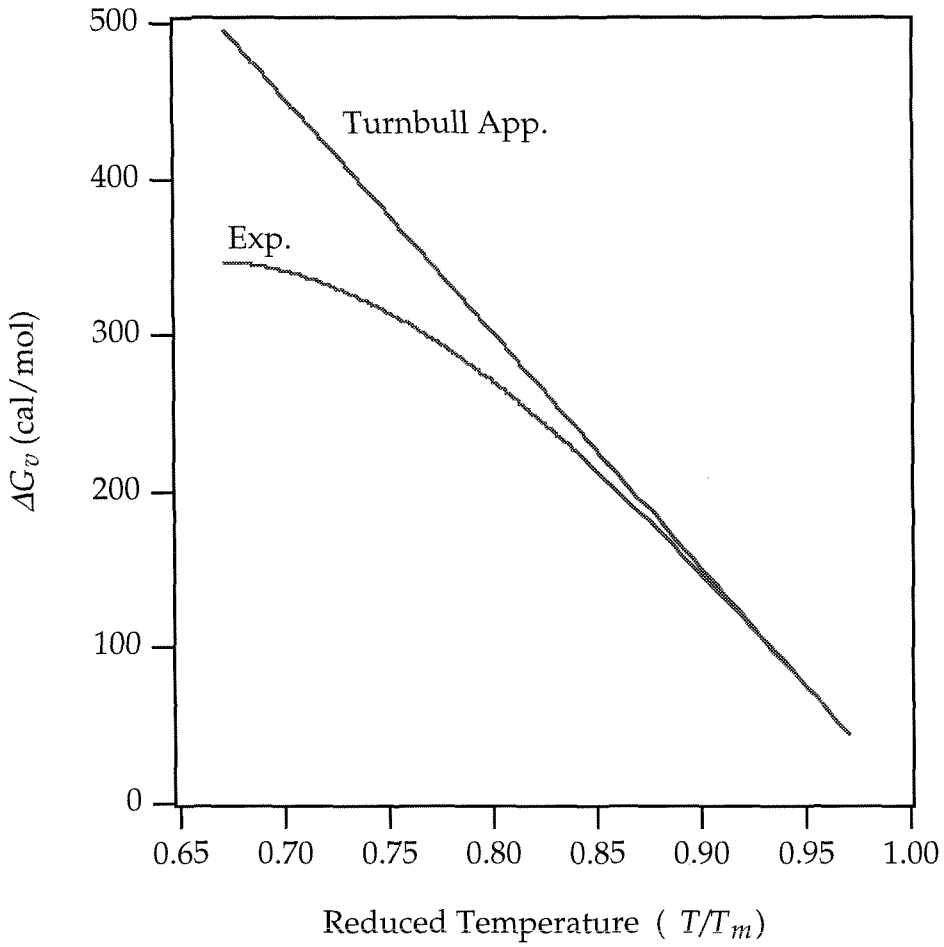

Figure 3.11: The free energy difference between undercooled liquid and corresponding crystal for $Zr_{41.2}Ti_{13.8}Cu_{12.5}Ni_{10.0}Be_{22.5}$ which is assumed to represent the eutectic alloy. Both the Turnbull approximation and experimentally extrapolated values are shown. Here, T_m is taken to be the eutectic temperature.

where we use the average values of K and C_p throughout the temperature range of ΔT. The critical cooling rate for glass formation is evaluated from the maximum possible value of R for a glassy sample.

The thermal conductivity of undercooled liquid can be calculated from the "Wiedemann-Franz" law which is stated as:

$$\frac{K\rho}{T} = L. \qquad (3.5)$$

T is the absolute temperature, ρ is the resistivity and L is the Lorenz number having a value of 2.45×10^{-8} watt ohm/deg^2 [12]. This expression should be valid for undercooled liquids due to their highly disordered nature. Taking $\rho = 2.5 \times 10^{-4}$ ohm cm., the value of glassy $Zr_{60}Be_{40}$ alloy [13], and $T = 780$ K we find an estimated value of $K = 7 \times 10^{-2}$ watt/cm. deg. The heat capacity of undercooled liquid can be calculated by the sum of the Dulong-Petit value of the corresponding crystal and using equation 3.1. We will get an average value of $C_p = 10$ cal/mol. or $C_p = 4$ J/cm^3 for the liquid. We can easily get 1.0 cm thick glassy ingots where heat is extracted from one direction. Using a value of 400 K for ΔT and plugging other numbers into equation 3.4, we find a average cooling rate of ~ 7 K/sec. for typical glassy ingots. In practice cooling rate changes with temperature, being highest around the melting point and decreasing as the glass transition is approached. As we have not yet set any upper bound for the maximum thickness of ingots which will form glass when cooled on metallic crucibles, the critical cooling rate could be substantially smaller.

3.5 TTT Diagram

TTT diagram (Time - Temperature - Transformations) and its derivative CCT (Continuous - Cooling - Transformations) have been used solely for estimating critical cooling rates [14]. These diagrams can be applied more generally to study the thermal stability of metallic glasses in the supercooled liquid region. This is especially true for very recent exceptional glass forming metallic alloys as they are more stable in the supercooled liquid region. The TTT diagram and its derivatives can also give us very useful information for fabrication of these hard and strong materials above glass transition using small forces. A preliminary attempt to construct the TTT diagram will be presented and it will be used to account for the observed thermal properties of our recently found excellent metallic glass formers [15].

The Uhlmann [16] and Davies [17] kinetic formulation was followed to construct a TTT diagram for the $Zr_{41.2}Ti_{13.8}Cu_{12.5}Ni_{10.0}Be_{22.5}$ alloy (which is assumed to represent the eutectic composition). A Doolittle-type expression was used to model the viscosity [18]

$$\eta = 0.0334 \exp\left[B \Big/ \exp\left[-\frac{C}{RT} \right] \right] \tag{3.6}$$

where the constants are determined by taking a viscosity of 10^{13} poise and 1 poise at the glass transition temperature and at the eutectic melting point respectively. The experimentally determined values of the free energy difference between the liquid and corresponding crystal were used. In order to get agreement with a critical cooling rate of 5 K/s, ΔG^* was set to 75 kT for a reduced undercooling $\Delta T_r = (T_m - T)/T_m = 0.2$. ΔG^* corresponds to the

energy barrier for nucleation in the kinetic formulation of Uhlmann and Davies. The CHT (Continuous- Heating -Transformations) curve was obtained approximately from the TTT curve using the method of Grange-Keifer [19].

In figure 3.12, TTT and CHT curves are shown together with DSC heating curves as well as a 5 K/sec cooling curve appropriate for a 1.0 cm thick glassy ingot. Also shown are experimental onset crystallization temperatures on the corresponding DSC heating curves. The observed crystallization temperatures are below the estimated temperatures from the calculated TTT diagrams. (When transient nucleation effects are included, it will push the TTT and CHT curves further to the right thus increasing the observed discrepancy.) At a heating rate of 200 K/min, no crystallization should be observed according to calculated TTT and CHT curves. To explain the differences between calculated and experimental crystallization temperatures, it is proposed that heterogeneous nucleation has intervened in the DSC experiments. This is supported by further experiments. For example, the development of a surface oxide has been observed above 675 K in samples scanned in flowing argon. Such oxidation can be suppressed by fluxing the sample surface with a layer of borosilicate glass or encapsulation in a thin glass ampoule. When this is done, surface oxidation is suppressed, and contact with the aluminum DSC pan is also prevented. Under these conditions, the experimental crystallization peaks have been found to shift to significantly higher temperatures. In fact, heterogeneous nucleation has previously been shown to be very important in the determination of critical cooling rates for glass formation as well as crystallization temperatures of glassy alloys. For example, Turnbull and co-workers undercooled liquid $Pd_{40}Ni_{40}P_{20}$

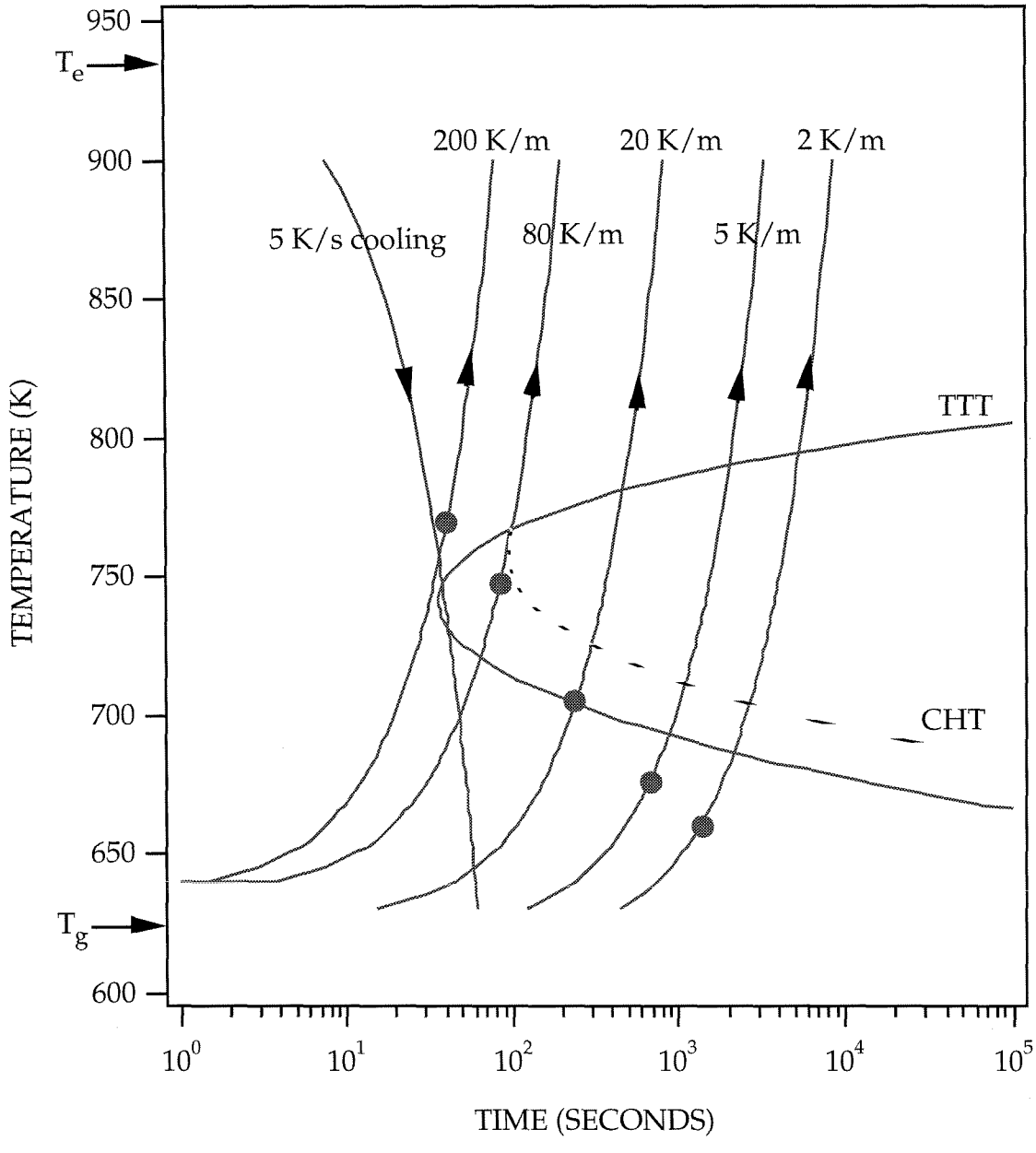

Figure 3.12: Calculated TTT and CHT curves for $Zr_{41.2}Ti_{13.8}Cu_{12.5}Ni_{10.0}Be_{22.5}$ are shown along with DSC heating curves at different heating rates and estimated critical cooling rate for glass formation. Also shown on the DSC heating curves are onset crystallization temperatures of the glassy alloy at corresponding heating rates (full circles).

samples with dimensions of one cm to the glassy state after removing heterogeneous nucleation catalysts by fluxing [20]. They estimated a critical cooling rate of order 1 K/s whereas it was earlier believed to be of order 10^3 K/s. They also showed that glassy $Pd_{40}Ni_{40}P_{20}$ can be heated to its melting point without crystallization at a heating rate of 2 K/s [21]. The effects of heterogeneous nucleation in glass formation and thermal stability of metallic glasses will be discussed in more detail in the next chapter.

An interesting feature of the TTT and CHT diagrams for this highly processable metallic glass is that the crystallization nose is very close to the continuous heating curves at the typical heating rates used in DSC experiments. For example, the continuous heating curve at the rate of 80 K/m just misses the crystallization nose. This will give a relatively wide supercooled liquid region above the glass transition as well as a strong dependence of crystallization temperatures on heating rates. The crystallization nose is far to the left in the TTT diagrams of conventional metallic glasses. In these systems it is necessary to use heating rates of 10^5-10^6 K/sec to encounter the crystallization nose. This is ordinarily not achieved in DSC experiments. Hence, typical DSC experiments give heating curves which fall to the far right of the crystallization nose of conventional metallic glasses. Here the slope of the TTT curve approaches zero. For very good glass forming alloys, the continuous heating curves at the typical heating rates used in DSC experiments should fall very close to the crystallization nose, where the TTT curve has a steeper slope and a rapidly changing value. As a result, crystallization temperatures should be strongly dependent on the typical heating rates used in DSC experiments. Thus any conclusions regarding the crystallization temperature and glass forming ability of these very good glass forming alloys should not be based on a single DSC

scan. This is illustrated in figure 3.13 where curve "a" represents a conventional metallic glass, e.g., $Zr_{65}Be_{35}$ and $Fe_{80}B_{20}$, curve "b" represents a thick glass former, e.g., $Pd_{77.5}Cu_6Si_{16.5}$ and $Zr_{60}Ni_{25}Al_{15}$, and curve "c" represents a bulk glass former such as $Zr_{41.2}Ti_{13.8}Cu_{12.5}Ni_{10.0}Be_{22.5}$. Two typical DSC heating rates are also shown. Obviously, the crystallization temperatures change more dramatically on curve "c" (representing the good glass former) for different heating rates. These TTT diagrams also suggest that the metallic glasses which require lower critical cooling rates have better stability above glass transition temperature, i.e., broader supercooled liquid region before crystallization on heating.

3.6 Origins of exceptional glass forming ability

We have seen in the previous chapter that the reduced glass transition temperature, $T_{rg} = T_g/T_m$ (where T_g is the calorimetrically defined glass transition temperature and T_m is the alloy melting point) has often been cited in the literature [14, 21] as a critical parameter which determines the glass forming ability of metallic alloys. High values of T_{rg} are associated with glass forming ability. Taking T_g = 625 K and T_m = 937 K (the eutectic temperature), we obtain T_{rg} = 0.67 for the eutectic alloy, which should have comparable glass forming ability as $Zr_{41.2}Ti_{13.8}Cu_{12.5}Ni_{10.0}Be_{22.5}$. This is among the highest values of T_{rg} reported for metallic alloys so far [14] and is consistent with the exceptional glass forming ability of the material.

To explain the exceptional glass forming ability of these alloys, both thermodynamic and kinetic factors must be taken into account. The large values of T_{rg} imply a small relative temperature range over which nucleation and growth of crystals can occur. From our DSC studies, we estimated the total

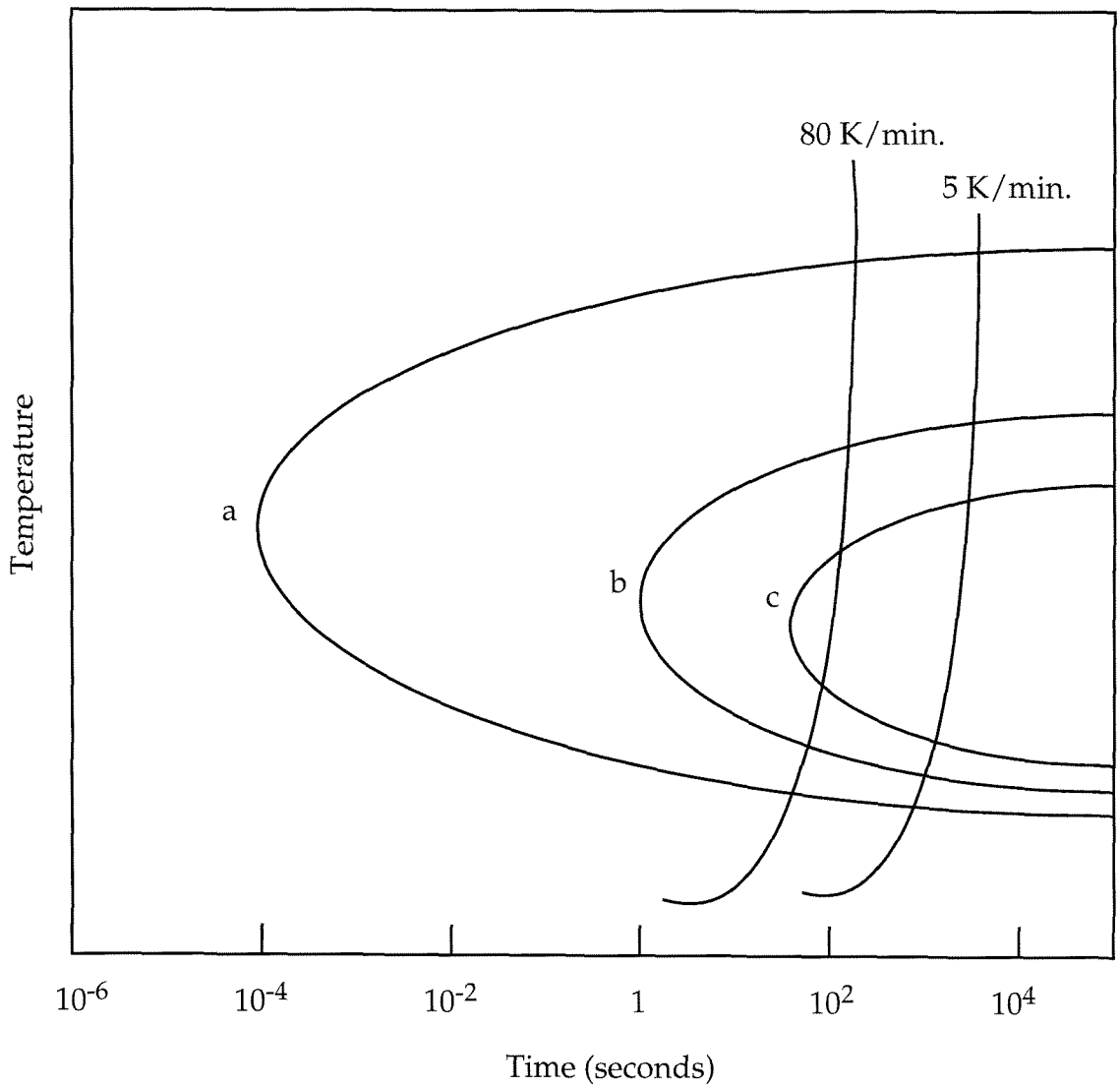

Figure 3.13: Schematic TTT diagrams for three different metallic glass formers. Curve a, b, c respectively represent a conventional metallic glass former, a moderately good glass former and an exceptionally good glass former. Also shown schematically are DSC traces at the heating rates of 80 K/min and 5 K/min. It is assumed that all the glassy alloys have the same value of T_g.

entropy of fusion, ΔS_m^f of these alloys, to be approximately 6.6 J/mole-K. This is a very low value compared to well known "Richard's rule" of $\Delta S_m^f \geq 8.4$ J/mole K for metallic alloys [23]. Using the Turnbull approximation [22] for the free energy difference between the liquid and crystalline phases in the undercooled regime,

$$\Delta G_m = \Delta S_m^f (T_m - T) + \text{higher order terms} \qquad (3.7)$$

gives a very small driving force for crystallization. The higher order terms involve the heat capacity difference between the liquid and crystal and generally reduce the driving force for crystallization relative to the first term. For example, at 780 K, corresponding to a reduced undercooling of 0.18 we estimate $\Delta G_m = 1.1$ kJ/mole. When heat capacity corrections are taken into account, figure 3.11 gives $\Delta G_m = 1.0$ kJ/mole. This relatively small driving force for crystallization will tend to result in a relatively large nucleation barrier for crystals in the restricted undercooled region. At lower temperatures, kinetic freezing of the melt sets in rapidly due to the small temperature interval between the melting point and glass transition (i.e., high value of T_{rg}). As evidenced by the TTT diagram, the undercooled liquid has a very small temperature range for crystallization.

A second factor which may influence crystallization is the "complexity" of the five component alloy. We note, for example, that the atomic radii of the elemental constituents vary over a large range. The atomic radius of Be is 0.111 nm, those of Ni and Cu are 0.124 nm, while those of Zr and Ti are 0.160 and 0.147. These differing sizes are expected to limit the solubilities of these elements in crystalline phases having a small number of non-equivalent

positions in the unit cell, thus requiring large chemical fluctuations to form critical nuclei of the crystalline phases. In support of this argument, we note that Tanner has studied glass formation by rapid quenching in Zr-Be and Ti-Be alloys [24]. In the Ti-Be system, glass formation is preempted by formation of a metastable CsCl-type structure near the equiatomic composition. Nucleation of this metastable phase is suppressed when Zr is substituted for Ti in the alloys. Apparently, the larger atomic diameter of Zr limits its solubility in the CsCl-type phase and makes nucleation of this phase more difficult in the ternary alloys. Masumoto and Inoue [25, 26] have suggested that atomic size differences in multicomponent alloys lead to efficient packing of atoms in the glassy phase. Recall that the atomic radius of elements in $Zr_{41.2}Ti_{13.8}Cu_{12.5}Ni_{10.0}Be_{22.5}$. alloy covers a broad range which will help in efficient packing. The packing should be further enhanced by isotropic metallic bonding which is characteristic of these metallic elements. It should be noted that Be, a crucial element for bulk glass formation, is the "smallest" atom which bonds metallically in the entire periodic table. This in turn leads to a smaller ground state energy difference between the amorphous and crystalline phases. This small difference together with the lowering of the free energy of the liquid due to chemical mixing entropy effects can be related to the existence of deep eutectic structures such as found in our alloys. The existence of deep eutectic structures will be discussed in more detail in chapter 5.

The crystal growth velocity is also an important factor in glass formation. Eutectic and dendritic crystallization may have substantially low growth velocities due to extensive solute partitioning [27]. For example, Boettinger demonstrated that there is a maximum crystal growth velocity for eutectic

crystallization of $Pd_{77.5}Cu_6Si_{16.5}$. This leads to glass formation at higher solidification velocities [27]. A low crystal growth velocity will be especially valuable in suppressing the effects of heterogeneous nucleation. When heterogeneous nucleation sites are dilute enough, the limited crystal growth will keep the bulk of the undercooled liquid unaffected. A good example of this is given by $Zr_{41.2}Ti_{13.8}Cu_{12.5}Ni_{10.0}Be_{22.5}$. glassy ingots. These samples have crystalline traces at the bottom surface. Crystallization does not extend to the ingot interior during cooling. This suggests a limited crystal growth velocity. This example also shows that there are no active or at least very few heterogeneous nucleation sites in the bulk of the $Zr_{41.2}Ti_{13.8}Cu_{12.5}Ni_{10.0}Be_{22.5}$ liquid. Comparing this to bulk glass formation in $Pd_{40}Ni_{40}P_{20}$ by fluxing, we see that this alloy is "self fluxing." We have, in fact, found that the liquid $Zr_{41.2}Ti_{13.8}Cu_{12.5}Ni_{10.0}Be_{22.5}$ alloy can dissolve up to 1% oxygen and still form bulk glass. It seems that the high oxygen solubility in the liquid results in an absence of oxide particles in the melt. Such particles would act as a catalyst for heterogeneous nucleation. This will be discussed in more detail in the next chapter.

References

[1] A. Peker and W. L. Johnson, Appl. Phys. Lett., **63**, 2342 (1993).

[2] R. B. Schwarz, Los Alamos National Laboratory (private communication, October 1993).

[3] L. A. Davis, in *Metallic Glasses: Papers Presented at a Seminar of the Materials Science Division of the ASM in 1976* (American Society for Metals, Ohio, 1978).

[4] H. A. Bruck, T. Christman, A. J. Rosakis, and W. L. Johnson, Script. Met., **30**, 429 (1994).

[5] S. Takayama and R. Maddin, Acta. Met. **23**, 943 (1975).

[6] H. J. Leamy, H. S. Chen, and T. T. Wang, Mett. Trans. **3**, 699 (1972).

[7] H. A. Bruck, A. J. Rosakis, and W. L. Johnson (private communication, 1993).

[8] B. S. Berry, in *Metallic Glasses: Papers Presented at a Seminar of the Materials Science Division of the ASM in 1976* (American Society for Metals, Ohio, 1978).

[9] Smithells Metals reference Book (edited by E. A. Brandes and E. B. Brook; Butterworth-Heinemann, Linacre House, Jordan Hill, Oxford) 15-2, 15-3 (1992).

[10] A. Peker, E. Bakke, and W. L. Johnson, (unpublished research, 1993-1994).

[11] H. S. Carslaw and J. C. Jaeger, *Conduction of heat in solids*, 2nd ed. (Clarendon Press, Oxford) p. 59.

[12] C. Kittel, *Introduction to Solid State Physics*, 6th ed. (Wiley, New York, 1986) p. 68.

[13] R. Hasegawa and L. E. Tanner, J. Appl. Phys **49**, 1196 (1978).

[14] H. A. Davies, in *Rapidly Quenched Metals III* , B. Cantor (ed.) (Metals Soc., London, 1978), Vol. 1, p. 1.

[15] A. Peker and W. L. Johnson, in *Prod. 8th Int. Conf. on Rapidly Quenched Metals,* to appear in Mater. Sci. Eng. (1994).

[16] D. R. Uhlmann, J. Non-Cryst. Solids, **7**, 337 (1972).

[17] H. A. Davies, Phys. Chem. Glasses, **17**, 159 (1976).

[18] P. Ramachandrarao, B. Cantor, and R. W. Cahn, J. Non-Cryst. Solids, **24**, 109 (1977).

[19] R. A. Grange and J. M. Keifer, Trans. Am. Soc. Metals, **29**, 85 (1941).

[20] H. W. Kui, A. L. Greer, and D. Turnbull, Appl. Phys. Lett., **45**, 615 (1984).

[21] H. W. Kui and D. Turnbull, Appl. Phys. Lett., **47**, 796 (1985).

[22] D. Turnbull, Contemp. Phys., **10**, 473 (1969).

[23] D. A. Porter and K. E. Easterling, *Phase Transformations in Metals and Alloys* (Van Nosttrand Reinhold, England) p. 11.

[24] L. E Tanner and R. Ray, Acta. Metall., **27**, 1727 (1979).

[25] T. Zhang, A. Inoue, and T. Masumoto, Mater. Trans., JIM, **32**, 1005 (1991).

[26] T. Zhang, A. Inoue, and T. Masumoto, Mater. Lett., JIM, **15**, 379 (1993).

[27] W. J. Boettinger, in *Rapidly Solidified Amorphous and Crystalline Alloys*, B. H. Kear, B. C. Giessen, and M. Cohen (eds.) (North Holland, 1982), p. 15.

Chapter 4

Heterogeneous nucleation and glass formation

In chapter 2, the theory of homogenous nucleation was presented and used in accounting for glass formation. However, homogenous nucleation is rarely realized in practice, as another mode of nucleation, heterogeneous nucleation, preempts homogenous nucleation. There are two sources of heterogeneous nucleation: the container and foreign particles (such as oxides). These are hard to avoid in routine practice of metallurgy, making heterogeneous nucleation very common. In fact, the theory of homogenous nucleation has very limited applicability for the same reason. In a few cases, experimental conditions have been achieved such that homogenous nucleation was realized or became competitive with heterogeneous nucleation.

In this chapter, I will discuss the origins of heterogeneous nucleation and its pronounced effect on glass formation. First, the theory of heterogeneous nucleation will be developed in analogy with that of homogenous nucleation. Then examples of heterogeneous nucleation induced by container walls will be presented for the bulk glass forming Zr-Ti-Cu-Ni-Be system. Some examples of metastable interfaces between the Zr-Ti-Cu-Ni-Be bulk glassy alloy and elemental crystalline phases will also be introduced. Later, the effect of heterogeneous nucleation induced by foreign particles, mainly oxides, will be

discussed in bulk glass formation of several different alloy systems. Finally, I will present examples demonstrating how thermal stability of metallic glasses is affected by heterogeneous nucleation.

4.1 Origins of heterogeneous nucleation

The principal resistance of an undercooled liquid to nucleation is related to the creation of an interface between the crystalline nuclei and liquid. Nucleation can be enhanced at small undercooling, when this effective interfacial energy is reduced. This can be effectively achieved by forming crystalline nuclei on the surface of the container or on foreign particles which exist incidentally (or are introduced intentionally) in the liquid. The existence of an interface between liquid and container (or foreign particles) before formation of a crystalline embryo is the primary cause of heterogeneous nucleation.

Let us consider a crystalline embryo forming on a flat container surface or foreign particle surface as shown in figure 4.1. If we assume the crystal-liquid interfacial energy γ_{XL} is isotropic as we did in the classical theory of homogenous nucleation, it can be shown that the total interfacial energy of the system is minimized if the crystalline embryo has the shape of a spherical cap [1]. The "wetting angle" θ can be expressed as

$$\cos\theta = (\gamma_{ML} - \gamma_{XM})/\gamma_{XL} \tag{4.1}$$

where γ_{XL}, γ_{XM}, γ_{ML} are the interfacial energy (or interfacial tension) between the crystal and the liquid, the crystal and the container, and the container and the liquid respectively [1]. This expression is derived from the balance of the interfacial tensions in the plane of the container (or foreign particle) wall. The wetting of container wall by the crystalline embryo can be enhanced

substantially if two crystals are lattice matched to each other (not necessarily in the same crystallographic planes). When their interatomic spacings differ significantly, a strain energy due to this mismatch will result in a high interfacial energy thus discouraging good wetting between the crystalline embryo and container wall [2]. Obviously, the same is true for the case of a foreign particle instead of the container.

The total Gibbs' free energy change upon formation of a crystalline embryo is given by [1]

$$\Delta G_{het} = \left\{ 4\pi r^2 \gamma_{XL} + \frac{4\pi}{3} r^3 \Delta G_v \right\} S(\theta) \tag{4.2}$$

where r is the radius of spherical cap and $S(\theta)$ is a shape term given by

$$S(\theta) = (2 + \cos\theta)(1 - \cos\theta)^2 / 4 . \tag{4.3}$$

Note that the expression for ΔG_{het} is the same as the one obtained for homogenous nucleation, equation 2.2, except for factor $S(\theta)$. The $S(\theta)$ has a numerical value less than 1 as shown in figure 4.2. The value of $S(\theta)$ approaches zero at small values of wetting angle θ; for example, $S(\theta)$ equals 0.0027 when θ is 20°. The critical radius r* and activation energy for heterogeneous nucleation, G^*_{het}, can be obtained by differentiation of equation 4.2, and they are given as:

$$r^*_{het} = -\frac{2\gamma_{XL}}{\Delta G_v} = r^*_{\text{hom}} \tag{4.4}$$

$$G^*_{het} = \left(\frac{16\pi}{3} \right) \left(\frac{\gamma_{XL}^3}{\Delta G_v^2} \right) = \Delta G_{\text{hom}} S(\theta) . \tag{4.5}$$

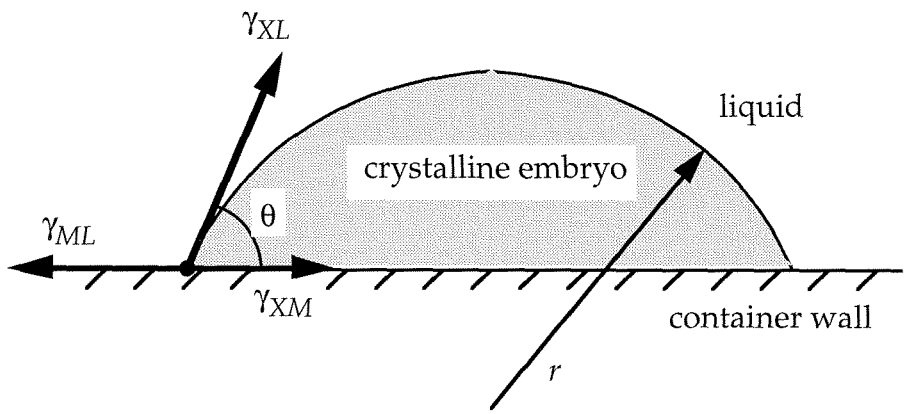

Figure 4.1: Heterogeneous nucleation of crystalline embryo having a shape of spherical cap on a flat container (or foreign particle such as oxide) wall.

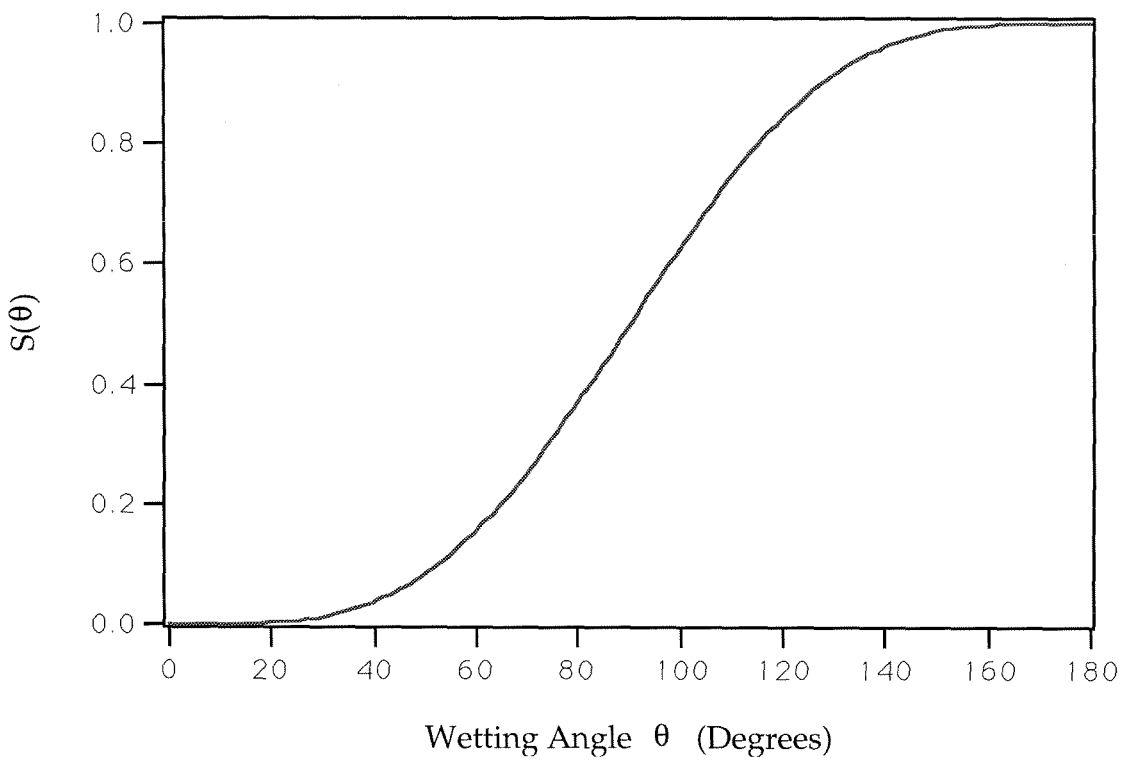

Figure 4.2: The value of the expression $S(\theta) = (2+\cos\theta)(1-\cos\theta)^2/4$ as a function of wetting angle θ.

Notice that the critical radius of a crystalline embryo has the same value for homogenous and heterogeneous nucleation, whereas the activation energy of nucleation can be substantially smaller for heterogeneous nucleation depending on the value of θ. This is illustrated in figure 4.3, where the total Gibbs free energy change of a crystalline embryo is shown as a function of its spherical radius for homogenous and heterogeneous nucleation. At small values of wetting angle, θ ~ 20°, the activation energy, G^*_{het}, decreases by three orders of magnitude.

Then the volume rate of heterogeneous nucleation is given by a similar expression for homogenous nucleation equation 2.6:

$$I_v^{het} = N_s v_o \exp\left[-\frac{\left(q + \Delta G^*_{het}\right)}{kT}\right] \tag{4.6}$$

where N_s is the number of atoms in contact with heterogeneous nucleation sites per unit volume of liquid [1].

The heterogeneous nucleation can be further enhanced by the crevices on the surfaces of container or foreign particle walls. This type of heterogeneous nucleation can be highly effective even at high values of θ. As an example, a special case will be presented where $\pi/4<\theta<\pi/2$. Let us consider a crack with a conical shape on the container wall (or foreign particle wall). For simplicity, it will be assumed that the base angle of the cone has the same value of the "wetting angle" θ as shown in figure 4.4. It can be shown that the total Gibbs' free energy change upon formation of a crystalline embryo at the crack tip is given by

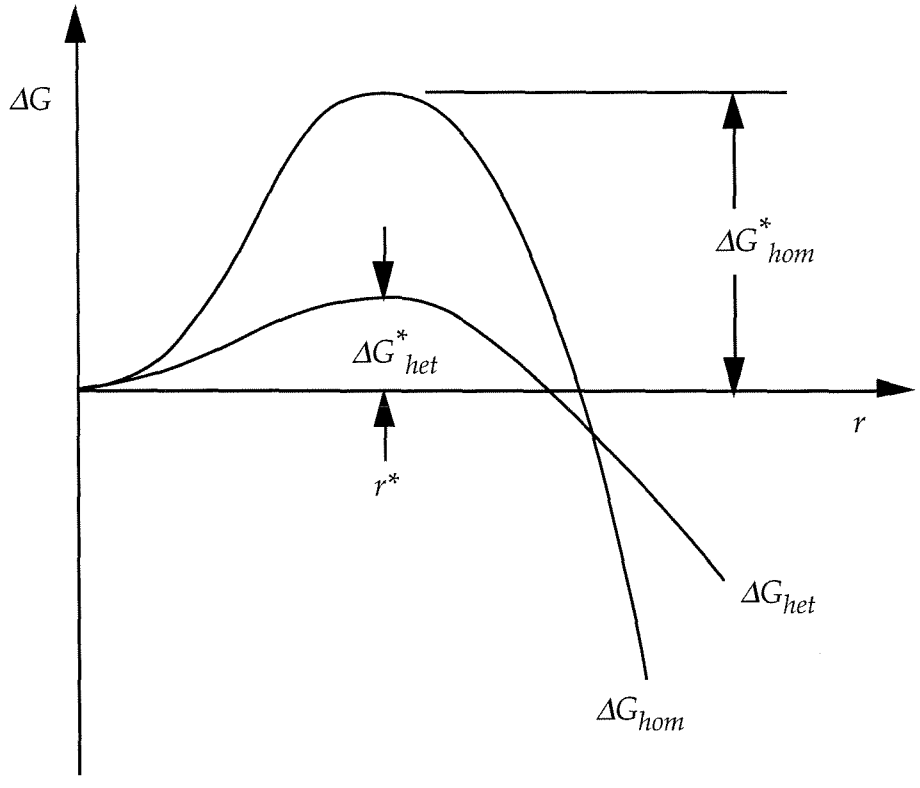

Figure 4.3: The total Gibbs' free energy change of a crystalline embryo for heterogeneous and homogenous nucleation as a function of its radius.

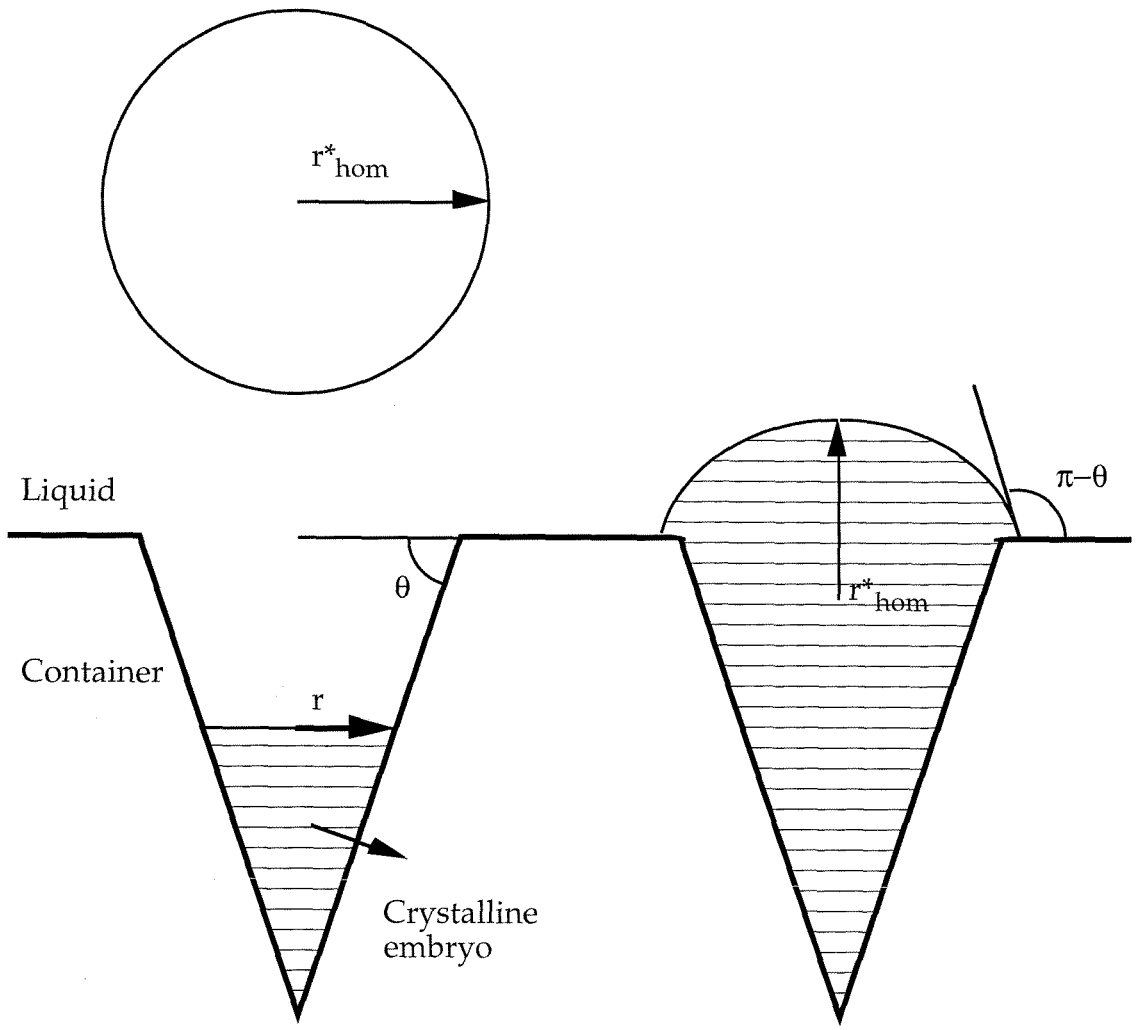

Figure 4.4: The formation of a crystalline embryo at the crack tip on a container wall (left). In this case r^*_{crack} is smaller than r^*_{hom} and the crystalline embryo can grow out of the crack into the bulk of liquid when the crack has a large enough opening radius (right). Also shown is the critical radius for homogenous nucleation, r^*_{hom}.

$$\Delta G_{crack} = \frac{\pi r^3 \tan\theta}{3}\Delta G_v + \pi r^2 \gamma_{XL}(1-\cot\theta) \tag{4.7}$$

where r is the radius of base of cone. Then, the critical radius for stable crystalline embryo at the crack tip, r^*_{crack}, is given by

$$r^*_{crack} = -\frac{2\gamma_{XL}}{\Delta G_v}\left(\frac{(\tan\theta)-1}{\tan\theta}\right) = r^*_{hom}\left(\frac{(\tan\theta)-1}{\tan^2\theta}\right). \tag{4.8}$$

From equation 4.7 we can deduce that

$$r^*_{crack} < r^*_{hom}\frac{1}{\tan\theta} < r^*_{hom}$$

for values of θ between $\pi/4$ and $\pi/2$. Thus a stable crystalline embryo with a smaller radius than r^*_{hom} can form at a crack tip. These embryos will grow from the crack tip to the crack opening. If the crack has a large enough opening radius (an opening radius of r^*_{hom} will suffice), the crystalline embryo can sustain its growth out of the crack thus starting crystallization into the bulk of liquid (figure 4.4). Otherwise the growth of the crystalline embryo will be limited to the inside of the crack. Using the general relation

$$\Delta G^* = 0.5\ V^*\ \Delta G_v \tag{4.9}$$

where V^* is the critical volume of crystalline embryo [1], we can deduce the heterogeneous nucleation if the crack tip has significantly smaller activation energy than heterogeneous nucleation on a flat wall. The above analyses can be further generalized to show that crevices on the surfaces of a container and foreign particles may greatly facilitate the heterogeneous nucleation.

4.2 Examples of heterogeneous nucleation in preparation of Zr-Ti-Cu-Ni-Be bulk glass forming system due to container walls

Figure 4.5 (a) shows an X-ray diffraction pattern taken from the as-cast surface of a 3.0 mm thick plate of $Zr_{41.2}Ti_{13.8}Cu_{12.5}Ni_{10.0}Be_{22.5}$ alloy produced by metallic mold casting. Obviously, there are glassy phases as well as crystalline phases in the cast sample. The relative amount of crystalline phases changes significantly depending on the composition of the bulk glass forming alloy and other parameters involved during processing of the alloy. What is not changing is the location of the crystalline phases within the samples. In all cases, the crystalline phases were found to be localized within the top few hundred microns of the surface layer. Progressively less crystalline phase was observed as one moves deeper from the sample surface. Figure 4.5 (b) shows the X-ray diffraction pattern of the same 3.0 mm thick $Zr_{41.2}Ti_{13.8}Cu_{12.5}Ni_{10.0}Be_{22.5}$ sample after it was polished to remove the upper 100 microns from the surface. No crystalline phases are observed within the resolution of X-ray diffraction, i.e., the sample is completely glassy in the interior. The cooling rate is generally higher at the surface of the sample as the liquid is in casual contact with the cooling medium at the surface. Based on the cooling rate considerations, one would expect crystals to form in the interior of the sample rather than at the surface if only homogenous nucleation is operational. This example is a vivid illustration of heterogeneous nucleation due to container walls in the Zr-Ti-Cu-Ni-Be bulk glass forming system. It seems that the crystals nucleate heterogeneously on the container walls but cannot grow more than a few hundred microns from the surface due to a very low crystal growth velocity. Thus, the rest of the liquid, the interior part, is left unaffected by surface heterogeneous nucleation provided no

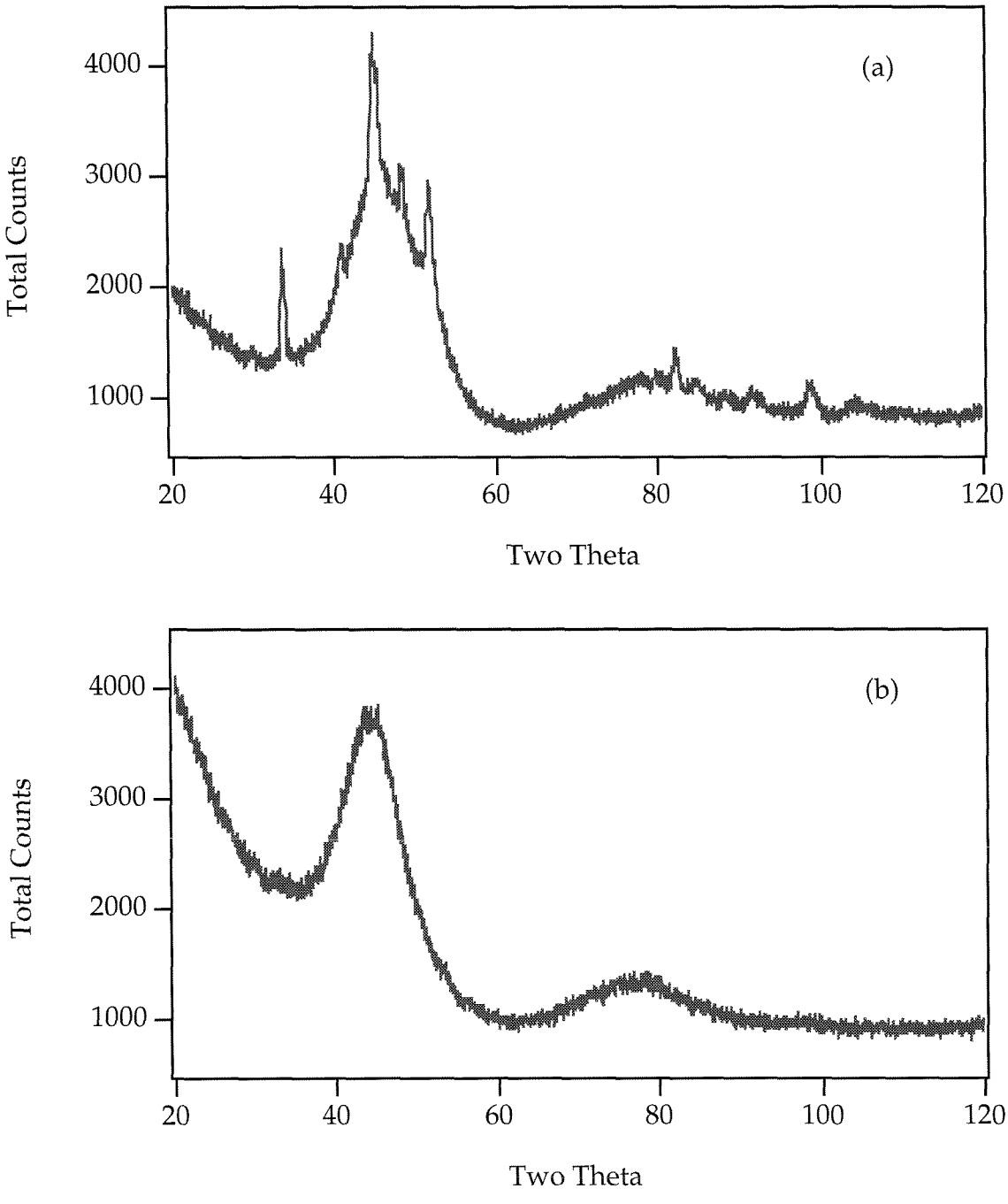

Figure 4.5: X-ray diffraction patterns taken from the surface of 3.0 mm thick $Zr_{41.2}Ti_{13.8}Cu_{12.5}Ni_{10.0}Be_{22.5}$ alloy obtained by metallic mold casting: (a) as-cast surface and (b) polished surface by 100 microns. Co Kα radiation.

other heterogeneous nucleation sites, such as oxide particles, exist in the bulk of the liquid.

However, one could argue that the polishing may damage the surface and may result in deformation induced amorphization as observed in some systems [3]. To clarify this point, two more examples will be presented. One way to avoid damaging the surface of the alloy is by using two different X-ray radiations to characterize the structure of the sample with respect to the depth from surface. A harder X-ray radiation can penetrate further into the bulk, thus giving more sampling of the interior compared to a soft X-ray radiation. This will give us a non-destructive method to find out the relative amount of crystalline phases at the surface and away from the surface. For this purpose Mo Kα and Cu Kα radiation were used. The linear absorption coefficient of Zr for Mo Kα radiation is 105 cm^{-1} whereas it is 890 cm^{-1} for Cu Kα radiation [4]. Mo Kα radiation can penetrate 8.5 times deeper into a Zr base sample than the Cu Kα radiation. For example, we can calculate from the relation [5]

$$I_x = I_0 e^{-\mu x} \tag{4.10}$$

that the intensity of Mo Kα radiation reduces to one-third of its initial value after passing through a Zr sample of ~ 100 micron thick. The corresponding thickness for Cu Kα radiation is ~ 12 microns. Thus Mo Kα radiation can give us more sampling from the interior, whereas Cu Kα radiation will sample mostly the volume close to the surface. Since Zr is the best element for this purpose (for the case of Mo Kα and Cu Kα radiation) [4], the composition of glass forming alloy is optimally set to the $Zr_{70}Ni_{7.5}Be_{22.5}$ such that all the other elements (Ti, Cu, and Ni) are minimized. Be is practically transparent to both radiations [4]. Figure

4.6(a) shows an X-ray diffraction pattern with Mo Kα radiation taken from the as cast surface of a 1.0 mm thick $Zr_{70}Ni_{7.5}Be_{22.5}$ alloy produced by metallic mold casting. Obviously there are both amorphous and crystalline phases. Figure 4.6 (b) shows the X-ray diffraction pattern with Cu Kα radiation taken from exactly the same region of the same sample. The amount of amorphous phase is drastically reduced. Again the crystalline phases are observed disproportionally on the surface. The interior of the sample has more amorphous phase. Figure 4.7 shows the X-ray diffraction pattern with Cu Kα radiation taken from the polished surface of the same sample. Only a trace amount of crystalline phases are left.

As a last example the glassy ingots produced by melting on water cooled metallic crucibles (Cu or Ag) are discussed. Figure 4.8 shows X-ray diffraction patterns taken from the various surfaces of a $Zr_{41.2}Ti_{13.8}Cu_{12.5}Ni_{10.0}Be_{22.5}$ ingot. The ingot weighs about 6 grams and it is approximately 7 mm thick. Shown in figure 4.8 (a) is a typical X-ray diffraction pattern taken from the bottom surface of the $Zr_{41.2}Ti_{13.8}Cu_{12.5}Ni_{10.0}Be_{22.5}$ ingot where casual contact with the silver (or copper) boat occurs. As evidenced by numerous Bragg peaks, the sample is crystalline on the bottom surface. Figure 4.8 (b) shows another X-ray diffraction pattern taken from a cross sectional surface of the $Zr_{41.2}Ti_{13.8}Cu_{12.5}Ni_{10.0}Be_{22.5}$ ingot parallel to the silver boat. The top surface of the ingot gives a similar X-ray diffraction pattern. The corresponding electron diffraction pattern as well as dark field and high-resolution TEM images taken from the interior of a similar ingot were already shown in chapter 3.1. The conclusion is $Zr_{41.2}Ti_{13.8}Cu_{12.5}Ni_{10.0}Be_{22.5}$ ingot is amorphous everywhere except the surface where it has contact with the container. The crystalline phases form a slight trace on the bottom of the surface.

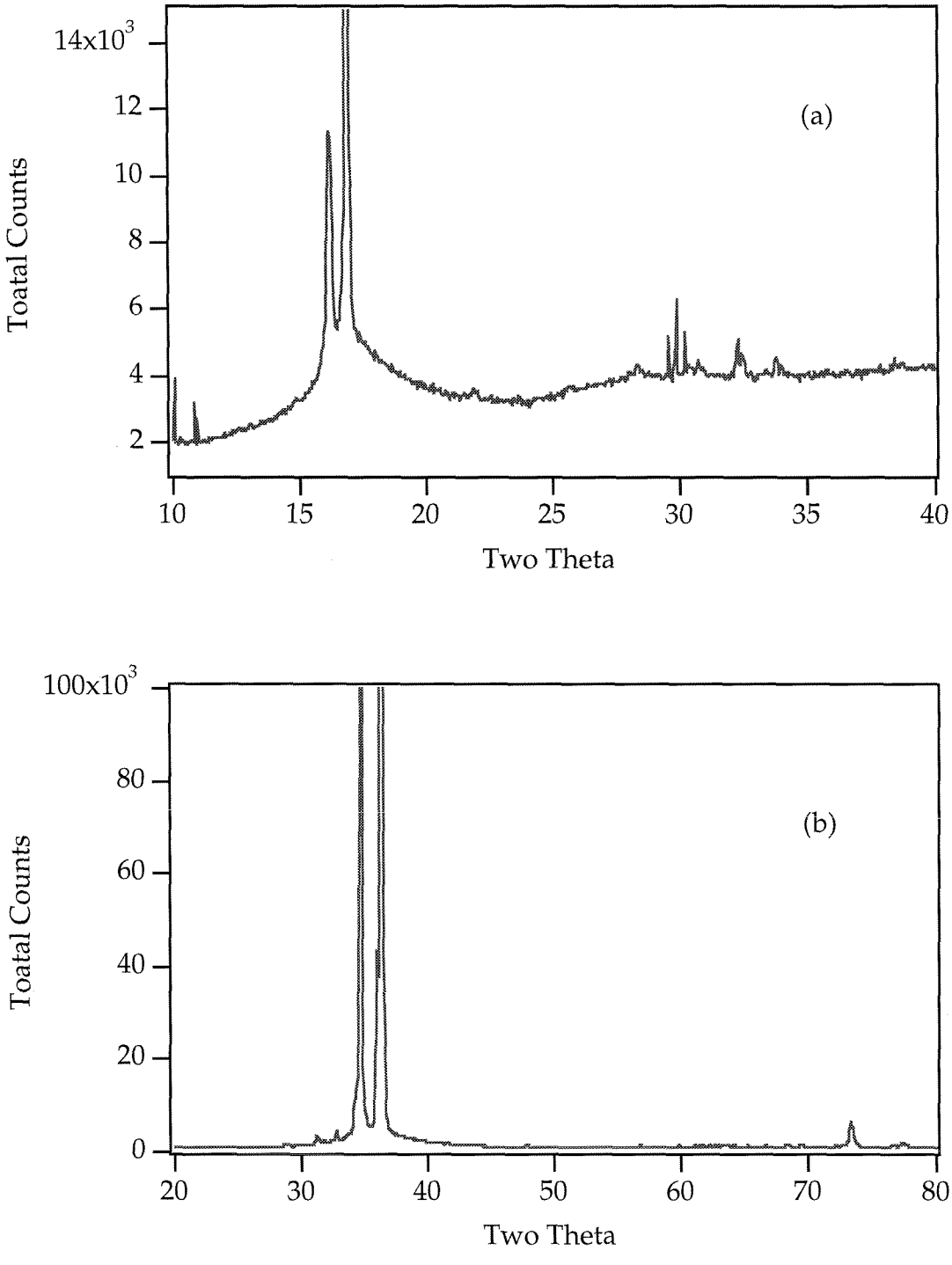

Figure 4.6: X-ray diffraction patterns with different radiation taken from the as-cast surface of 1.0 mm thick $Zr_{70}Be_{22.5}Ni_{7.5}$ alloy obtained by metallic mold casting: (a) Mo Kα radiation and (b) Cu Kα radiation.

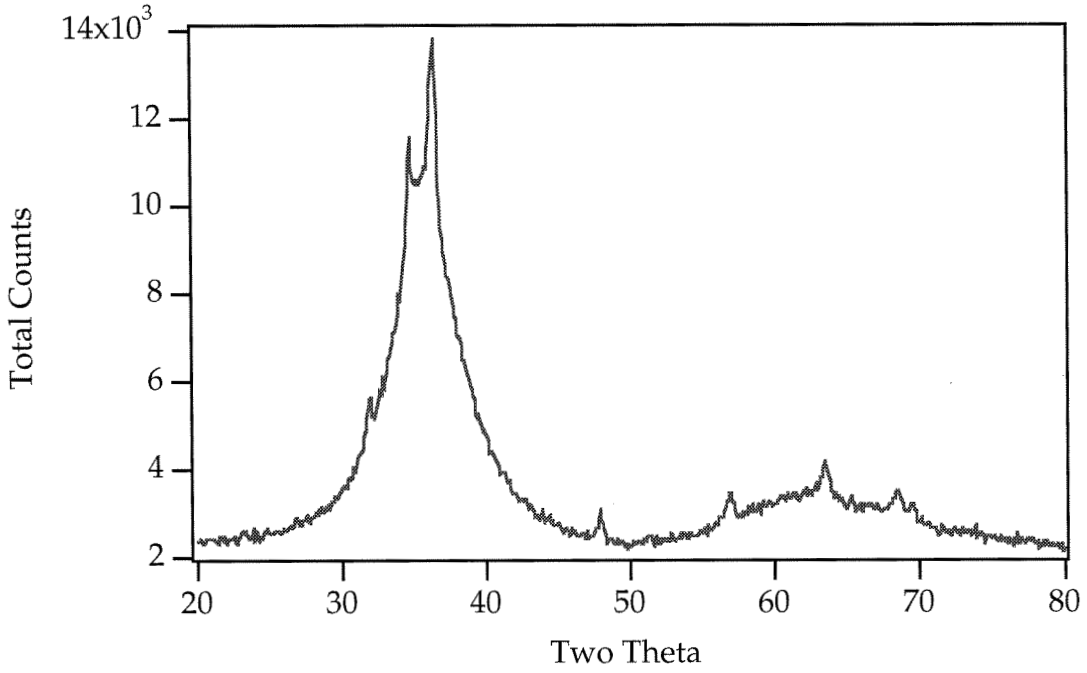

Figure 4.7: X-ray diffraction pattern taken from the polished surface (by ~100 microns) of a 1.0 mm thick $Zr_{70}Be_{22.5}Ni_{7.5}$ alloy obtained by metallic mold casting. Cu Kα radiation.

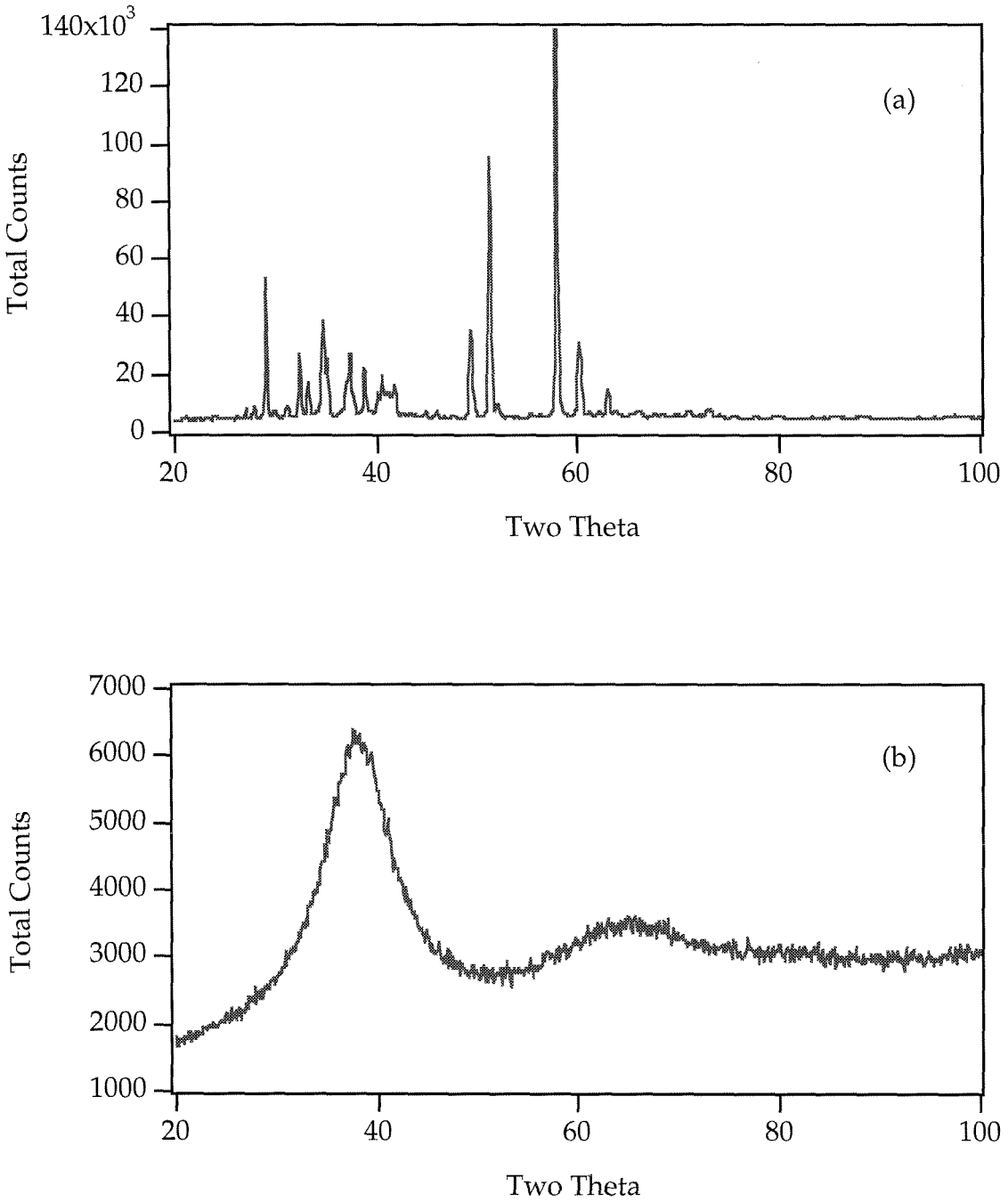

Figure 4.8: X-ray diffraction patterns taken from various parts of a 6 gram ingot of $Zr_{41.2}Ti_{13.8}Cu_{12.5}Ni_{10.0}Be_{22.5}$ alloy: (a) Bottom surface where contact with the silver boat occurs and (b) cross section surface parallel to the plane of the silver boat surface. Cu Kα radiation.

Given the above examples, how can one solve the problem of heterogeneous nucleation due to container walls if one has to use a container? The first try is to use a container which is not crystalline. When the container is amorphous, we expect a higher interfacial energy for the amorphous container-crystal interface than of the amorphous container-liquid interface, i.e., the liquid will wet the amorphous container better than the crystal. To test this idea we have used a fused silica tube as a container. The glassy nature of the fused silica also gives a relatively smoother surface compared to the crystalline surfaces, thus making heterogeneous nucleation less effective from crevices. The $Zr_{41.2}Ti_{13.8}Cu_{12.5}Ni_{10.0}Be_{22.5}$ samples were sealed in glass tubes under an inert atmosphere. After the samples were melted, the glass tube was plunged into the water and stirred until solidification was complete. The outcome was superb. No crystalline phases were observed in any part of the sample. A typical X-ray diffraction pattern of this sample is shown in figure 3.3. The wetting angle between the fused silica and glassy $Zr_{41.2}Ti_{13.8}Cu_{12.5}Ni_{10.0}Be_{22.5}$ alloy was determined to be less than 20°. This very low wetting angle evidences a very low interfacial energy between the liquid $Zr_{41.2}Ti_{13.8}Cu_{12.5}Ni_{10.0}Be_{22.5}$ and fused silica as predicted. In fact, the glassy $Zr_{41.2}Ti_{13.8}Cu_{12.5}Ni_{10.0}Be_{22.5}$ alloy and fused silica glass container made an extremely strong bond (as strong as the base glassy alloy) evidencing good wetting. This is a profound observation when we consider the extremely brittle behavior of fused silica. This strong bond could be utilized by employing silica as a reinforcing and weight reduction material in the metallic glass alloys.

Another approach to the solve surface nucleation problem is to use a container made out of a crystalline phase which can form a metastable interface with a molten glass forming alloy. For example, the growing amorphous phase and

crystalline elemental phases form metastable interfaces in the solid state amorphization of Ni-Zr diffusion couples [6,7]. Further, it is found that the equilibrium intermetallic phases almost invariably nucleate on the Zr side of the growing amorphous phase, i.e., the interface of amorphous phase and crystalline Ni seems less likely to induce nucleation [7]. Recently, our experiments reveal that similar metastable interfaces can be formed between the liquid $Zr_{41.2}Ti_{13.8}Cu_{12.5}Ni_{10.0}Be_{22.5}$ and crystalline Ti and Zr [8]. Though our work is still in progress, we have promising results showing that Ti and Zr can be used as containers in processing of Zr-Ti-Ni-Cu-Be metallic glasses. The preparation and characterization of these metastable interfaces are described in the following paragraphs.

The ingot of elemental Zr (or Ti) and previously prepared ingot of $Zr_{41.2}Ti_{13.8}Cu_{12.5}Ni_{10.0}Be_{22.5}$ alloy were put on a water cooled copper boat under a Ti-gettered inert atmosphere. Initially they were separated at a distance so that each of them can be melted separately. First, the ingot of Zr (or Ti) was melted to dissolve any surface oxide so that a clean metallic surface can be exposed. After the ingot of Zr was cooled, the ingot of $Zr_{41.2}Ti_{13.8}Cu_{12.5}Ni_{10.0}Be_{22.5}$ alloy was melted and driven onto the cold Zr ingot. This formed a strong bond between the elemental Zr and the frozen alloy. (When the joined metal piece was torn apart, the Zr failed before the interface.) The molten alloy was further frozen to the glass as evidenced by a highly reflective surface and the lack of recalescence. The glassy nature of the amorphous ingot was further confirmed by TEM and X-ray analyses. The interface between elemental Zr and glassy alloy was analyzed by a Philips EM 430 300 -keV transmission electron microscope with high resolution and analytical capabilities. Figure 4.9 shows a high resolution TEM image of this interface. As evidenced by the existence of lattice fringes on one

side and lack of lattice fringes on the other side, there are obviously both a glassy phase and a crystalline phase (which belongs to the elemental Zr) separated by an atomically sharp interface. The EDAX analyses (Energy Dispersive X-ray Spectroscopy) showed that there is no chemical mixing on the elemental Zr-side of the interface. The electron diffraction further confirmed the glassy nature of the $Zr_{41.2}Ti_{13.8}Cu_{12.5}Ni_{10.0}Be_{22.5}$ alloy side of the interface and the nature of the equilibrium crystalline phase of elemental Zr. No other crystalline intermetallic phases were observed along the interface separating the original elemental Zr from the amorphous alloy. Since the amorphous alloy was solidified from the melt at a relatively low cooling rate, we can conclude that the interface with elemental Zr is not a favorable site for hetoregeneous nucleation of crystalline intermetallic phases from the undercooled alloy melt! The undercooled liquid is in metastable equilibrium with crystalline Zr along the interface.

Figure 4.10 shows a dark field TEM image of the interface of the glassy $Zr_{41.2}Ti_{13.8}Cu_{12.5}Ni_{10.0}Be_{22.5}$ alloy and crystalline elemental Ti prepared with the same method described above. The electron diffraction confirmed the glassy nature of the $Zr_{41.2}Ti_{13.8}Cu_{12.5}Ni_{10.0}Be_{22.5}$ alloy side of the interface. Further, the EDAX analyses detected no chemical mixing on the crystalline elemental Ti-side of the interface. Thus, the glassy phase and crystalline elemental Ti are separated by a sharp boundary and no nucleated intermetallic phase has been observed from the interface. Similarly, $Zr_{41.2}Ti_{13.8}Cu_{12.5}Ni_{10.0}Be_{22.5}$ molten alloy can also form a metastable interface with elemental Ti.

If we have to use a crystalline container, removing the crevices on container walls should be very useful to prevent heterogeneous nucleation. Crevices are very effective in inducing heterogeneous nucleation even at high values of wetting

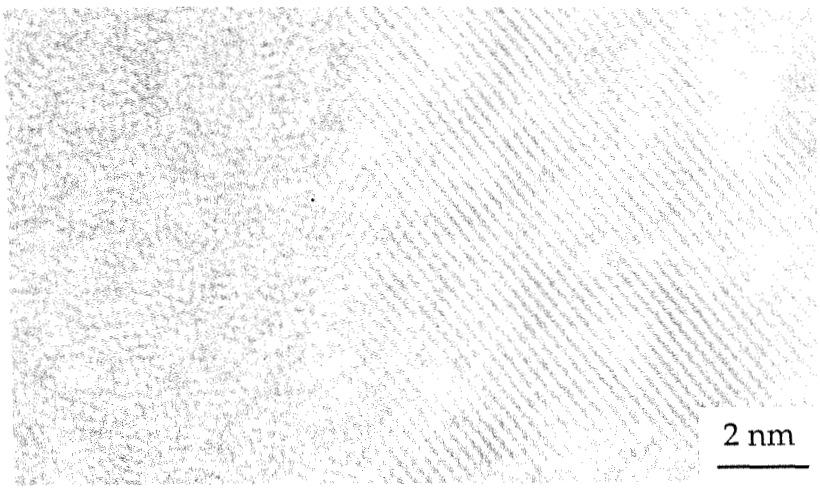

Figure 4.9: The high resolution transmission electron image of metastable interface of $Zr_{41.2}Ti_{13.8}Cu_{12.5}Ni_{10.0}Be_{22.5}$ glassy alloy with elemental Zr. Glassy alloy is on the left side.

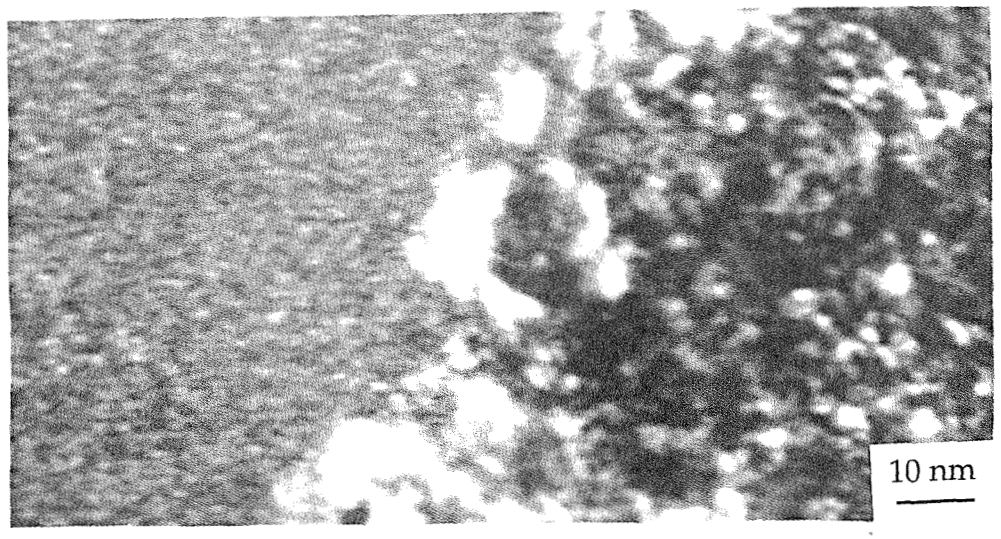

Figure 4.10: The darkfield TEM image of metastable interface of $Zr_{41.2}Ti_{13.8}Cu_{12.5}Ni_{10.0}Be_{22.5}$ glassy alloy with elemental Ti. Glassy alloy is on the left side.

angle between the crystalline embryo and container. Recently, Schwarz used an electropolished copper hearth as a water cooled metallic crucible to prepare glassy $Zr_{41.2}Ti_{13.8}Cu_{12.5}Ni_{10.0}Be_{22.5}$ ingots by plasma arc melting [9]. The electropolishing removes all the asperities and crevices on the copper hearth making an almost atomically smooth surface. According to the experiments of Schwarz, no crystalline phases were observed on the surface of these plasma melted amorphous ingots, which weigh as much as 200 grams [9].

4.3 Heterogeneous nucleation from foreign particles and its effect on bulk glass formation

We have seen in chapter 2 that the metallic alloys having a reduced glass transition temperature, $T_{rg} \sim 2/3$ (where T_m, the melting point, can be taken as the solidus temperature in the case of a general alloy), should exhibit very low rates of homogenous nucleation and should be bulk glass formers as suggested by Turnbull [10]. However, prior to 1982, no metallic glass could be made with a thickness of more than a few mm, although there were known metallic alloys having T_{rg} =0.66, such as $Pd_{40}Ni_{40}P_{20}$ and $Nb_{40}Ni_{60}$ several years earlier [11]. The main obstacle was believed to be heterogeneous nucleation due to container walls and foreign particles such as oxides. In the early eighties, Turnbull and his co-workers used fluxing to prevent heterogeneous nucleation in $Pd_{40}Ni_{40}P_{20}$ melts and obtained the largest bulk metallic glass samples at that time using cooling rates of ~1-2 K/s [12]. By contrast, no glassy alloy of $Nb_{40}Ni_{60}$ thicker than one mm has yet been obtained.

The $Zr_{41.2}Ti_{13.8}Cu_{12.5}Ni_{10.0}Be_{22.5}$ alloy, which we have discovered recently, also has T_{rg} =0.67 and bulk pieces of this alloy readily undercool to glass unlike any

other glass forming alloy. Although the alloys, $Zr_{41.2}Ti_{13.8}Cu_{12.5}Ni_{10.0}Be_{22.5}$, $Pd_{40}Ni_{40}P_{20}$ and $Nb_{40}Ni_{60}$, have almost the same T_{rg}, their bulk glass forming ability shows drastic differences. For example, the $Zr_{41.2}Ti_{13.8}Cu_{12.5}Ni_{10.0}Be_{22.5}$ alloy is prone to surface heterogeneous nucleation due to container walls, whereas no sign of any significant crystallization has been observed in its interior. The $Pd_{40}Ni_{40}P_{20}$ alloy needs a careful and delicate fluxing treatment for bulk glass formation. Otherwise, its glass forming ability is very limited. For the time being we do not know whether or not we can find a similar fluxing treatment for $Nb_{40}Ni_{60}$. These differences can be accounted for by heterogeneous crystal nucleation induced by crystalline debris incidentally existing in the bulk of the liquid. These crystalline debris can be various types of refractory particles; oxides are possibly the most common form of them. It seems that the flux used in the $Pd_{40}Ni_{40}P_{20}$ experiment, B_2O_3 which is also a glass, can dissolve the oxide particles thus eliminating heterogeneous nucleation and giving rise to bulk glass formation.

Since no flux has been used in production of $Zr_{41.2}Ti_{13.8}Cu_{12.5}Ni_{10.0}Be_{22.5}$ bulk glasses, there should be another mechanism to eliminate the heterogeneous nucleation sites in the bulk of the liquid. This can be achieved if liquid reacts with incidentally existing crystalline debris, such as oxides, and dissolves them without detrimentally effecting its bulk glass forming ability. We can examine this by intentionally introducing crystalline debris into the liquid such as by slight oxidization. To test this proposition, $Zr_{41.2}Ti_{13.8}Cu_{12.5}Ni_{10.0}Be_{22.5}$ bulk glassy ingots were oxidized in a controlled atmosphere of oxygen by heating to the melting point of the crystalline alloy on a water cooled copper boat with a levitation melting system. Upon subsequent cooling, recalescence was observed evidencing crystallization. The alloy was visibly oxidized and exhibited a rough

surface with a dark color rather than a smooth and reflecting surface unique to the glassy phase. The oxidizing atmosphere was then replaced with a clean inert atmosphere as in the routine preparation of glassy ingots. In the next few heating and cooling cycles (from ambient temperature to the melting point), the alloy crystallized on cooling. This could be easily detected by the final surface luster and recalescence during cooling. Solid particles, most probably oxides, were also observed floating on the surface of the liquid. After keeping the alloy above the melting point for a few minutes, it was observed that these oxide particles gradually dissolved. Following the dissolution of the oxide debris, the alloy again froze to glass upon subsequent cooling. We have found that liquid samples as large as 9 grams can dissolve up to 1 atom percent oxygen (as detected by weight measurements) and still form glass on a water cooled metallic crucible as easily as non-oxidized samples, provided that all solid oxide debris is dissolved in the melt before cooling.

It can be said that Zr and Ti have the distinguishing property of forming crystalline solid solutions with oxygen content up to 30 atom percent. This large oxygen solubility [13] may eliminate the oxide formation which creates the sites for heterogeneous nucleation. We believe that what is significant is not the oxygen solubility in solid solutions, but rather oxygen solubility in undercooled liquid! The maximum oxygen solubility in undercooled liquid Zr can be estimated from the metastable liquidus line of *ZrO* in the Zr-O phase diagram [13]. The metastable liquidus line can be constructed by extending the thermodynamic liquidus line of *ZrO* in the direction of less oxygen in the Zr-O phase diagram. This also approximately gives the equilibrium and metastable liquidus line of *ZrO* in a Zr- base alloy which has a very depressed melting point such as $Zr_{41.2}Ti_{13.8}Cu_{12.5}Ni_{10.0}Be_{22.5}$. This is illustrated in figure 4.11. The

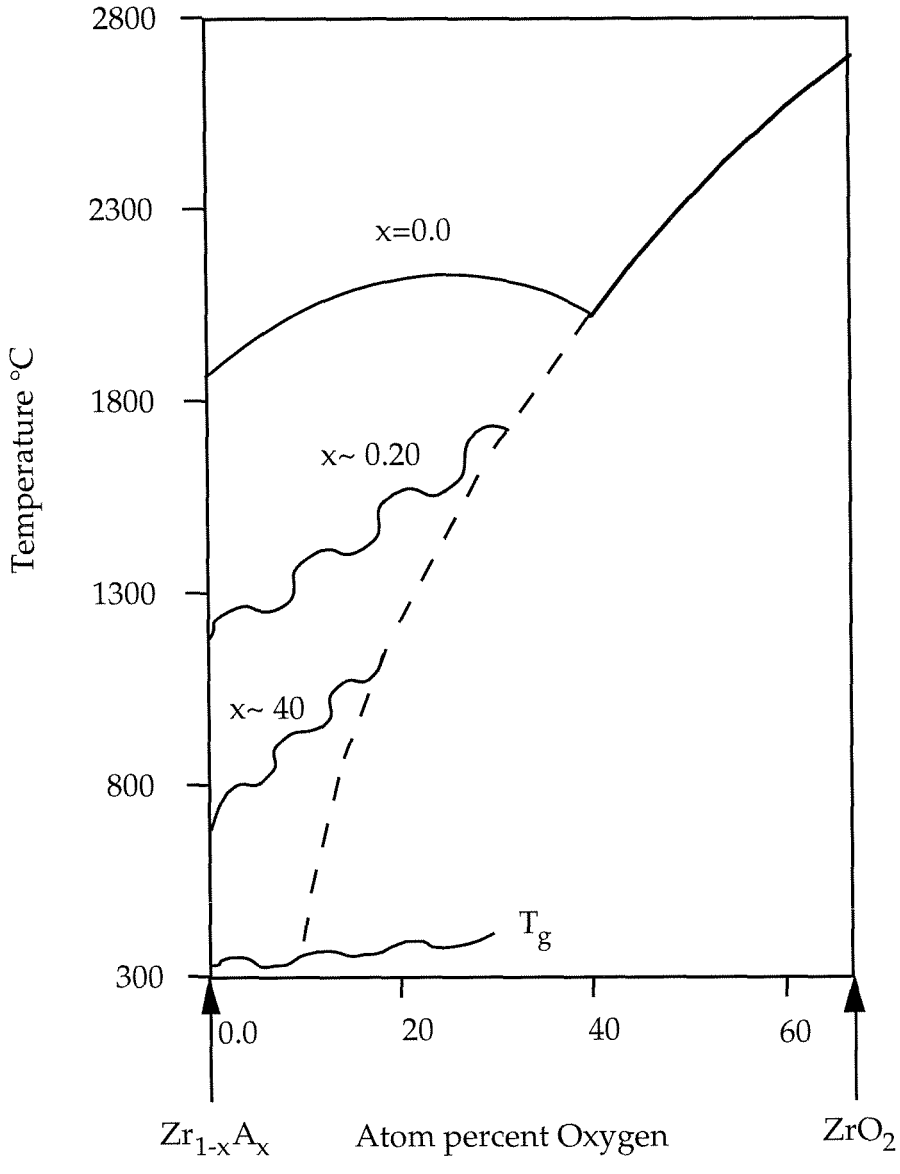

Figure 4.11: Construction of metastable liquidus line of ZrO_2 in a Zr alloy. "A" corresponds to an alloying element(s) which depresses the liquidus line of Zr base crystalline solid solutions.

metastable liquidus line suggests a maximum oxygen content of ~10 atom percent at 350 °C and ~20 atom percent at 1100 °C in the undercooled liquid Zr or Zr base alloy. (The additional alloying elements may have detrimental effects on the oxygen solubility in the liquid Zr-base alloy, thus overestimating the maximum oxygen content.) The oxide, *ZrO*, starts to precipitate from the melt at higher oxygen content. These oxide precipitates will serve as heterogeneous nucleation sites for further crystallization.

Let us consider the $Zr_{41.2}Ti_{13.8}Cu_{12.5}Ni_{10.0}Be_{22.5}$ alloy which has a glass transition temperature, T_g = 350 °C. When this alloy was kept above its melting point for a certain time in a reasonably clean atmosphere, all the incidentally existing oxygen should be dissolved in the liquid. As we cool down the liquid, no oxides should precipitate down to the glass transition temperature provided the oxygen content is low enough. Upon further cooling, the undercooled liquid configurationally freezes to glass below the glass transition temperature, 350 °Ç. As the metastable liquidus line of ZrO suggests, the amount of oxygen that can be dissolved in the undercooled liquid $Zr_{41.2}Ti_{13.8}Cu_{12.5}Ni_{10.0}Be_{22.5}$ down to 350 °C is significantly larger than the amount of oxygen incidentally existing in an alloy which is prepared in a reasonably clean atmosphere. This is also demonstrated by the experiment presented above. When all the incidentally existing oxides are dissolved in the liquid and the precipitation of oxides is hindered thermodynamicaly at lower temperatures, there will not be any heterogeneous nucleation sites, thus making bulk glass formation much easier. We have found that the Zr-Ti-Cu-Ni-Be system has an exceptionally large bulk glass forming range [14]. Further, the bulk glass forming alloys are extremely forgiving to impurities in the constituent raw elements [15]. In fact, a substantial

amounts of elements other than Zr, Ti, Cu, Ni and Be can be added to this system without damaging the bulk glass formation [14]. All of these observations suggest that the Zr-Ti-Cu-Ni-Be bulk glass forming alloy will tend to react with any crystalline debris incidentally existing in the liquid state provided necessary time and temperature are provided. The dissolving of the crystalline debris will not affect the bulk glass formation as the alloy system has a large bulk glass formation range including elements other than its constituents.

In the case of $Nb_{40}Ni_{60}$ and $Pd_{40}Ni_{40}P_{20}$, the maximum solubility of oxygen in the undercooled liquid should be extremely low. This can be shown from the phase diagrams of Ni-O and Nb-O [12]. The liquidus lines of NbO and NiO exhibit a shallow depression with lowering oxygen content, i.e., the oxygen content of the liquidus lines of oxides of Nb and Ni decreases very rapidly with respect to temperature. We can roughly construct the metastable liquidus lines for these systems as described above. The case of Nb-A-O has been illustrated in figure 4.12, where A stands for an element depressing the liquidus line of a Nb alloy (such as Ni). As seen in figure 4.12, the metastable liquidus line of NbO reaches ~0.0 percent oxygen content at temperatures ~ 1000 °C. At higher temperatures the Nb-base liquid has some increasing solubility of oxygen with increasing temperature (e.g., a few percent at 1300 ° C). The case of Ni also shows very similar behavior. For liquid alloys having an oxygen content > 0, oxides will precipitate at lower temperatures (below 1000 °C), whereas all the oxygen can be dissolved in the liquid at high temperatures. This is possibly the cause of heterogeneous nucleation in $Nb_{40}Ni_{60}$ and $Pd_{40}Ni_{40}P_{20}$ alloys. The liquid alloys can pick up and dissolve some small amount of oxygen at high temperatures employed in the alloy preparation (or its constituent elements). However, crystalline oxides will precipitate in the undercooled liquid thus inducing

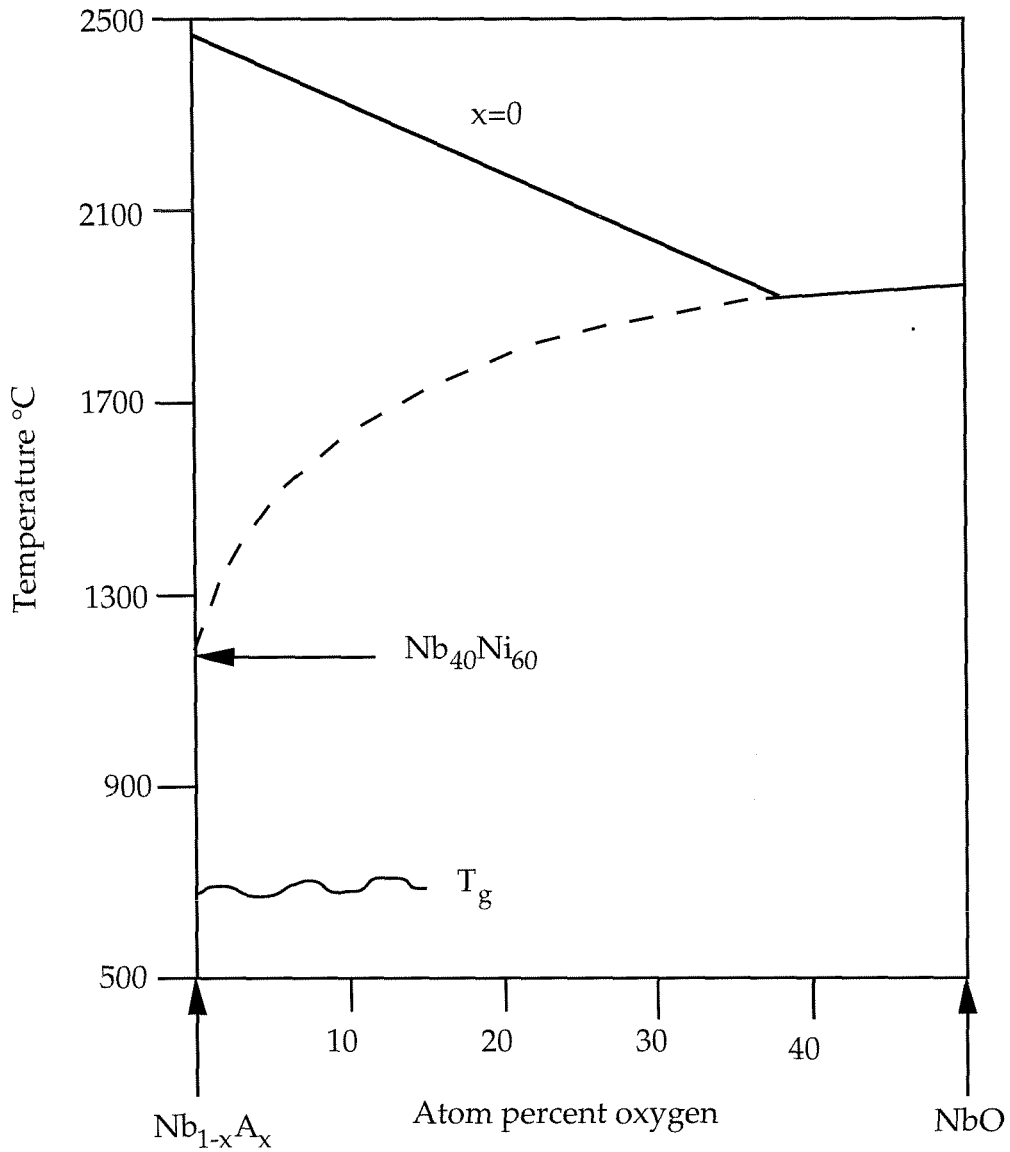

Figure 4.12: Construction of metastable liquidus line of NbO in a Nb alloy. "A" corresponds to an alloying element(s) which depresses the liquidus line of Nb base crystalline solid solutions.

heterogeneous nucleation sites even at the very small oxygen concentrations suggested by the phase diagrams.

We can further elaborate our discussion to account for the success of fluxing in $Pd_{40}Ni_{40}P_{20}$ bulk glass formation and for predicting whether or not we can have similar success for $Nb_{40}Ni_{60}$. It was found that the equilibrium crystalline compounds of $Nb_{40}Ni_{60}$ can dissolve a significant amounts of oxygen such as η phase, $Nb_{50}Ni_{50}O_x$ (W_3Fe_3C type) [16]. Thus the oxygen (or oxide particles) will be dissolved in crystalline compounds upon crystallization of $Nb_{40}Ni_{60}$. As the liquid state can also dissolve a significant amount of oxygen above the melting point, the fluxing medium will not have any chance to dissolve any oxide particles and will not be effective. Alternatively, the oxygen (oxide particles) should not be dissolved by crystalline compounds for fluxing techniques to be effective. It seems that the oxides of $Pd_{40}Ni_{40}P_{20}$ precipitate and stay separate from the equilibrium compounds. This will allow the oxide particles to be dissolved by the fluxing medium (B_2O_3) allowing bulk glass formation.

Finally, I would like to point out that the $Zr_{41.2}Ti_{13.8}Cu_{12.5}Ni_{10.0}Be_{22.5}$ alloy is ideally suited for containerless undercooling experiments in view of the experimental observations presented in the last two sections of this chapter. That is, there are no effective heterogeneous nucleation sites in the interior of the molten alloy. Further, surface nucleation is caused by container walls. The earlier undercooling experiments in undercooled metallic melts were severely limited by heterogeneous nucleation and high critical cooling rates for glass formation. In our experiments the critical cooling rate of $Zr_{41.2}Ti_{13.8}Cu_{12.5}Ni_{10.0}Be_{22.5}$ was estimated to be less than 5 K/s. This number has been estimated for the conditions where effective heterogeneous nucleation

sites, such as container walls, exist. We believe that the critical cooling rate of this system may be several orders of magnitude less when the condition of homogenous nucleation is achieved. This extremely low cooling rate for glass formation is good enough for any conceived undercooling experiment to cover the whole temperature range from the glass transition to the melting point. This allows us to perform a true test of the homogenous nucleation theory in the high undercooling regime of this alloy in a containerless experiment, such as in the TEMPUS facility in the Space Shuttle. For example, undercooling of 3 mm diameter liquid balls of $Zr_{41.2}Ti_{13.8}Cu_{12.5}Ni_{10.0}Be_{22.5}$ alloy down to the glass transition has recently been realized in containerless undercooling experiments made possible by the high vacuum electrostatic levitation unit at the Jet Propulsion Laboratory [16]. In the experiments, the sample cools only by radiation. The estimated cooling rates are about 5 K/s.

4.4 Heterogeneous nucleation and thermal stability of metallic glasses

We have seen in the previous chapter that the TTT diagrams suggest a higher thermal stability above glass transition for metallic glasses requiring lower cooling rates provided there exists a single mode of crystallization at all temperatures. In practice, this may not be achieved as different crystallization modes may become effective at high temperatures (around melting point) and low temperature (around glass transition). For example, there is a significant difference between observed thermal stability of glassy $Zr_{41.2}Ti_{13.8}Cu_{12.5}Ni_{10.0}Be_{22.5}$ alloy above the glass transition and the predicted thermal stability from the TTT diagram (which is constructed according to the observed critical cooling rate). This was attributed to a more effective nucleation

of crystals induced by oxidation of glassy alloy around the glass transition temperature. However, it was just demonstrated that there is a significant oxygen solubility in undercooled liquid $Zr_{41.2}Ti_{13.8}Cu_{12.5}Ni_{10.0}Be_{22.5}$, and this plays an important role in its bulk glass formation by melt quenching through elimination of heterogeneous nucleation from oxide particles. These two apparently conflicting observations can be explained easily when we consider the temperature dependence of the diffusion of oxygen into the bulk of the undercooled liquid. Recall that it takes some time to dissolve the oxide particles at the melting point in the oxidation experiment presented above. When we quench the $Zr_{41.2}Ti_{13.8}Cu_{12.5}Ni_{10.0}Be_{22.5}$ alloy from the melt, it is always sealed in a closed container under a reasonably clean inert atmosphere. Since the liquid can dissolve all the incidentally existing oxygen (not more than a few ppm) in a reasonably short time, the diffusion of oxygen at the melting temperature is expected to be relatively fast. Meanwhile, the DSC (Differential Scanning Calorimetry) and other annealing experiments suggest that the $Zr_{41.2}Ti_{13.8}Cu_{12.5}Ni_{10.0}Be_{22.5}$ glassy alloy has limited diffusion of oxygen at low temperatures (around the glass transition). For example, we have observed that an oxide layer grows on $Zr_{41.2}Ti_{13.8}Cu_{12.5}Ni_{10.0}Be_{22.5}$ glassy samples above 400 °C during our thermal analyses which is carried under a nominally pure flowing argon atmosphere. As the glassy alloy has no means to dissolve this oxide layer (unless heated to the elevated temperatures), this growing oxide layer may induce nucleation of crystals. Such oxidation can be suppressed by fluxing the sample surface with a layer of borosilicate-glass or encapsulation in a thin glass ampoule. A small sample of $Zr_{41.2}Ti_{13.8}Cu_{12.5}Ni_{10.0}Be_{22.5}$ alloy (~40 mg) was sealed in borosilicate-glass tube and heated. Since borosilicate glass softens around the melting temperature of $Zr_{41.2}Ti_{13.8}Cu_{12.5}Ni_{10.0}Be_{22.5}$ alloy, the

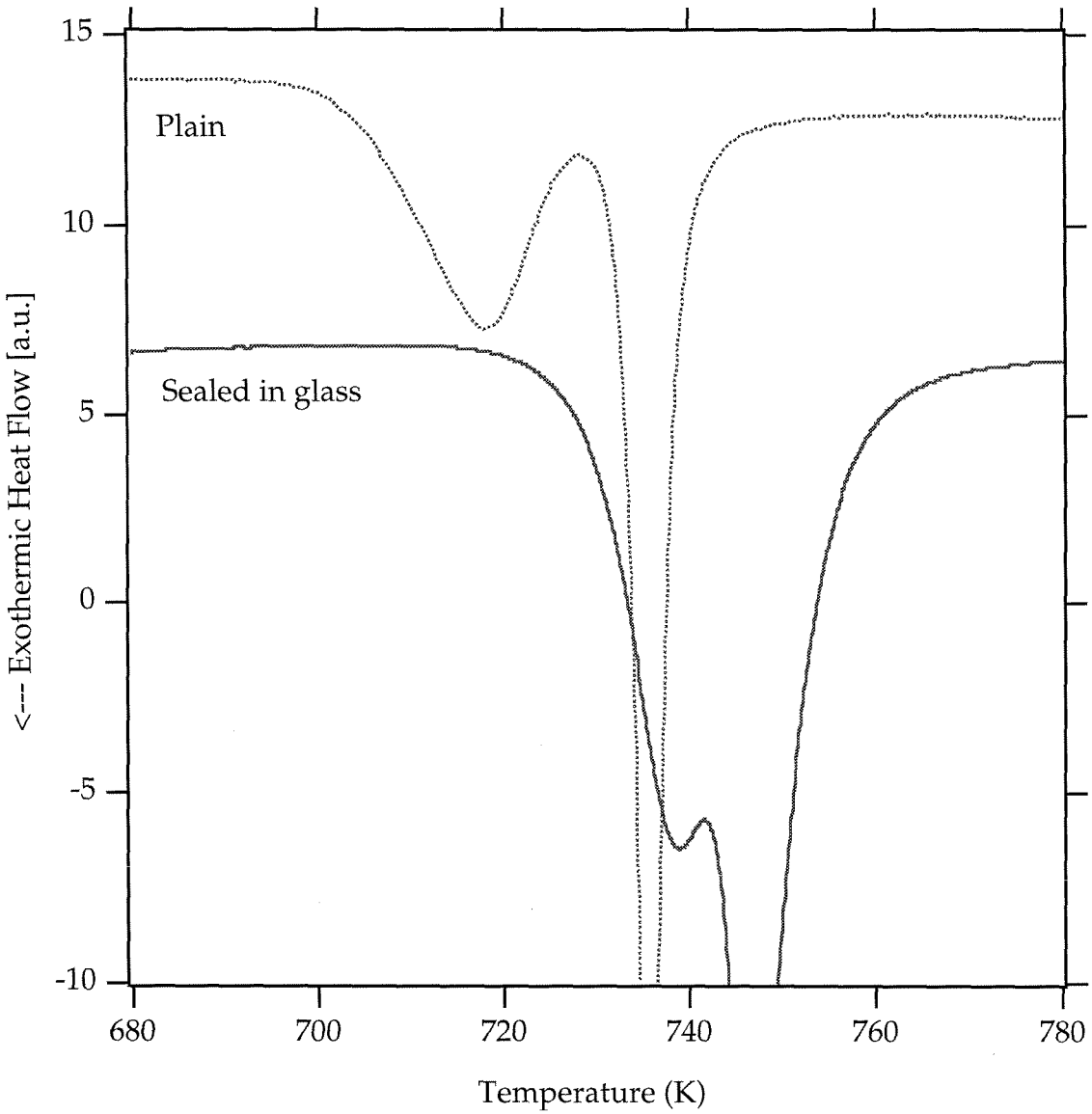

Figure 4.13: DSC scans of two $Zr_{41.2}Ti_{13.8}Cu_{12.5}Ni_{10.0}Be_{22.5}$ glassy alloys at a heating rate of 20 K/min. The dashed curve corresponds to a plain glassy sample whereas the solid curve is for a glassy sample sealed in a borosilicate-glass ball.

sample can be completely covered with a thin shell of glass. The molten sample was then water quenched resulting in a glassy sample sealed in a borosilicate-glass ball. When this is done, surface oxidation is suppressed and contact with the aluminum DSC pan is prevented. The crystallization peaks of the amorphous alloy as observed by DSC shift to significantly higher temperatures under these conditions. Figure 4.13 shows DSC scans of two $Zr_{41.2}Ti_{13.8}Cu_{12.5}Ni_{10.0}Be_{22.5}$ glassy alloy samples at a heating rate of 20 K/min. One of the samples is sealed in a borosilicate-glass ball as described above, and the other is a plain glassy sample used in routine thermal analyses experiments. Obviously, the sealed glassy sample crystallizes at temperatures 20-30 °C higher than the plain glassy sample. However, this sealing technique has limitations at higher temperatures as the borosilicate-glass layer cracks due to thermal expansion and accompanying thermal stresses.

The mechanism of nucleation of crystals induced by oxidation requires further explanation. There is increasing experimental evidence which suggests that the nucleation of crystals may occur as a result of a composition shift at the surface driven by selective oxidation. This is not the same as the heterogeneous nucleation described in the beginning of this chapter in which the nucleation of crystals is eased by the reduced effective interfacial energy rather than by a composition shift in undercooled liquid. For example, the study of the surface of the glassy $Zr_{41.2}Ti_{13.8}Cu_{12.5}Ni_{10.0}Be_{22.5}$ alloy by XPS (X-ray photoemission spectroscopy) technique has shown that the surface oxide contains only elements of Zr, Ti, Be. As the oxide layer grows, other elements, Ni and Cu, are expelled into the interior from surface oxide layer [18]. Zr, Ti and Be have high negative free energy for the formation of oxides [19]. It seems that the growing oxide

layer cannot accommodate any elements with low negative free energy of oxide formation. Quite possibly, there exists a quaternary oxide of Zr-Ti-Be-O with a still higher negative free energy for formation as suggested by the Ti-Be-O system [20]. This will further encourage the rejection of Ni and Cu from the oxide layer. The depletion of Ni and Cu in the surface layer (and Ni and Cu enrichment in the layer beneath the oxide surface) will drive this region out of the good glass forming range. Then the nucleation of crystals may occur much more easily in these compositionally altered regions. Crystallization may occur either homogeneously or heterogeneously (provided the growing oxide layer is crystalline).

Schneider et al. also observed that the growing native oxide layer on $Zr_{55}Ni_{25}Al_{20}$ glassy alloys does not contain Ni [21]. The oxide of the glassy alloy contains only Zr and Al which have comparable heat of formation of oxides (both much higher than Ni). Their observations further suggest that the oxide growth is in fact limited by the uphill diffusion of Ni into the amorphous matrix. As the growing oxide was found to be amorphous in the early stages, they proposed that the crystallization of the glassy alloy is started by an unfavorable glass forming composition shift beneath the oxide layer.

This type of crystallization was previously observed in other systems such as in glassy $Fe_{90}Zr_{10}$ alloys [22]. Selective oxidation of Zr occurs as it has a high affinity for oxygen. Then a Zr depleted region forms locally at the surface of glassy ribbons which results in crystallization of α-Fe at temperatures much lower than otherwise required for primary crystallization.

The effect of oxidation on thermal stability of glassy alloys depends on the temperature at which the oxidation starts. If oxidation starts below the glass

transition temperature, its detrimental effect on the thermal stability of the glassy alloy can be quite significant. As different elements in the glassy alloy will have different affinities for oxygen, we expect a strong temperature dependence of oxidation on composition. For example, Altonian etal observed that severe oxidation of $Zr_{50}Cu_{50}$ starts around 500 °C in DSC experiments [23]. In fact, they observed that this oxidation starts after crystallization of the glassy alloy. In this case the thermal stability of $Zr_{50}Cu_{50}$ glassy alloy is least affected by oxidation as the glass transition of this alloy is around 400 °C. When we introduce another element which has a higher oxygen affinity to these glassy alloys, the thermal stability of the new glassy alloy may change unfavorably even though it may become a better glass former. To illustrate this, I will give three good glass forming alloys as examples. Their compositions, estimated critical cooling rates $\dot{T}_c$, reduced glass transition temperatures T_{rg}, and thermal stabilities above glass transition as quantified by $\Delta T = T_x - T_g$ are given table 4.1. The corresponding DSC scans of the glassy alloys are also shown in figure 4.14. The replacement of Zr by Ti effectively reduces the critical cooling rate for glass formation. Our previous analyses of the TTT diagrams suggest that the thermal stability of glassy alloy should favorably increase in parallel with the lower critical cooling rate provided the same mode of crystallization remains effective from the glass transition temperature to the melting point. The initial increase in thermal stability of glassy alloys with Ti addition is in good agreement with this prediction. However, the further replacement of Zr by Ti deteriorates the thermal stability of glass alloys while it still lowers the critical cooling rate. The $(Zr_{0.65}Ti_{0.35})_{55}Cu_{7.5}Ni_{10.0}Be_{27.5}$ glassy alloy has a critical cooling rate at least two orders of magnitude less than the $Zr_{55}Cu_{7.5}Ni_{10.0}Be_{27.5}$ glassy alloy, though it has a relatively poor thermal stability above glass transition. These observations

can be explained by oxidation above the glass transition as seen in the thermal stability of $Zr_{41.2}Ti_{13.8}Cu_{12.5}Ni_{10.0}Be_{22.5}$ metallic glass. It seems that Ti has a higher affinity for oxygen than that of Zr at lower temperatures, i.e., around the glass transition temperature. This will result in oxidation of $(Zr_{1-x}Ti_x)_{55}Cu_{7.5}Ni_{10.0}Be_{27.5}$ glassy alloy at lower temperatures, when the Ti concentration is high enough to govern the oxidation of the glassy alloy. This oxidation may induce crystallization by heterogenous nucleation on forming oxide or by the selective oxidation mechanism described above. All these observations suggest that the thermal stability and glass forming ability of glassy alloys cannot generally be correlated from our routine DSC experiments.

Table 4.1: Various properties of three highly processable metallic glasses.

Alloy composition	T_{rg}	ΔT	$\dot{T}_c$
$Zr_{55}Ni_{10}Cu_{7.5}Be_{27.5}$	~ 0.60	~ 110 K	~ 500 K/s
$(Zr_{0.85}Ti_{0.15})_{55}Ni_{10}Cu_{7.5}Be_{27.5}$	-	~ 125 K	~ 50 K/s
$(Zr_{0.65}Ti_{0.35})_{55}Ni_{10}Cu_{7.5}Be_{27.5}$	~ 0.67	~ 70 K	~ 5 K/s

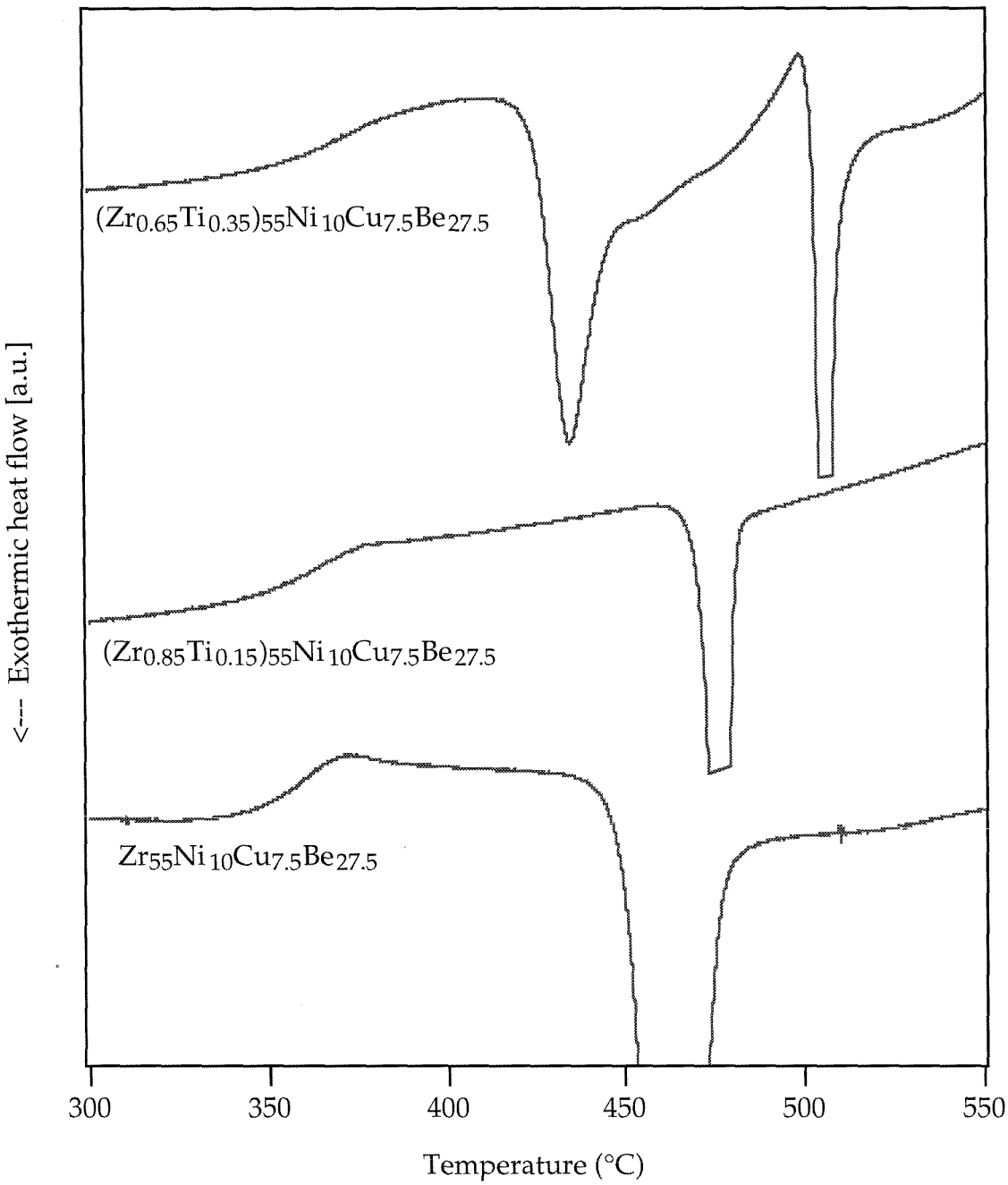

Figure 4.14: DSC scans of three bulk glassy alloys at a heating rate of 20 K/min.

References

[1] D. A Porter and K. E. Easterling, *Phase Transformations in Metals and Alloys* (Van Nostrand Reinhold International, England, 1981), Chap. 4.

[2] W. Kurz and D. J. Fisher, *Fundamentals of Solidification* (Trans Tech Publications, Switzerland, 1986), Chap. 2.

[3] Phil Ashkenazy, Ph.D. Thesis, California Institute of Technology (1992).

[4] B. D. Cullity, *Elements of X-Ray Diffraction*, 2nd ed. (Addison- Wesley Publishing Company, Inc., 1978), p. 512-513.

[5] B. D. Cullity, *Elements of X-Ray Diffraction*, 2nd ed. (Addison- Wesley Publishing Company, Inc., 1978), p. 13.

[6] W. L. Johnson, Mat. Sci. Engg, **97**, 1 (1988).

[7] W. L. Johnson, Prog. Mater. Sci., **30**, 81 (1986).

[8] A. Peker, C. Garland, and W. L. Johnson, unpublished research (1993-1994).

[9] R. B. Schwarz, Los Alamos National Laboratory (private communication, October 1993).

[10] D. Turnbull, Contemp. Phys., **10**, 473 (1969).

[11] H. A. Davies, in *Rapidly Quenched Metals III*, B. Cantor (ed.) (Metals Soc., London, 1978), Vol. 1, p. 1.

[12] H. W. Kui, A. L. Greer, and D. Turnbull, Appl. Phys. Lett., **45**, 615 (1984).

[13] T. B. Massalski, *Binary Alloy Phase Diagrams* (American Society of Metals, Metals Park, OH, 1986).

[14] A. Peker and W. L. Johnson, U.S. Patent No. 5,288,344, assigned to California Institute of Technology (Feb. 1994).

[15] A. Peker and W. L. Johnson, unpublished research (1993).

[16] D. E. Polk, C. E. Dube, and B. C. Giessen, in *Rapidly Quenched Metals III*, B. Cantor (ed.) (Metals Soc., London, 1978), Vol. 1, p. 220.

[17] Y. Kim, W. Q. Rim, and W. L. Johnson, Jet Propulsion Laboratory and California Institute of Technology (private communication, February 1994).

[18] M. LaMadrid, A. Peker, R. Houseley, and W. L. Johnson, unpublished research (1993-1994).

[19] F. S. Galasso, *Structure and Properties of Inorganic Solids* (Pergamon Press Inc., New York, 1970).

[20] B. C. Giessen, J. C. Barrick, and L. E. Tanner, Mat. Sci. Engg, **38**, 211 (1979).

[21] S. Schneider, X. Sun, M.-A. Nicolet, and W. L. Johnson, California Institute of Technology (private communication, January 1994).

[22] U. Koster and U. Schunemann, in *Rapidly Solidified Alloys: Processes, Structures, Properties, Applications*, H. H. Liebermann (ed.) (Marcel Dekker Inc., New York, 1993).

[23] Z. Altounian, T. Guo-hua, and J. Strom-Olsen, J. Appl. Phys., **53**, 4755 (1982).

Chapter 5

Conclusion: How to find bulk metallic glasses

Crystallization from the liquid state involves two processes: nucleation and growth of crystalline nuclei. Obviously, glass will form easily when there is no detectable nucleation of crystals as the liquid cools from its thermodynamic freezing point to the glass transition. Slow crystal growth kinetics will also result in glass formation in the case that crystals nucleate, provided that nucleation is not copious. (Slow crystal growth velocities are especially favored when heterogeneous nucleation is effective.) As such, bulk glass forming systems should have slow kinetics for either nucleation or crystal growth, compared to conventional metallic glass forming alloys. To design bulk glass forming systems, we must then determine the thermodynamic parameters governing the kinetics of nucleation and crystal growth and their critical values required for slow kinetics. This was the subject of chapter 2, and here it will be revisited briefly. Accordingly, we can use this knowledge in engineering (or explaining) bulk glass forming systems.

First consider the kinetics of homogenous nucleation. The rate of homogenous nucleation is given by [1]

$$I_v = \frac{A}{\eta(T)} \exp\left(-B \frac{\gamma_{XL}^3}{\Delta G_v^2} \right). \tag{5.1}$$

Here, the atomic mobility is assumed to be inversely proportional to viscosity. Metallic liquids have viscosity values typically 0.01 -10 poise around the melting point. This corresponds to adequately high atomic mobility for nucleation of crystals provided the thermal activation barrier is small. However, the homogenous nucleation rate is generally too small to detect at low undercooling ($\Delta T_r < 0.2$) for metallic systems. This is due to the fact that $\Delta G_v^2 / \gamma_{XL}^3$ is very small and positive definite just below T_m, the thermodynamic melting point. On the other hand, the liquid is assumed to be frozen (i.e., no atomic mobility) just below glass transition where the viscosity is assumed to be 10^{13} poise. Thus, no homogenous nucleation is expected below the glass transition temperature. The viscosity therefore becomes the governing factor for the homogenous nucleation rate at large values of undercooling. As the rate of homogenous nucleation is inversely proportional to the viscosity, a steeply rising viscosity from the melting point down to the glass transition will give rise to a suppressed homogenous nucleation rate. A narrower region between the melting point and glass transition will yield a relatively more steeply rising viscosity from the melting point downward for a given form of viscosity-temperature relation. Turnbull quantified this by introducing the reduced glass transition temperature [2]. Assuming a Fulcher type viscosity-temperature relation, he showed that the homogenous nucleation rate becomes too small to detect, thus allowing bulk glass formation, when reduced glass transition T_{rg} approaches 0.67. It should be kept in mind that these numbers strongly depend on the assumed functional form of viscosity with respect to the temperature (or undercooling). However, a higher reduced glass transition temperature is always favorable for lower homogenous nucleation rates, whatever the functional form of viscosity.

The crystal growth velocity is also inversely related to viscosity. The corresponding equation for partitionless growth is given by [1,3]

$$u_c = \frac{A}{\eta(T)}\left[1-\exp\left(-\frac{\Delta G_m}{RT}\right)\right]. \qquad (5.2)$$

Other types of crystal growth velocities (eutectic and dendritic) should have a similar dependence on viscosity. Again, a high reduced glass transition temperature (a steeply rising viscosity from the melting point) is favorable for better glass formation.

The glass transition temperature has generally been found to be slowly varying with composition. Thus, deep eutectic systems are invariably associated with a high reduced glass transition temperature and in turn with good glass formation. Deep eutectic systems possess other benefits for glass formation besides high reduced glass transition. For example, relatively large values of viscosity and relatively low values of the entropy of fusion have been found in deep eutectic systems around the melting point (possibly due to ordering of liquid). These will favor better glass formation through low nucleation rates and low crystal growth velocities as suggested by equations 5.1 and 5.2. In addition to these, the eutectic type of growth itself may favor glass formation substantially since its kinetics are much slower compared to other growth types (e.g., partionless growth). Boettinger, for instance, has demonstrated that there is a maximum crystal growth velocity for eutectic crystallization of $Pd_{77.5}Cu_6Si_{16.5}$ [4]. This results in glass formation at higher solidification velocities. Again, his analysis for glass formation requires a high reduced glass transition temperature. Near deep eutectics, the proximity of glass transition results in a drastic decrease of the diffusion coefficient which in turn gives an upper bound for the eutectic growth

rate into the viscous liquid. This analysis predicts an extended range of glass formation at a given cooling rate around the eutectic composition, unlike the Davies-Uhlmann kinetic analysis.

Thus, the first condition for bulk glass formation can be summarized as deep eutectic systems where "deep eutectic" is quantified by reduced glass transition temperature T_{rg}. I will take $T_{rg} \sim 0.67$ as a necessary condition for bulk glass formation (requiring a critical cooling rate of 1-10 K/s) as it is in good agreement with the earlier and recently found bulk glass formers. For thick glass formation (requiring a critical cooling rate of 100-1000 K/s), a corresponding value of $T_{rg} \sim$ 0.60 seems to be supported by experimental data. Table 5.1 lists some glass forming alloys with their reduced glass transition temperatures and critical cooling rates.

Table 5.1: Some bulk and thick glass forming alloy compositions, their reduced glass transition temperature T_{rg}, and critical cooling rates $\dot{T}_c$.

Composition	T_{rg}	$\dot{T}_c$
$Zr_{41.2}Ti_{13.8}Cu_{12.5}Ni_{10}Be_{22.5}$ [5, 8]	0.67	<1 K/s
$Pd_{40}Ni_{40}P_{20}$ [6]	0.66	~1 K/s
$Zr_{65}Cu_{17.5}Ni_{10}Al_{7.5}$ [7]	0.60	~100 K/s
$Zr_{55}Cu_{22.5}Be_{22.5}$ [8]	0.58	<500 K/s

The second criteria for bulk glass formation will be taken as avoidance of heterogeneous nucleation sites introduced through "impurity phases." As we have seen in chapter 4, heterogeneous nucleation can be a devastating factor for glass formation even at high values of reduced glass transition temperature. A relatively small crystal growth velocity may lessen this effect. Unfortunately, the kinetics of homogenous nucleation rates usually correlate with those of crystal growth rate, thus still making the heterogeneous nucleation effective at high reduced glass transition temperatures and near eutectic systems (i.e., at relatively small crystal growth velocities). Thus more effective measures of suppressing heterogenous nuclation are required. Two previously described methods are fluxing and utilizing melt chemistry to dissolve the impurity phases. The latter can be incorporated into alloy design along with the first criteria (high reduced glass transition temperature). As the liquid states of Zr-base and Ti-base alloys have relatively high reactivity for dissolving impurity phases, they offer a better opportunity to avoid heterogeneous nucleation sites in the bulk of liquid compared to the other alloy systems. The former technique, fluxing, can be practiced after an alloy which satisfies the first criteria of bulk glass formation is found. Obviously, our tools to suppress the heterogeneous nucleation are relatively new and more work is needed in this area.

We need to know the glass transition temperature and melting point of an alloy to decide its potential to form bulk glass. The glass transition temperature of metallic alloys tends to increase with alloying though its dependence on composition and alloying elements is relatively weak compared to the liquidus temperature of the alloy. We can obtain a rough estimate for the glass transition temperature of a new alloy based on our knowledge of currently known metallic

glasses. For example, we expect a glass transition temperature of 350 °C-400 °C for Zr-base metallic glasses, 700 °C - 750 °C for Ta-base metallic glasses, etc. [9]. From these numbers, we can estimate the required melting point of these alloys to have a T_{rg} ~0.67. As the melting point of metallic systems can change drastically with alloying, knowledge of liquidus temperature becomes a highly desirable thermodynamic parameter for estimating the glass forming ability.

If we knew all the thermodynamic phase diagrams of binary, ternary, quaternary, pentiary and higher order systems, we could locate abnormally deep eutectics which would be potentially good bulk glass formers. We already have satisfactory knowledge of thermodynamic phase diagrams for binary systems for the purpose of glass formation, and almost all promising binary glass formers have been worked out throughout the first 30 years of metallic glass research. However, most of the known good metallic glass formers have turned out to be ternary or higher order systems. Obviously, we have to look for good glass formation in ternary and higher order systems. Unfortunately, our knowledge is rather limited concerning phase diagrams of ternary systems, and almost non existent on higher order systems. For the time being, the wide availability of experimental ternary and higher order phase diagrams is far from complete. It will take thousands of years to experimentally determine all ternary phase diagrams at our current tempo. Quite possibly, a very selective approach for ternary and quaternary phase diagram determination will pay off in the long run, though this will not be available in the near future. As phase diagram calculations and computer modeling are in early stages, this will not be a good option in the near future. A rigorous ternary phase diagram calculation is still considered to be a formidable task. Further, extensive experimental data will be needed as input for a good phase diagram calculation.

As we are deprived of all rigorous techniques to determine higher order deep eutectic systems in the near future, we have to devise more simple approaches which will be useful in locating deep eutectics in ternary and higher order systems. Massalski et al. proposed an experimental method coupled with analytical techniques to determine the eutectic composition (if it exists) in a limited range of a given system [10]. However, this method has its limitations and will not be practical without some guidelines which suggest possible eutectic compositions.

One proven method is to start with a binary alloy which already has a deep eutectic and make these eutectics deeper by alloying. Hard work, intuition and some luck are necessary, as this technique requires trial and error. A first approach to alloying is to prepare combinations of these deep eutectic binary alloys. The currently known good metallic glass formers are combinations of two or more deep eutectic binary alloys such as Pd-Ni-P, Mg-Cu-Y, and Zr-Ti-Ni-Cu-Be good glass forming systems.

A more systematic approach would be to search for suitable eutectic systems such that the elements of one eutectic system will suppress the stability of the crystalline phases of the other eutectic system. Usually, elements with different atomic radius have proven useful as in the cases of recently found exceptionally good glass forming Zr-Cu-Ni-Al and Zr-Ti-Ni-Cu-Be-X systems (X stands for all other elements in periodic table and can be a significant part of the alloy content). Here, this approach will be exercised in the example of Zr-Ti-Ni-Cu-Be bulk glass forming system.

Figures 5.1, 5.2, 5.3, and 5.5 show the binary phase diagrams of Ti-Ni, Zr-Cu, Zr-Ni, and Ti-Cu [11]. These systems show generally similar features with low lying eutectics over the central portions of the phase diagrams. The existence of intermetallic compounds, which are usually size compounds (Laves phases), prevent the binary systems from exhibiting much deeper eutectic features. Figures 5.4 and 5.6 show the hypothetical phase diagrams of Zr-Ni and Ti-Cu, in which the intermetallic compounds are assumed to be non-existent. Obviously, the hypothetical eutectics are much deeper than existing in the real binary systems and would be easy bulk glass formers. Our objective is to attain these hypothetical phase diagrams by the help of additional alloying elements

Figures 5.7 and 5.8 show the binary phase diagrams of Zr-Be and Ti-Be systems [11]. The Zr-Be and Ti-Be systems differ from the above binary systems in that crystalline intermetallic phases are confined to the Be-rich portion of the phase diagram. For example, in Zr-Be shown in figure 5.7, the most Zr-rich crystalline intermetallic is $ZrBe_2$, a Laves phase which forms peritectically at 1508 K. This is separated from the Zr-base terminal solutions by a broad and deep eutectic feature with a eutectic temperature of 1238 K at 35 at. % Be.

The essential motivation in developing bulk glass forming alloys is to find the deepest eutectic features obtainable in the pseudo-ternary phase diagrams. The absence of Zr-rich (Ti-rich) phases in the Zr-Be and Ti-Be systems provides a key. It suggests, for instance, that Be will have limited solubility in crystalline binary phases such as Zr_2Cu, $ZrCu$, Zr_2Ni, and $ZrNi$, since analogous phases are absent in the Zr-Be system. As further support for this conjecture, the metallic radius of Be is substantially smaller than that of Cu and Ni (R_{Be}= 0.112 nm, while R_{Cu}=0.128 nm, and R_{Ni}=0.124 nm), and much smaller than that of Zr, R_{Zr}=0.160

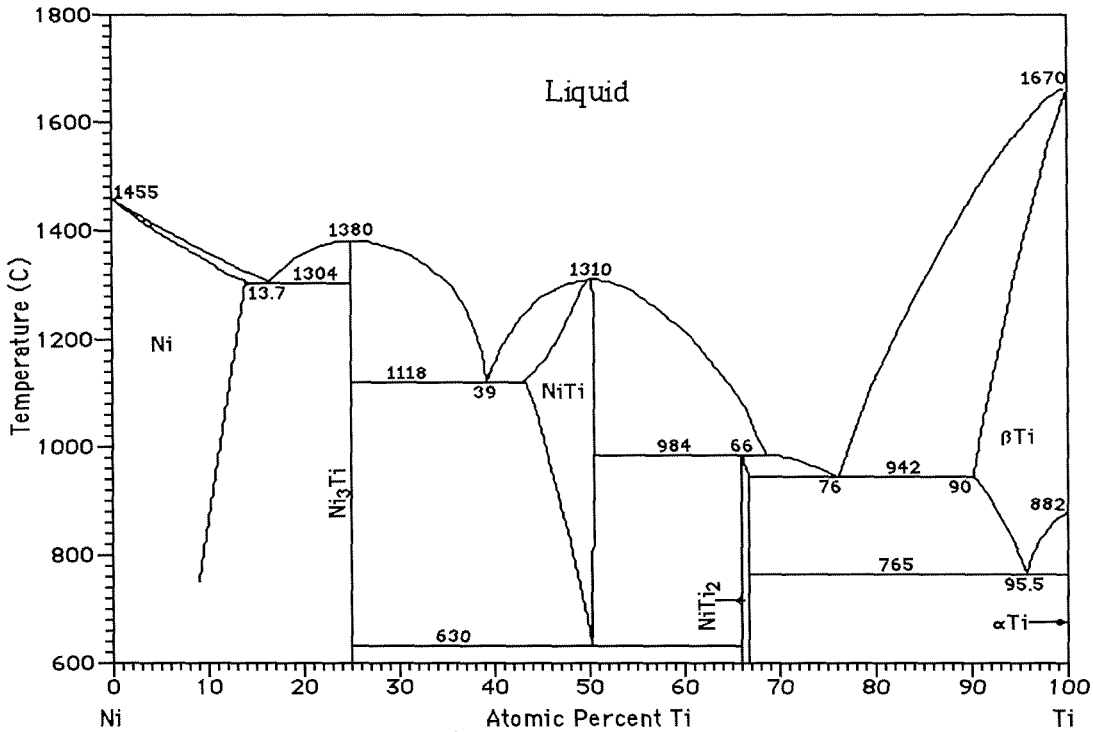

Figure 5.1: Phase Diagram of the Ti-Ni system. Reproduced from ref. 11.

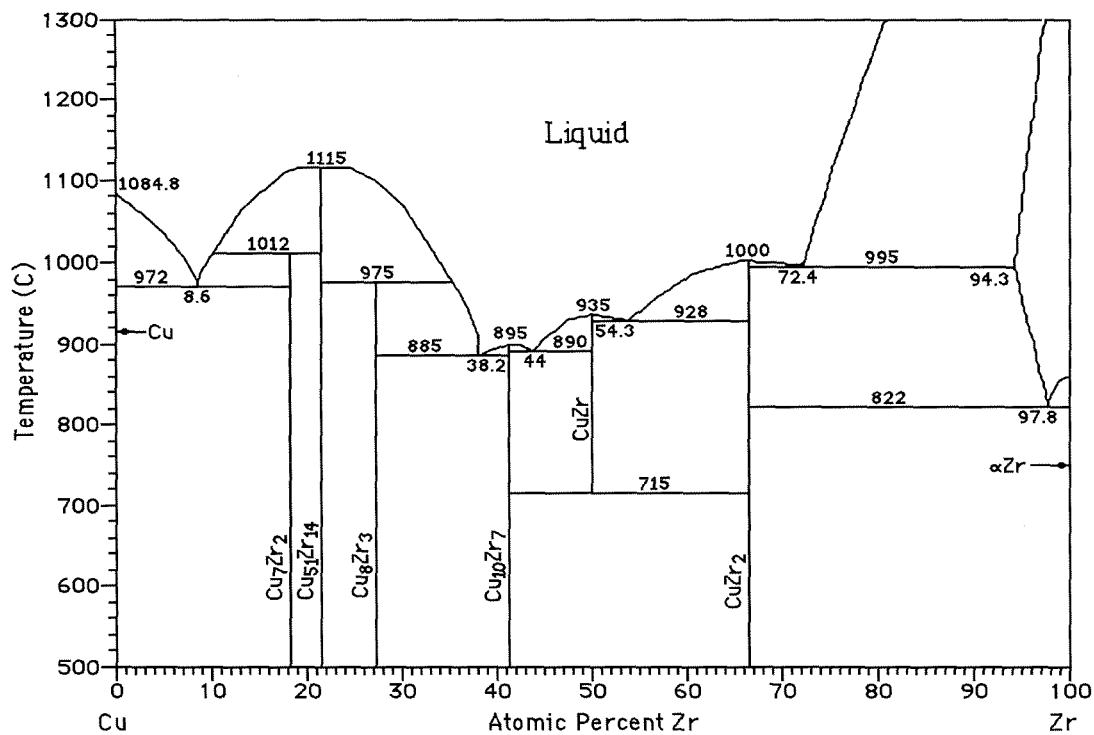

Figure 5.2: Phase Diagram of the Zr-Cu system. Reproduced from ref. 11.

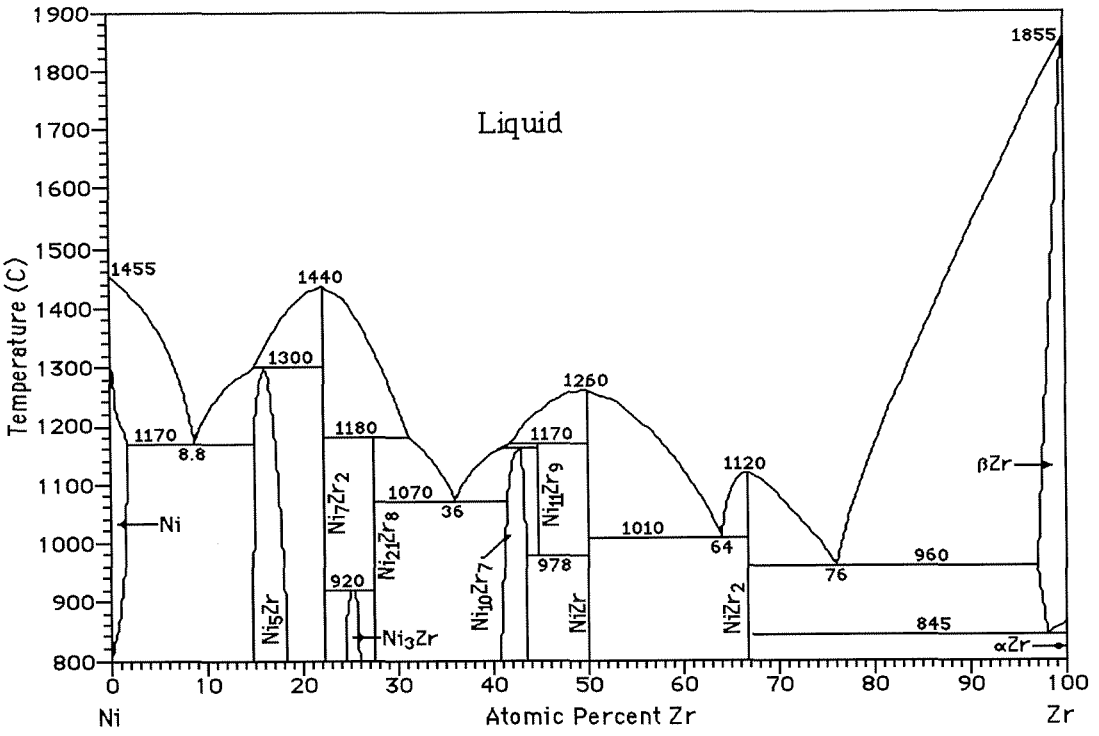

Figure 5.3: Phase Diagram of the Zr-Ni system. Reproduced from ref. 11.

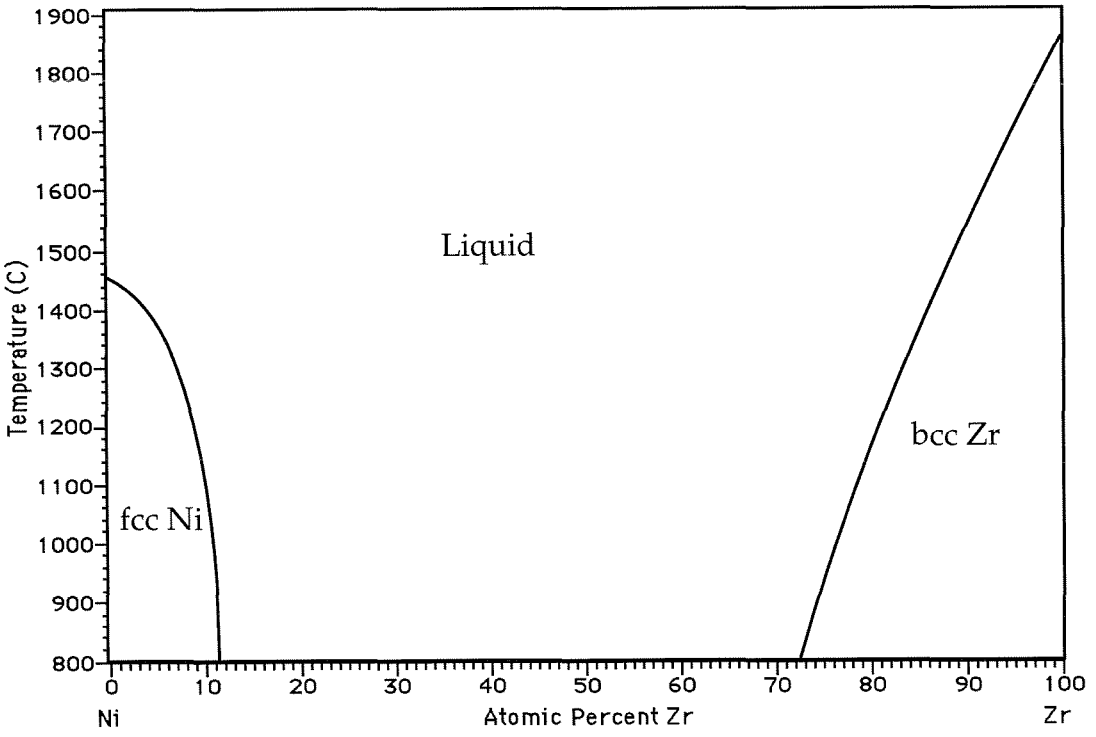

Figure 5.4: Hypothetical phase diagram of the Zr-Ni system.

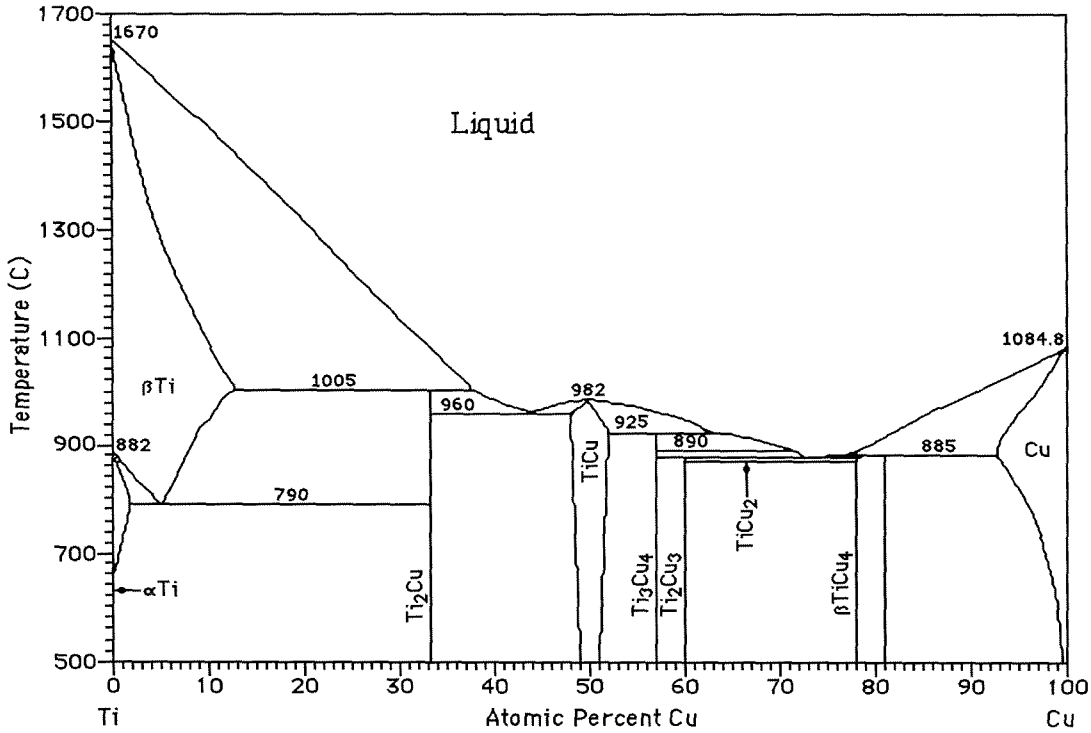

Figure 5.5: Phase Diagram of the Ti-Cu system. Reproduced from ref. 11.

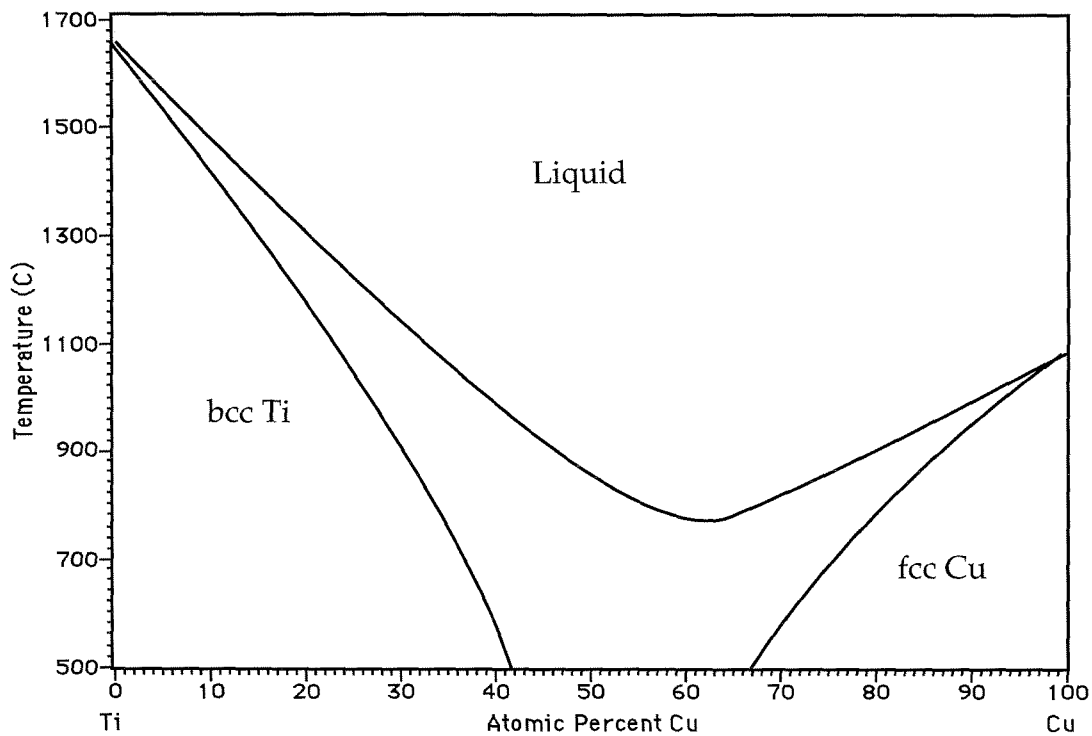

Figure 5.6: Hypothetical phase diagram of the Ti-Cu system.

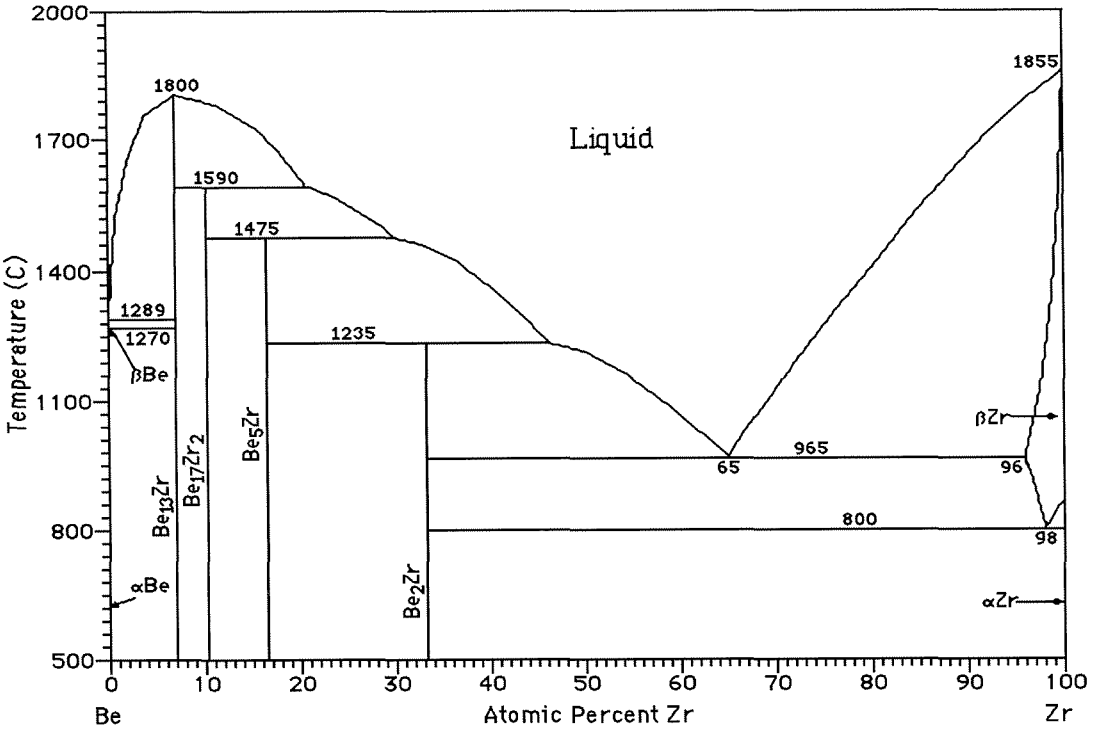

Figure 5.7: Phase Diagram of the Zr-Be system. Reproduced from ref. 11.

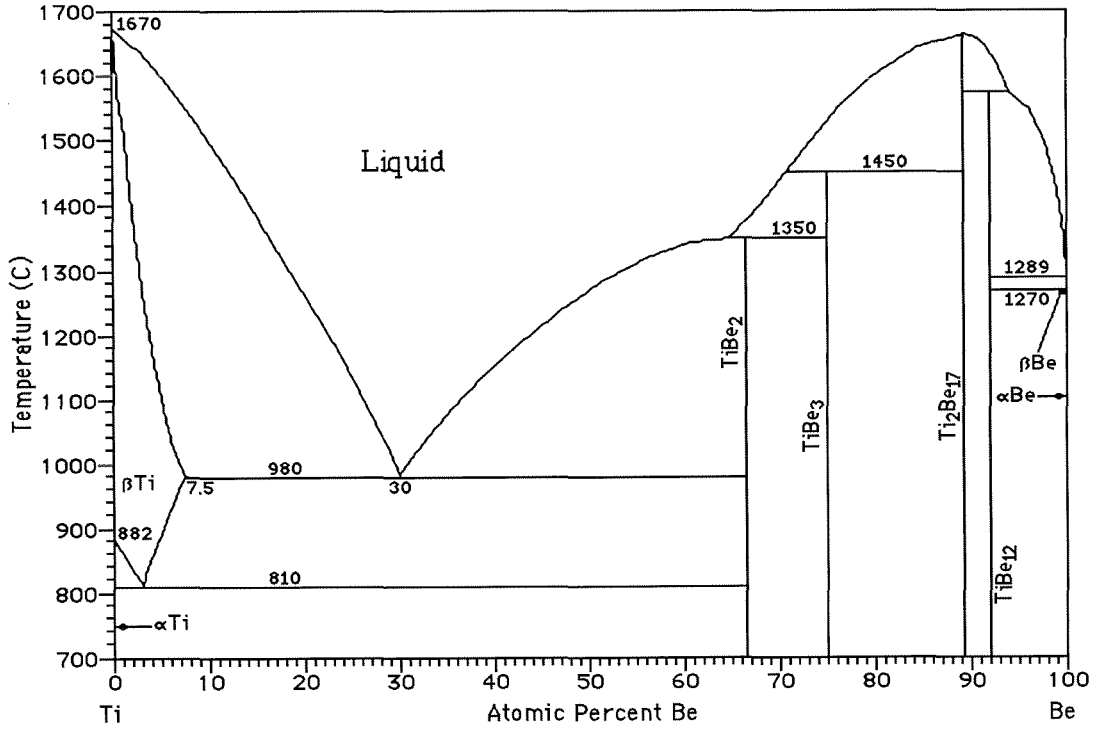

Figure 5.8: Phase Diagram of the Ti-Be system. Reproduced from ref. 11.

nm) [12]. In compounds such as Zr_2Ni (Al_2Cu-*type*), substitution of Be on the Ni-site in the crystal should be accompanied by substantial lattice strain. This in turn should reduce the stability of the compound as Be is substituted in the form $Zr_2(Ni_{1-X}Be_X)$. A similar argument applies to crystalline compound $Zr(Ni_{1-X}Be_X)$. Such compounds should have limited solubility for Be. In the absence of a new ternary Zr-rich Zr-Ni-Be phase, one would expect to find a ternary eutectic feature in the Zr-rich portion of the ternary diagram. This eutectic should lie at Be concentrations exceeding the solubility limits of the above crystalline phases. Further, this ternary eutectic should lie lower at temperature than the binary eutectics or the corresponding liquidus features in the binary Zr-Cu and Zr-Ni systems. Such a deep eutectic region in fact exists in the ternary and pseudo-ternary phase diagrams. For example, high temperature DSC scans of the melting curves of several ternary Zr-Cu-Be alloys are shown in figure 5.9. The alloys have compositions varying over a substantial region of the Zr-rich part of the ternary diagram. All four alloys have a solidus temperature of about $T_s \approx 1070$ K while the liquidus curves vary from 1080 to 1125 K. These temperatures lie well below the corresponding binary eutectic temperatures in the Zr-Be Diagram (eutectic at 35 at. % Be with $T_e = 1238$ K), or the Zr-Cu system (eutectics at 28 and 46 at. % Cu with $T_e = 1273$ K, and 1201 K respectively). In higher order alloys, this broad region of low lying solidus and liquidus features becomes even more pronounced. Figure 3.10 shows the high temperature DSC scan of the melting transition for the pentiary alloy $Zr_{41.2}Ti_{13.8}Cu_{12.5}Ni_{10}Be_{22.5}$. Here, $T_s = 937$ K while $T_l \approx 985$ K. This pseudo-ternary alloy exhibits an exceedingly low melting region. In this region, one finds $T_{rg} \approx 0.67$.

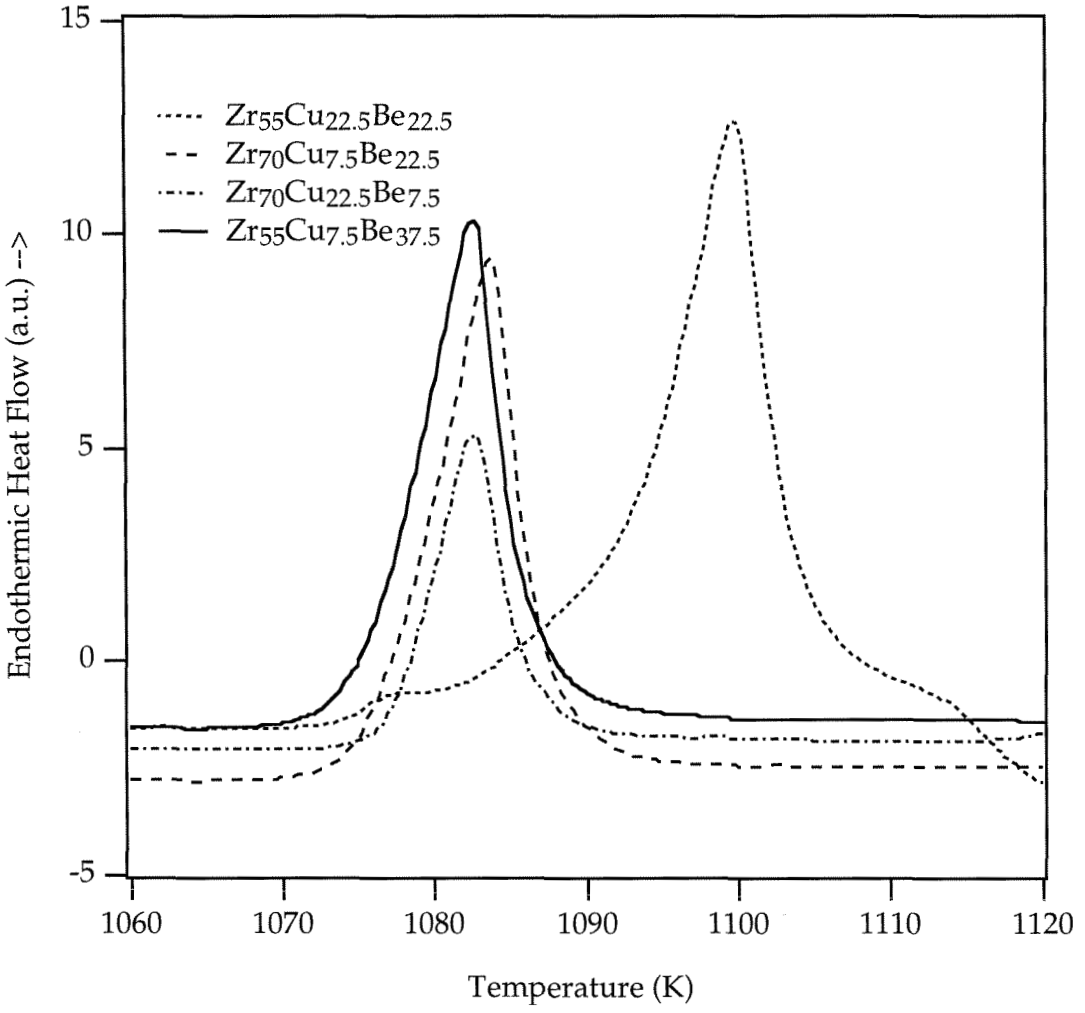

Figure 5.9: High temperature DSC scans of the melting endotherms for a series of ternary Zr-Cu-Be alloys.

The Zr-Ti-Ni-Cu-Be alloys of interest here can best be viewed as pseudo-ternary alloys of the type $(Zr\text{-}Ti)_{1-X-Y}(Ni,Cu)_XBe_Y$, or more generally as:

$$(ETM)_{1-X-Y}(LTM)_XBe_Y.$$

where ETM is an early transition metal (e.g. Ti, Zr, Nb, V, etc.) and LTM is a late transition metal (e.g., Cu, Ni, Co, Fe) [13-15]. Figure 5.10 shows the region where bulk glass forming alloys were found. An extremely large region of this pseudo-ternary system was found to exhibit glass formation at cooling rates as low as 1 K/s. Obviously Be is a very effective alloying element to improve bulk glass formation. We have not yet found such an effective alloying element to improve glass formation. Thus, there should be something unique with Be!

Figure 5.11 shows a plot of metallic radii of selected elements (most common elements in metallic glass research). Obviously, Be stands out with its metallic radius. This may explain the unique effectiveness of Be for bulk glass formation in $(ETM)_{1-X-Y}(LTM)_XBe_Y$ system. Be is neither small enough to fit into interstitial sites nor big enough for substitutional solutions without causing substantial strain energy in crystalline phases. The unique size of Be makes crystalline solution phases highly unstable due to strain energy, whereas liquid can sustain larger atomic size differences. This small atom will also increase the packing efficiency and the entropy of mixing of the liquid state. By contrast, Be cannot be replaced by other metalloid atoms (e.g., B, C, Si) which form strong covalent bonds. Such covalent bonding results in highly refractory and easy nucleating crystalline compounds. Figures 5.12, 5.13, 5.14, and 5.15 show the binary phase diagrams of Zr-Si, Ti-C, Ti-B, and Zr-B [11].

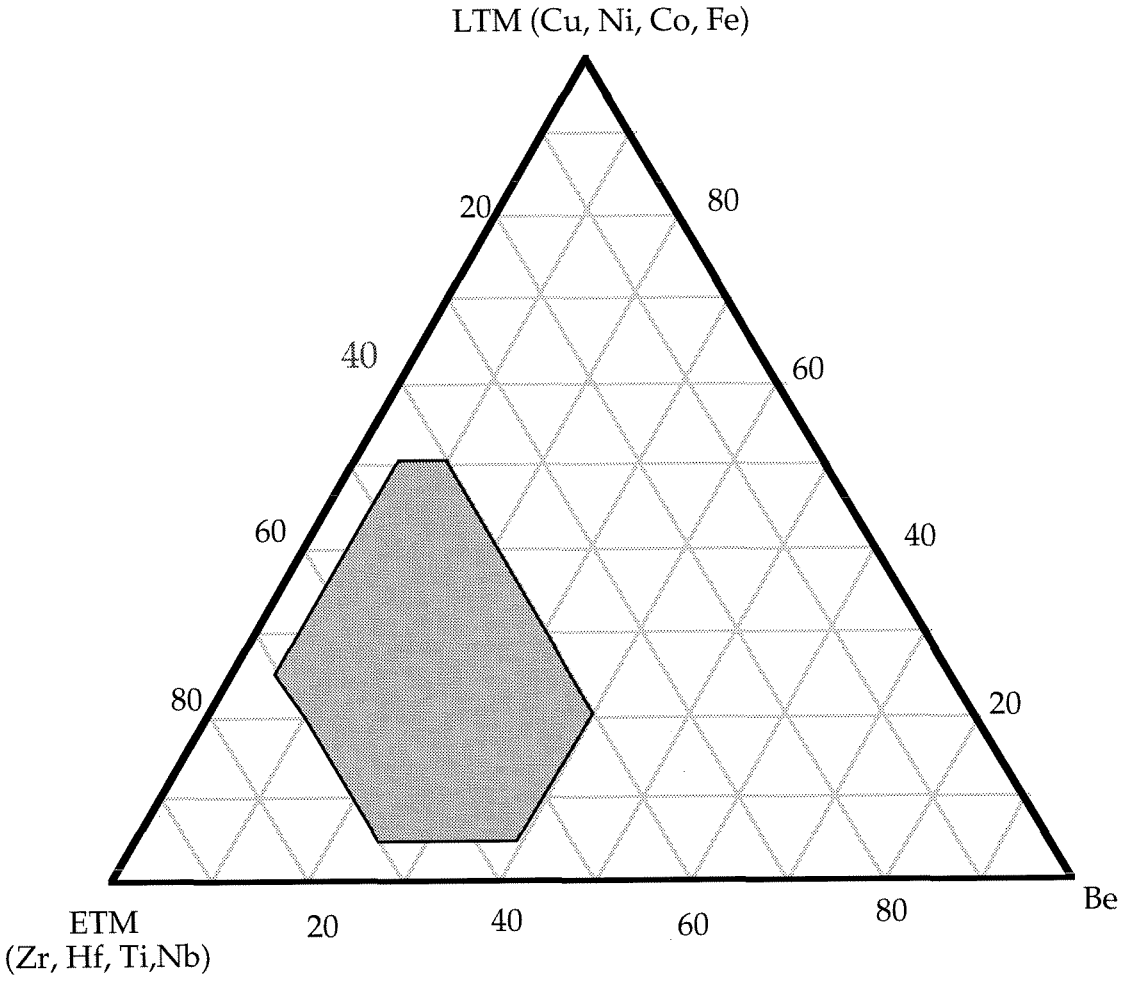

Figure 5.10: Schematic ternary phase diagram showing the region in which bulk glass forming alloys were found in ETM-LTM-Be alloys.

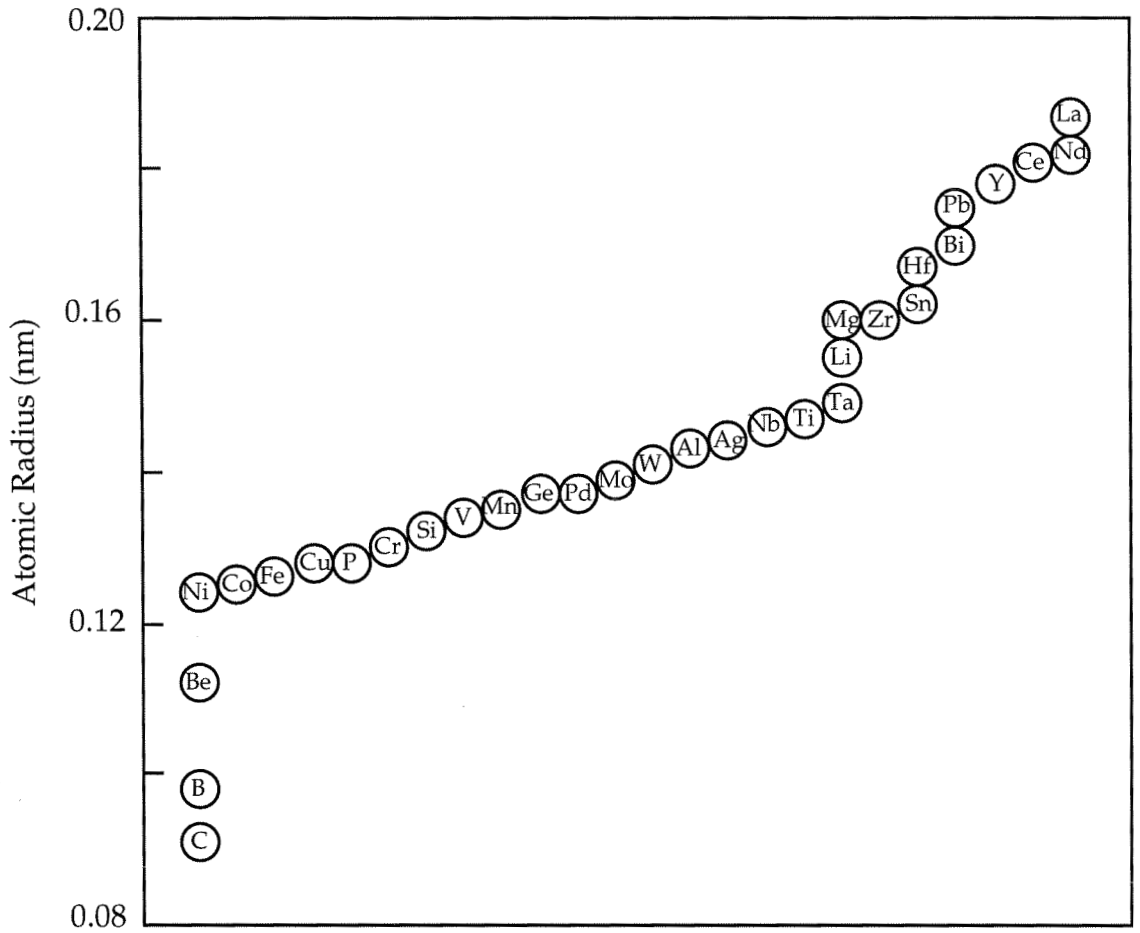

Figure 5.11: Metallic radii of selected elements. The data is taken from ref. 12.

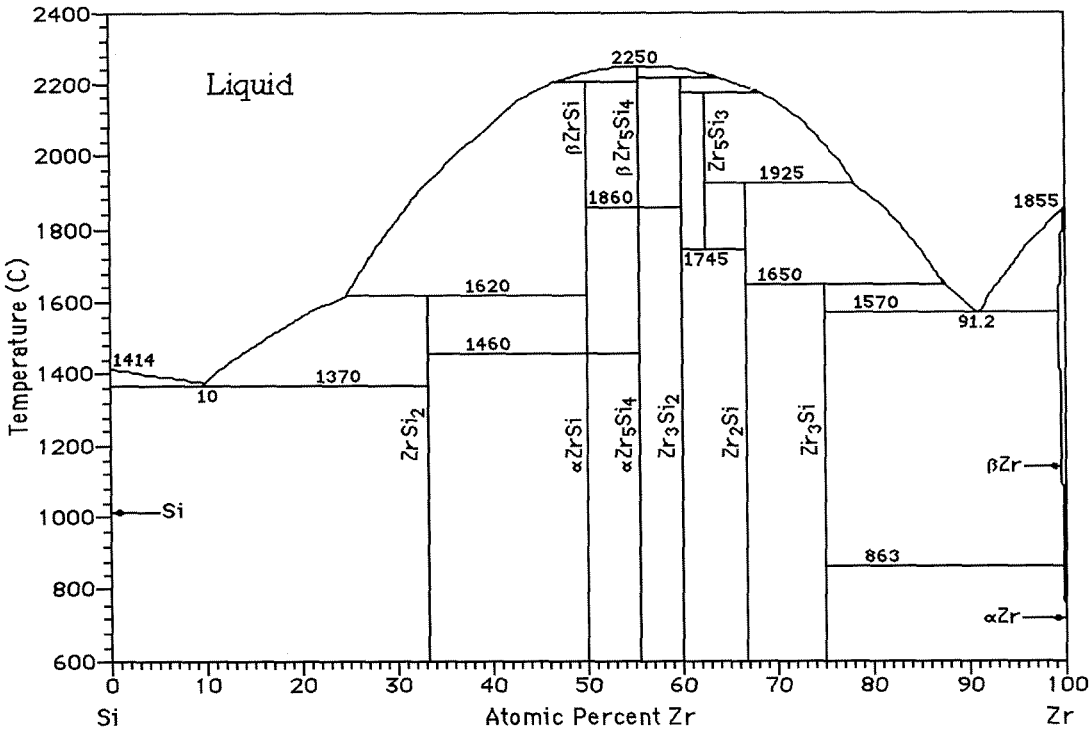

Figure 5.12: Phase Diagram of the Zr-Si system. Reproduced from ref. 11.

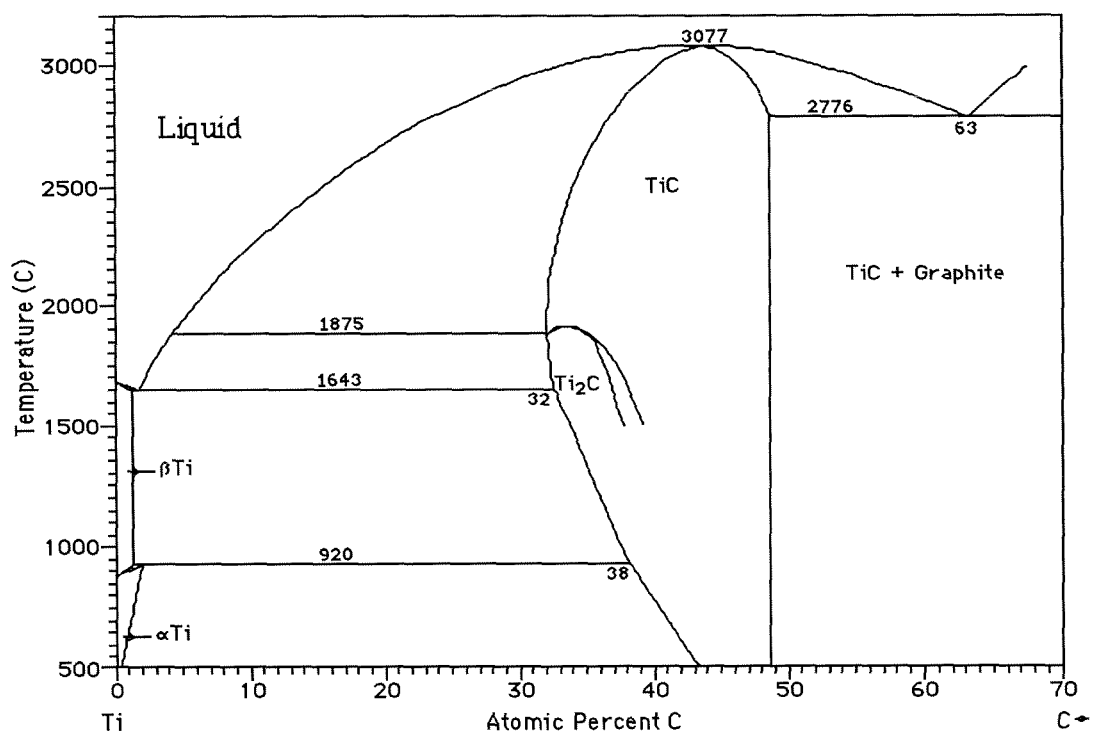

Figure 5.13: Phase Diagram of the Ti-C system. Reproduced from ref. 11.

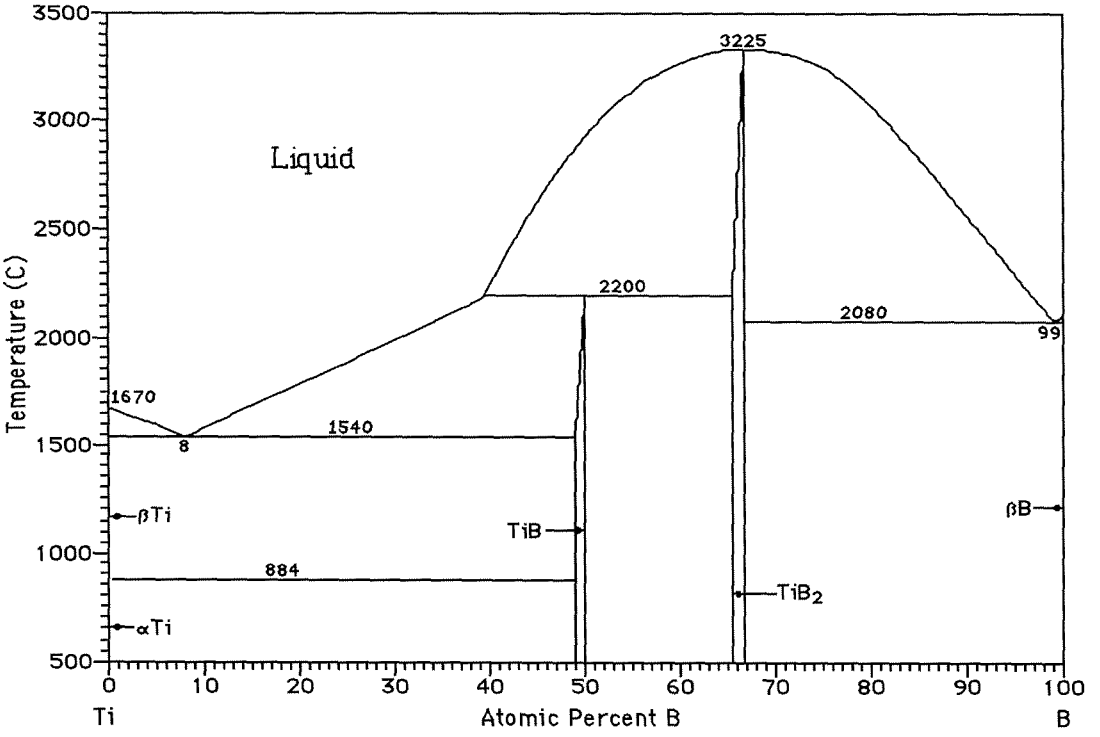

Figure 5.14: Phase Diagram of the Ti-B system. Reproduced from ref. 11.

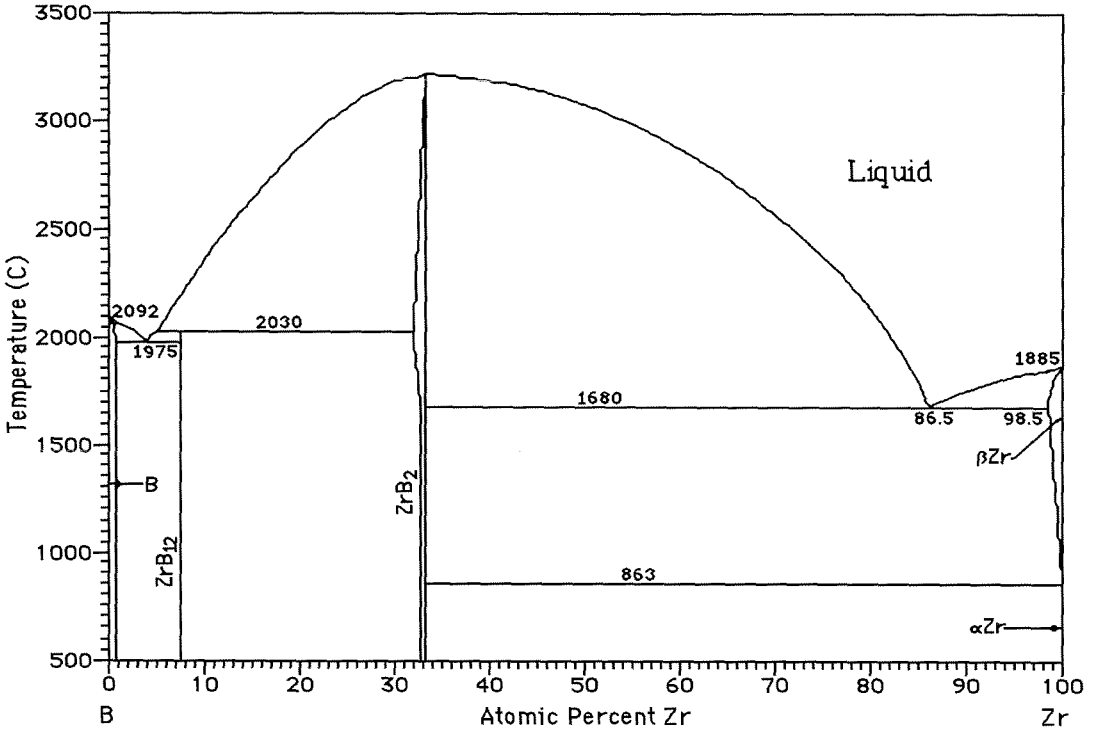

Figure 5.15: Phase Diagram of the Zr-B system. Reproduced from ref. 11.

We can increase the reduced glass transition temperature T_{rg} to the limit of 0.67 by increasing the glass transition temperature and/or reducing the melting point of the alloy. Pure metals have T_{rg} much smaller than 0.5 and most of the deep eutectic binary alloys have T_{rg} from 0.5 to 0.6. In earlier research aimed at developing metallic glasses, attention was devoted to the reduction in melting point through alloying, as the glass transition temperature was found to be slowly changing with composition. However, increasing of T_{rg}, by increasing T_g, should not be overlooked as an efficient method. To increase T_{rg} from 0.6 to 0.65, the reduction of melting point should be 1.6 times the increase in glass transition temperature. An increase of glass transition temperature by 40-50 °C can be very critical as it becomes harder to increase T_r after it reaches a value of 0.60.

As a final comment, I include the following quotations from two currently known experts in the field of materials science [16].

D. DeFontaine: *I would like to raise a point regarding the size of the task ahead of us if we are to meet the needs of the industrial world. If we take 80 elements as being important, there are 3,000 possible binary systems. In the last 50 years, it appears on the average that we have completed work on one binary per week. There are approximately 50,000 ternaries. Assuming conservatively that at the same tempo of work it takes five times as long to complete a study on a ternary system as it does on a binary, it would be possible to complete ten a year. This takes us forward 5,000 years. If we go to quaternary systems and assume that by that time our techniques have advanced sufficiently so that we can do a complete quaternary system in about the same time it now takes us to do a ternary system, it would appear that an additional 100,000 years would be required. This overly simplified statement brings out the enormity of the task before us. It seems*

to me that we must ask ourselves what are the realistic goals and where do we stop. We must be honest with the industrialists and say that we never really are going to be able to develop all the information that is needed in the next hundred thousand years.

***J. F. Elliot**: I feel that the question is highly pertinent. One of the answers is that we must be highly selective as to the systems on which we work because of limitations of funding and of the available manpower. It seems to me that the latter is the more important constraint. We must also be aware that there are limits to the patience of those who ultimately must pay the bills --the public. We must provide the industrial researcher with background information to assist him to get started in his work even though he may have to develop detailed information on the system that is of immediate interest to him.*

References

[1] D. R. Uhlmann, in *Materials Science Research*, Vol. 4 (Plenum, New York, 1969).

[2] D. Turnbull, Contemp. Phys., **10**, 473 (1969).

[3] D. Turnbull, J. Chem. Phys., **66**, 609 (1962).

[4] W. J. Boettinger, in *Rapidly Solidified Amorphous and Crystalline Alloys*, B. H. Kear, B. C. Giessen, and M. Cohen (eds.) (North Holland, 1982), p. 15.

[5] A. Peker and W. L. Johnson, Appl. Phys. Lett., **63**, 2342 (1993).

[6] H. W. Kui, A. L. Greer, and D. Turnbull, Appl. Phys. Lett., **45**, 615 (1984).

[7] T. Zhang, A. Inoue, and T. Masumoto, Mater. Trans., JIM, **32**, 1005 (1991).

[8] This thesis.

[9] A. Peker and W. L. Johnson, unpublished research (1991).

[10] T. B. Massalski, Y. W. Kim, L. F. Vassamillet and R. W. Hopper, Mat. Sci. Engg, **47**, K1 (1981).

[11] T. B. Massalski, *Binary Alloy Phase Diagrams* (ASM International, Metals Park, OH, 1990).

[12] L. Pauling, *Theory of Alloy Phases* (American Society for Metals, Metals Park, OH, 1956).

[13] A. Peker and W. L. Johnson, U.S. Patent No. 5,288,344, assigned to California Institute of Technology (Feb. 1994).

[14] A. Peker and W. L. Johnson, U.S. Patent application (April 1994).

[15] W. L. Johnson and A. Peker, to appear in *Science and Technology of Rapid Solidification Processing Technologies, NATO ASI Series,* M. A. Otooni (ed.), (West Point, June 1994).

[16] In *Applications of Phase Diagrams in Metallurgy and Ceramics*, G. C. Carter (ed.), NBS Special Publication 496, p. 1373.

APPENDIX I

The bulk glass forming Zr-Ti-Cu-Ni-Be alloys can be viewed as pseudo-ternary alloys of the type

$$(Zr_{1-X}Ti_X)_{100-b-c}(Cu_{1-Y}Ni_Y)_b(Be)_c$$

where X and Y are atomic fractions and a, b and c are atomic percentages [1-3]. Generally, a is in the range of from 30 to 75%, b is in the range of from 2 to 60%, c is in the range of 2 to 52%, and X and Y are in the range of from 0 to 1 for good glass formation by rapid quenching technique ($\dot{T}$~10^4-10^6 K/s). Table A. 1 lists glassy alloys of this type obtained by rapid quenching ($\dot{T}$~10^4-10^6 K/s). Thick glass formation ($\dot{T}$~10^2-10^3 K/s) is generally observed when a is in the range of from 38 to 72%, b is in the range of from 5 to 52%, c is in the range of 5 to 42% and X and Y are in the range of from 0 to 1. Table A. 2 lists glassy alloys prepared in the form of 1.0 mm thick strips. Bulk glass formation ($\dot{T}$~1-10 K/s) is generally observed when a is in the range of from 42 to 68%, b is in the range of from 10 to 45%, c is in the range of 12 to 35%, and X is in the range of from 0.15 to 0.65. Table A. 3 lists glassy alloys prepared in the form of at least 5.0 mm thick ingots. The molten alloys listed in table A. 3 usually freeze to glassy ingots on a water cooled copper (or silver) boat under a clean inert atmosphere. When the value of (bY) --which gives the Ni content in atom percent-- is in the range of from 5 to 15%, the largest ranges of a, b, c and X are obtained for bulk glass formation. Figure A.1 shows glass formation at two different cooling rates

($\dot{T}$~10 K/s and $\dot{T}$~500 K/s) for $(Zr_{0.75}Ti_{0.25})_{100-b-c}(Cu_{1-Y}Ni_Y)_bBe_c$ alloy system, where Ni content (the value of bY) is from 5 to 15 atom percent. Table A.4 lists thermal properties of 1.0 mm thick $Zr_{100-b-c}Cu_bNi_{10}Be_c$ glassy alloys. Listed are the onset glass transition temperature T_g, the onset crystallization temperature T_x, and supercooled liquid region ΔT, which is defined as $\Delta T = T_x - T_g$.

The $(Zr_{1-X}Ti_X)_{100-b-c}(Cu_{1-Y}Ni_Y)_b(Be)_c$ glass forming alloy system can also accommodate substantial amount of other elements without damaging its glass forming ability. Generally, this alloy system can comprise any transition metal from 0 to 30 atom percent, metalloids from 0 to 10 atom percent, any metal from lanthanides and actinides from 0 to 15 atom percent, and a few atom percent of any other element (including Oxygen) for thick and bulk glass formation. For example, the Zr-Ti moiety can contain additional metals selected from the group of from 0 to 20 atom percent Nb, from 0 to 20 atom percent V, from 0 to 15 atom percent Y, from 0 to 10 atom percent Cr, and up to 10 atom percent of any other early transition metal for thick glass formation ($\dot{T}$~10^2-10^3 K/s). When Zr-Ti moiety contains additional metals selected from the group of from 0 to 10 atom percent Nb, from 0 to 10 atom percent V, from 0 to 5 atom percent Y, from 0 to 5 atom percent Cr, and up to 5 atom percent of any other early transition metal, bulk glass formation at cooling rates as low as 10 K/s can still be obtained. Zr can be completely replaced by Hf in any of these alloys without damaging the glass forming ability. Further, the Cu-Ni moiety can contain additional metals selected from the group of from 0 to 25 atom percent Co, from 0 to 15 atom percent Fe, from 0 to 10 atom percent Mn and up to 10 atom percent of any other late transition metal for thick glass formation ($\dot{T}$~10^2-10^3 K/s). When Cu-Ni moiety contains additional metals selected from the group of from 0 to 15 atom

percent Co, from 0 to 10 atom percent Fe, and up to 5 atom percent of any other transition metal, bulk glass formation at cooling rates as low as 10 K/s can still be obtained.

When other transition metals are included, the $(Zr_{1-X}Ti_X)_{100-b-c}(Cu_{1-Y}Ni_Y)_b(Be)_c$ system can be generalized to

$$ETM_{100-b-c}LTM_bBe_c,$$

where ETM is a combination of early transition metals (e.g. Zr, Hf, Ti, Nb, V, Cr, etc.) and LTM is a combination of late transition metals (e.g. Cu, Ni, Co, Fe etc.). Generally, the values of a, b, and c are still valid as described above for glass formation at different cooling rates. Table A. 5, A.6, and A.7 list alloys of $ETM_{100-b-c}LTM_bBe_c$ type prepared at different cooling rates. Listed in table A. 8 are glassy alloys of Zr-Ti-Ni-Cu-Be-M prepared in the form of 1.0 mm strips, where M stands for a metalloid atom (Si, B, Al).

It should be noted that the above boundaries are only approximately given. A variation of glass forming ability is observed slightly inside and/or outside of the these given boundaries. Also, the given cooling rates, $\dot{T}$, are approximately estimated cooling rates effective in the preparation of glassy alloys and they are not necessarily the critical cooling rates, $\dot{T}_c$, for glass formation.

TABLE A.1: Readily glass forming ($\dot{T} < 10^4$-10^6 K/s) Zr-Ti-Ni-Cu-Be alloys.

$Ti_{40}Cu_{37.5}Ni_{15}Be_{7.5}$	$Ti_{45}Cu_{32.5}Ni_{15}Be_{7.5}$
$Ti_{45}Cu_{27.5}Ni_{15}Be_{12.5}$	$Ti_{50}Cu_{27.5}Ni_{15}Be_{7.5}$
$Ti_{50}Cu_{17.5}Ni_{10}Be_{22.5}$	$Ti_{55}Cu_{22.5}Ni_{15}Be_{7.5}$
$Ti_{55}Cu_{17.5}Ni_{10}Be_{17.5}$	$Ti_{60}Cu_{17.5}Ni_{10}Be_{12.5}$
$Ti_{60}Cu_{7.5}Ni_{10}Be_{22.5}$	$Ti_{65}Cu_{17.5}Ni_{10}Be_{7.5}$
$Ti_{55}Ni_{27.5}Be_{17.5}$	$Ti_{70}Ni_{7.5}Be_{22.5}$
$Ti_{26.2}Zr_{8.8}Cu_{47.5}Ni_{10}Be_{7.5}$	$Ti_{30}Zr_{10}Cu_{22.5}Ni_{15}Be_{22.5}$
$Ti_{30}Zr_{10}Cu_{12.5}Ni_{10}Be_{37.5}$	$Ti_{41.2}Zr_{13.8}Cu_{17.5}Ni_{10}Be_{17.5}$
$Ti_{48.8}Zr_{16.2}Cu_{17.5}Ni_{10}Be_{7.5}$	$Ti_{32.5}Zr_{32.5}Cu_{17.5}Ni_{10}Be_{7.5}$
$Zr_{22.5}Ti_{7.5}Cu_{37.5}Ni_{10}Be_{22.5}$	$Zr_{26.2}Ti_{8.8}Cu_{22.5}Ni_{10}Be_{32.5}$
$Zr_{25}Cu_{37.5}Ni_{15}Be_{22.5}$	$Zr_{30}Cu_{37.5}Ni_{10}Be_{22.5}$
$Zr_{35}Cu_{22.5}Ni_{10}Be_{32.5}$	$Zr_{35}Cu_{7.5}Ni_{10}Be_{47.5}$
$Zr_{55}Cu_{5}Ni_{7.5}Be_{32.5}$	$Zr_{75}Cu_{7.5}Ni_{10}Be_{7.5}$
$Zr_{30}Ni_{47.5}Be_{22.5}$	$Zr_{30}Cu_{47.5}Be_{22.5}$
$Zr_{70}Cu_{22.5}Be_{7.5}$	$Zr_{75}Ni_{12.5}Be_{12.5}$

TABLE A.2: Thick glass forming ($\dot{T} < 10^2$-10^3 K/s) Zr-Ti-Ni-Cu-Be alloys.

$Zr_{30}Ti_{10}Cu_{22.5}Ni_{10}Be_{27.5}$	$Zr_{33.8}Ti_{11.2}Cu_{7.5}Ni_5Be_{42.5}$
$Zr_{45}Ti_{15}Cu_{17.5}Ni_{10}Be_{12.5}$	$Zr_{48.8}Ti_{16.2}Cu_{2.5}Ni_{10}Be_{22.5}$
$Zr_{48.8}Ti_{16.2}Cu_{12.5}Ni_{10}Be_{12.5}$	$Zr_{48.8}Ti_{16.2}Cu_{17.5}Ni_{10}Be_{7.5}$
$Zr_{52.5}Ti_{17.5}Cu_{7.5}Ni_{10}Be_{12.5}$	$Zr_{37.5}Ti_{12.5}Ni_{37.5}Be_{12.5}$
$Zr_{52.5}Ti_{17.5}Ni_{7.5}Be_{22.5}$	$Zr_{20}Ti_{20}Cu_{22.5}Ni_{15}Be_{22.5}$
$Zr_{20}Ti_{20}Cu_{12.5}Ni_{15}Be_{37.5}$	$Zr_{22.5}Ti_{22.5}Cu_{12.5}Ni_{10}Be_{32.5}$
$Zr_{22.5}Ti_{22.5}Cu_{7.5}Ni_{10}Be_{37.5}$	$Zr_{25}Ti_{25}Cu_{27.5}Ni_{15}Be_{7.5}$
$Zr_{25}Ti_{25}Cu_{17.5}Ni_{15}Be_{22.5}$	$Zr_{27.5}Ti_{27.5}Cu_{17.5}Ni_{10}Be_{27.5}$
$Zr_{30}Ti_{30}Cu_{17.5}Ni_{10}Be_{12.5}$	$Zr_{35}Ti_{35}Ni_{7.5}Be_{22.5}$
$Ti_{30}Zr_{10}Cu_{42.5}Ni_{10}Be_{7.5}$	$Ti_{37.5}Zr_{12.5}Cu_{27.5}Ni_{15}Be_{7.5}$
$Ti_{37.5}Zr_{12.5}Cu_{17.5}Ni_{10}Be_{22.5}$	$Ti_{41.2}Zr_{13.8}Cu_{12.5}Ni_{10}Be_{22.5}$
$Ti_{45}Zr_{15}Cu_{17.5}Ni_{10}Be_{12.5}$	$Ti_{52.5}Zr_{17.5}Ni_{7.5}Be_{22.5}$
$Zr_{40}Cu_{22.5}Ni_{15}Be_{22.5}$	$Zr_{55}Cu_{7.5}Be_{37.5}$
$Zr_{70}Ni_{7.5}Be_{22.5}$	$Zr_{60}Ni_{12.5}Be_{27.5}$

TABLE A.3: Bulk glass forming ($\dot{T} < 10$ K/s) Zr-Ti-Ni-Cu-Be alloys.

$Zr_{33.8}Ti_{11.2}Cu_{32.5}Ni_{10}Be_{12.5}$	$Zr_{33.8}Ti_{11.2}Cu_{27.5}Ni_{10}Be_{17.5}$
$Zr_{33.8}Ti_{11.2}Cu_{22.5}Ni_{10}Be_{22.5}$	$Zr_{33.8}Ti_{11.2}Cu_{17.5}Ni_{10}Be_{27.5}$
$Zr_{33.8}Ti_{11.2}Cu_{17.5}Ni_{10}Be_{32.5}$	$Zr_{33.8}Ti_{11.2}Cu_{7.5}Ni_{10}Be_{37.5}$
$Zr_{37.5}Ti_{12.5}Cu_{32.5}Ni_{10}Be_{7.5}$	$Zr_{37.5}Ti_{12.5}Cu_{27.5}Ni_{10}Be_{12.5}$
$Zr_{37.5}Ti_{12.5}Cu_{22.5}Ni_{10}Be_{17.5}$	$Zr_{37.5}Ti_{12.5}Cu_{17.5}Ni_{10}Be_{22.5}$
$Zr_{37.5}Ti_{12.5}Cu_{12.5}Ni_{10}Be_{27.5}$	$Zr_{37.5}Ti_{12.5}Cu_{7.5}Ni_{10}Be_{32.5}$
$Zr_{41.2}Ti_{13.8}Cu_{17.5}Ni_{10}Be_{17.5}$	$Zr_{41.2}Ti_{13.8}Cu_{12.5}Ni_{10}Be_{22.5}$
$Zr_{41.2}Ti_{13.8}Cu_{7.5}Ni_{10}Be_{27.5}$	$Zr_{41.2}Ti_{13.8}Cu_{2.5}Ni_{10}Be_{32.5}$
$Zr_{45}Ti_{15}Cu_{12.5}Ni_{10}Be_{17.5}$	$Zr_{45}Ti_{15}Cu_{7.5}Ni_{10}Be_{22.5}$
$Zr_{45}Ti_{15}Cu_{2.5}Ni_{10}Be_{27.5}$	$Zr_{48.8}Ti_{16.2}Cu_{7.5}Ni_{10}Be_{17.5}$
$Zr_{52.5}Ti_{17.5}Cu_{2.5}Ni_{10}Be_{17.5}$	$Zr_{30}Ti_{10}Cu_{22.5}Ni_{15}Be_{22.5}$
$Zr_{41.2}Ti_{13.8}Ni_{22.5}Be_{27.5}$	$Zr_{27.5}Ti_{27.5}Cu_{12.5}Ni_{10}Be_{22.5}$
$Zr_{27.5}Ti_{27.5}Cu_{7.5}Ni_{10}Be_{27.5}$	$Zr_{30}Ti_{30}Cu_{7.5}Ni_{10}Be_{22.5}$
$Zr_{35.8}Ti_{19.2}Cu_{7.5}Ni_{10}Be_{27.5}$	$Zr_{46.8}Ti_{8.25}Cu_{7.5}Ni_{10}Be_{27.5}$
$Zr_{33}Ti_{22}Cu_{12.5}Ni_{10}Be_{22.5}$	

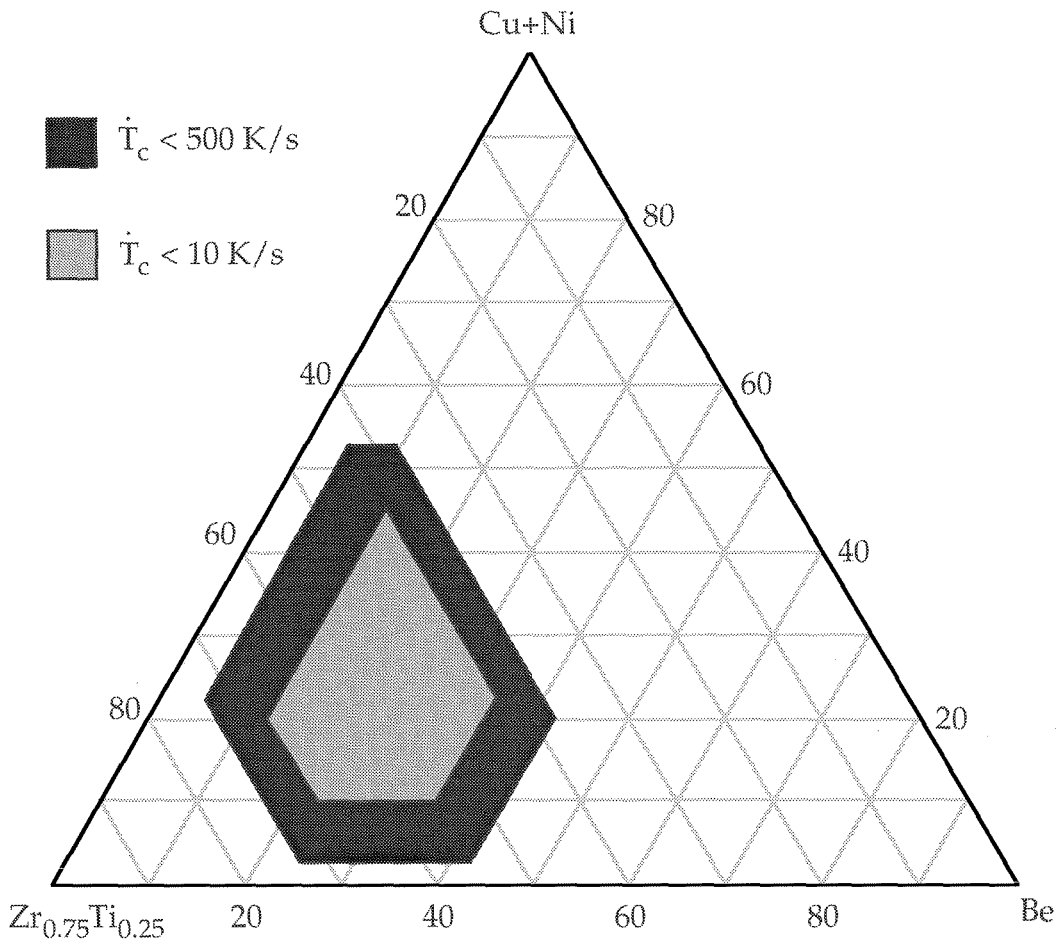

Figure A.1: Glass forming range for $(Zr_{0.75}Ti_{0.25})_{100-b-c}(Cu_{1-Y}Ni_Y)_bBe_c$ alloys for two different cooling rates. Ni content (the value of b_Y) is from 5 to 15 atom percent.

TABLE A.4: Thermal properties of $Zr_{100-b-c}Cu_bNi_{10}Be_c$ glassy alloys prepared in the form of 1.0 mm strips.

Composition	T_g(°C)	T_x(°C)	ΔT(°C)
$Zr_{70}Cu_{7.5}Ni_{10}Be_{12.5}$	304	361	57
$Zr_{65}Cu_{17.5}Ni_{10}Be_{7.5}$	324	391	67
$Zr_{65}Cu_{12.5}Ni_{10}Be_{12.5}$	317	390	73
$Zr_{65}Cu_{12.5}Ni_{10}Be_{17.5}$	317	396	79
$Zr_{60}Cu_{17.5}Ni_{10}Be_{12.5}$	338	418	80
$Zr_{55}Cu_{22.5}Ni_{10}Be_{12.5}$	355	428	73
$Zr_{55}Cu_{17.5}Ni_{10}Be_{17.5}$	349	430	81
$Zr_{55}Cu_{12.5}Ni_{10}Be_{22.5}$	347	433	86
$Zr_{55}Cu_{17.5}Ni_{10}Be_{27.5}$	343	455	112
$Zr_{55}Cu_{12.5}Ni_{10}Be_{22.5}$	347	433	86
$Zr_{50}Cu_{27.5}Ni_{10}Be_{12.5}$	378	445	67
$Zr_{50}Cu_{22.5}Ni_{10}Be_{17.5}$	372	450	78
$Zr_{50}Cu_{17.5}Ni_{10}Be_{22.5}$	361	453	92
$Zr_{50}Cu_{12.5}Ni_{10}Be_{27.5}$	360	464	104
$Zr_{50}Cu_{7.5}Ni_{10}Be_{32.5}$	362	466	102
$Zr_{45}Cu_{37.5}Ni_{10}Be_{7.5}$	404	459	55
$Zr_{45}Cu_{32.5}Ni_{10}Be_{12.5}$	395	454	59
$Zr_{45}Cu_{27.5}Ni_{10}Be_{17.5}$	389	456	67
$Zr_{45}Cu_{22.5}Ni_{10}Be_{22.5}$	383	464	81
$Zr_{45}Cu_{12.5}Ni_{10}Be_{32.5}$	375	460	85
$Zr_{45}Cu_{7.5}Ni_{10}Be_{37.5}$	373	451	78

TABLE A.5: Bulk glass forming ($\dot{T}$ < 10 K/s) ETM-LTM-Be type alloys.

$Hf_{41.2}Ti_{13.8}Cu_{12.5}Ni_{10}Be_{22.5}$	$Zr_{41.2}Ti_{13.8}Cu_{7.5}Co_{15}Be_{22.5}$
$Zr_{33}Ti_{11}Hf_{11}Cu_{12.5}Ni_{10}Be_{22.5}$	$Zr_{41.2}Ti_{13.8}Cu_{12.5}Ni_{10}Be_{20}Si_{2.5}$
$Zr_{34.5}Ti_{11.5}Nb_9Cu_{12.5}Ni_{10}Be_{22.5}$	$Zr_{41.2}Ti_{13.8}Cu_{12.5}Ni_{10}Be_{20}B_{2.5}$
$Zr_{36}Ti_{12}V_7Cu_{12.5}Ni_{10}Be_{22.5}$	

TABLE A.6: Thick glass forming ($\dot{T}$ < 10^2-10^3 K/s) ETM-LTM-Be type alloys.

$Zr_{33}Ti_{11}Y_{11}Cu_{12.5}Ni_{10}Be_{22.5}$	$Zr_{41.2}Ti_{13.8}Cu_{7.5}Fe_{15}Be_{22.5}$
$Zr_{36}Ti_{12}Cr_7Cu_{12.5}Ni_{10}Be_{22.5}$	$Zr_{41.2}Ti_{13.8}Mn_{15}Cu_{7.5}Be_{22.5}$
$Zr_{33.8}Ti_{11.2}Cr_{10}Cu_{17.5}Ni_{10}Be_{17.5}$	$Zr_{55}Fe_{7.5}Be_{37.5}$

TABLE A.7: Readily glass forming ($\dot{T}$ < 10^4-10^6 K/s) ETM-LTM-Be type alloys.

$Zr_{30}Ti_{10}V_{15}Cu_{12.5}Ni_{10}Be_{22.5}$	$Nb_{25}Zr_{22.5}Ti_{7.5}Cu_{12.5}Ni_{10}Be_{22.5}$
$Zr_{41.2}Ti_{13.8}Fe_{22.5}Be_{22.5}$	$Zr_{30}Nb_{20}Ni_{30}Be_{20}$

TABLE A.8: Thick glass forming ($\dot{T}$ < 10^2-10^3 K/s) Zr-Ti-Ni-Cu-Be-M type alloys.

$Zr_{41.2}Ti_{13.8}Cu_{12.5}Ni_{10}Be_{7.5}Al_{15}$	$Zr_{41.2}Ti_{13.8}Cu_{12.5}Ni_{10}Be_{17.5}Si_5$
$Zr_{41.2}Ti_{13.8}Cu_{12.5}Ni_{10}Be_{12.5}Al_{10}$	$Zr_{41.2}Ti_{13.8}Cu_{12.5}Ni_{10}Be_{17.5}B_5$

References

[1] A. Peker and W. L. Johnson, U.S. Patent No. 5,288,344, assigned to California Institute of Technology (Feb. 1994).

[2] A. Peker and W. L. Johnson, U.S. Patent application (April 1994).

[3] W. L. Johnson and A. Peker, to appear in *Science and Technology of Rapid Solidification Processing Technologies, NATO ASI Series,* M. A. Otooni (ed.), (West Point, June 1994).